Improvement on the performance of spray deposited $CuInS_2/In_2S_3$ solar cell using extremely thin absorber layer with mixed phases of $CuInS_2$ and Cu_2S

Thesis submitted to

Cochin University of Science and Technology

in partial fulfilment of the requirements

for the award of the degree of

Doctor of Philosophy

In **Physics**

Under the Faculty of Science

By

SANTHOSH M.V

Thin Film Photovoltaic Division
Department of Physics
Cochin University of Science and Technology
Cochin- 682 022, Kerala, India

August 2015

Improvement on the performance of spray deposited $CuInS_2/In_2S_3$ solar cell using extremely thin absorber layer with mixed phases of $CuInS_2$ and Cu_2S

Ph.D thesis in the field of Thin Film Photovoltaics

Author

Santhosh M.V
Thin Film Photovoltaic Division
Department of Physics
Cochin University of Science and Technology
Cochin-682 022, Kerala, India
E-mail: ssanthu1987@gmail.com

Supervising Guide:

Dr. K.P.Vijayakumar
Professor (Retd) & CSIR Emeritus Scientist
Department of Physics
Cochin University of Science and Technology
Cochin-682 022, Kerala, India
E-mail: kpv@cusat.ac.in

Cochin University of Science and Technology
Cochin-682 022, Kerala, India
www.cusat.ac.in

August 2015

Department of Physics
Cochin University of Science and Technology
Cochin- 682 022, Kerala, India

Dr.K.P.Vijayakumar
Professor (Retd) & CSIR Emeritus Scientist
Phone: 0484 2577404, E-mail: kpv@cusat.ac.in

Certificate

Certified that the thesis entitled **"Improvement on the Performance of Spray Deposited $CuInS_2/In_2S_3$ Solar Cell Using Extremely Thin Absorber Layer with Mixed Phases of $CuInS_2$ and Cu_2S"** submitted by **Mr. Santhosh M. V.** is an authentic record of research work carried out by him under my supervision at the Department of Physics in partial fulfilment of the requirements for the award of degree of Doctor of Philosophy of Cochin University of Science and Technology and the work embodied in this thesis has not been included in any other thesis submitted for the award of any degree.

Dr. K.P. Vijayakumar
(Supervising Guide)

Cochin -22
Date:

Department of Physics
Cochin University of Science and Technology
Cochin- 682 022, Kerala, India

Dr.K.P.Vijayakumar
Professor (Retd) & CSIR Emeritus Scientist
Phone: 0484 2577404, E-mail: kpv@cusat.ac.in

Certificate

This is to certify that the thesis entitled **"Improvement on the Performance of Spray Deposited $CuInS_2/In_2S_3$ Solar Cell Using Extremely Thin Absorber Layer with Mixed Phases of $CuInS_2$ and Cu_2S"** submitted by **Mr. Santhosh M.V.**, has incorporated all the relevant corrections and modifications suggested by the audience during the pre-synopsis seminar and recommended by the Doctoral Committee.

Dr. K.P. Vijayakumar
(Supervising Guide)

Cochin -22
Date:

Declaration

I hereby declare that the work presented in the thesis entitled **"Improvement on the performance of spray deposited $CuInS_2/In_2S_3$ solar cell using extremely thin absorber layer with mixed phases of $CuInS_2$ and Cu_2S"** is based on the original work done by me under the guidance of **Dr. K.P.Vijayakumar**, Professor (Retd) and CSIR Emeritus Scientist, Department of Physics, Cochin University of Science and Technology, Cochin- 682 022, India and has not been included in any other thesis submitted for the award of any degree.

Cochin- 22 **Santhosh M. V.**

Date :

Acknowledgements

Support and prayers of many people strengthen me to complete my work. I would like to write my humble gratitude to all those who were with me during this journey.

First of all I express my heartfelt gratitude to my supervising guide Dr. K. P. Vijayakumar, Professor (Retd) and CSIR Emeritus Scientist, Department of Physics, Cochin University of Science and Technology, who enabled me to full fill the criteria of this degree. I am thankful for his patience and support. I gratefully acknowledge Prof (Retd) C. Sudha Kartha for her apt advices and contributions during my research work.

I express my sincere gratitude to Prof. S. Jayalakshmi, Head, Department of Physics and to all former heads of Physics department during my research work for providing me the facilities of this prestigious department. I am indebted to Prof (Retd) M. Sabir for his help and encouragement. I also express my gratitude to Dr. K. Rajeev Kumar for being my research committee member. I acknowledge my thanks to Prof. M. K. Jayaraj for allowing me to utilize the equipment facility under 'DST Nano Mission Initiative' programme. I express my deepest gratitude to teaching faculty of Department of Physics, CUSAT for their love and concern from my post-graduation study onwards. I acknowledge office staffs of Department of Physics and in administrative sections for their help.

I would also like to thank Dr. Y. Kashiwaba and Ms. T. Abe of Iwate University, Japan, for collaboration and XPS analysis of my sample. Helps offered by Dr. K. B. Jinesh is also greatly acknowledged.

The financial assistance from MNRE and CUSAT is greatly acknowledged. I remember helps and love from my seniors Dr. Tina Sebastian, Dr. Vimal Kumar T V, Dr. Sajeesh T H, Dr. Rajesh Menon, Dr. Angel Susan Cherian, Dr. Rajeshmon, Dr. Poornima and Dr. Anita R Warrior. I am also indebted to Deepu, Sreejith, Titu, Gincy and Gisa for their whole-hearted support and encouragements. I have great pleasure in thanking them most sincerely for their timely helps and fruitful discussions. Especially, I remember with gratitude for the selfless support from Deepu who is with me from M.Sc. onwards. I would also like to thank Rajesh C S, Anshad, Aswathy, Jisha, Jubi mol and Sona for their friend ship and support. I express my gratitude to Anas, Saneesh, Nithya, Jalaja,Vipin, Sreeroop and Aneesh George for their friend ship during the course of my research work.

Interactions with my friends Abhilash, Hasna, Sajan, Shijeesh, Anand, Manoj, Jubeesh, Jishnu, Sagar, Dr. Tharanath, Dr. Sanal K C, Dr. Arun Aravind, Dr. Sreekanth Varma, Dr. R. Sreekumar, Dr. Rajiv, Dr. Priyesh, Dr. Nijo Varghese, Lija, Lisha, Dintomon, Aravind, Vinod, Rasheed, Satheesan, Kurias, Subin Thomas and Dr. Mothy Mohan helped me a lot to keep a cheerful atmosphere in the Department. Especially, gratitude to my roommate Abhilash is beyond the words. I am also thankful for the interactions of M. Sc and M. Phil students who have done their projects in our lab.

Finally and most importantly, I am indebted to my family for their continuous support and understandings. I am not able to express my gratitude to each of them with this sheet of paper.

Santhosh M.V

Preface

Inclination in today's worldwide energy consumption graph demands further invention, development and implementation of clean and sustainable energy sources. In this scenario, photovoltaic devices can play a major role. But contemporary photovoltaic industry is dominated by costly silicon based solar cells. This "cost factor" mainly hinders popularity of these devices as it is not affordable to common people. Also, technology of silicon based solar cell is now experiencing saturation in terms of material development, efficiency and cost effectiveness. Compound semiconductors based on 'earth abundant' elements are excellent alternative to silicon. As they have direct band gap and higher absorption coefficient, less material is required for efficient light absorption when comparing with silicon. Moreover, for the deposition of most of these semiconductors, a variety of simple, low cost, chemical methods can be employed. Thus thin film solar cells based on compound semiconductors are capable of making photovoltaics competitive with traditional means of energy production.

Recent developments in thin film solar cell technologies based on chalcogenide materials like $CuInSe_2$, $CuInS_2$, Cu_2S, $CuGaSe_2$ and $CuIn_{1-x}Ga_xSe_2$ are promising signs to outclass the limitations in Si based solar cell industry. These materials and their further solar cell fabrication technologies are cost effective. This thesis deals with material study, fabrication and characterization of thin film solar cells using automated chemical spray pyrolysis (CSP) machine. CSP is simple, versatile and cost effective chemical method for thin film deposition, suitable for large area deposition. For the absorber layer in thin film solar cells, we chose $CuInS_2$ and Cu_2S. $CuInS_2$ is ideal absorber material because of its direct band gap of 1.5 eV and high absorption coefficient of the order 10^5 cm^{-1}, both favorable for efficient solar energy absorption. Theoretically efficiency of 28.5 % was calculated for $CuInS_2$ based solar cells, which is high when comparing with

other chalcopyrites. Cu_2S is also another well-established absorber material that can be simply deposited by chemical methods such as chemical spray pyrolysis. In this work, spray pyrolysis has been effectively used to deposit thin films having mixed phases of both $CuInS_2$ and Cu_2S. After incorporating multiple absorption bands in the absorber layer, this new material was used to fabricate an extremely thin absorber (ETA) solar cell with In_2S_3 as buffer layer. This thesis has been structured in to six chapters and in the following section; we give brief description on topics included in different chapters.

CHAPTER 1 deals with basic concepts and developments in the field of photovoltaics. Important output parameters of a solar cell that are used to compare its performance with other solar cells are discussed briefly. A detailed description on chemical spray pyrolysis, deposition technique used for solar cell fabrication in the present study, is also included. Review on $CuInS_2$, Cu_2S and solar cells based on these materials are also done. In final section of this chapter, significance of the present work is also incorporated.

CHAPTER 2 deals with fabrication of $CuInS_2/In_2S_3$ solar cells in superstrate structure using spray pyrolysed microporous TiO_2 as 'electron conducting layer'. There is a brief review on $CuInS_2$ solar cells in superstrate configuration. Deposition and characterization of $CuInS_2$ absorber layer by optimizing the spray rate is also discussed. Microporous TiO_2 electron conducting layer was spray deposited using commercially available TiO_2 powder and different characterization tools are used for its study. An "all sprayed solar cell" having $FTO/TiO_2/In_2S_3/CuInS_2/Ag$ structure fabricated using the optimized spray conditions for individual layers showed an efficiency of 0.61 %. When the "sprayed FTO" back contact is replaced with "sputtered ITO", the device shows an efficiency of 1.17 %.

CHAPTER 3 briefly discusses fabrication of $TCO/CuInS_2/In_2S_3/Ag$ solar cells using single and double layered structure for the absorber layer. Device fabricated on ITO with optimized thicknesses of absorber and buffer

layer shows efficiency of 2.59 %. Large area device having active area of 5 cm^2 was also fabricated using the same configuration and its performance was monitored for 100 days. On sprayed FTO, device shows efficiency of 0.94 %. XPS depth profile analysis of these solar cells indicated diffusion of Cu from $CuInS_2$ to In_2S_3 buffer layer, which can deteriorate performance of the device. An Al_2O_3 inter layer was deposited between $CuInS_2$ and In_2S_3 layer employing 'atomic layer deposition' in the cell structure and the diffusion of Cu was very much controlled. In the next stage, spray pyrolysis itself was effectively used to deposit a resistive $CuInS_2$ in the cell structure for controlling Cu diffusion. Comparing with devices having single layered absorber, it shows better values of open circuit voltage (V_{oc}) and fill factor, but current density (J_{sc}) decreases, in effect efficiencies are almost same for both configurations.

CHAPTER 4 describes "Extremely Thin Absorber (ETA)" layer solar cells fabricated using mixed phase $CuInS_2$-Cu_2S as absorber layer and In_2S_3 as buffer layer. Detailed description on the CSP deposition and characterisation of this 'mixed phase absorber layer' is also included. ETA solar cells fabricated in the following structure ITO/$CuInS_2$-Cu_2S/In_2S_3/Ag has efficiency of 3.82 %. Thicknesses of both absorber and buffer layers are optimized for this device. Detailed analysis of transmission spectra of the solar cells fabricated without top electrode is also incorporated in this chapter. The cells shows ~ 45 % transmission in the visible region, and on changing the input power accordingly, device will show efficiency of ~ 6 %; these solar cells can be used as 'window glass' that can simultaneously trasmit sunlight and capture power from it.

CHAPTER 5 deals with fabrication of ETA solar cells using mixed phase $CuInS_2$-Cu_2S absorber by utilizing Cu diffusion in Cu_2S/In_2S_3 heterojunction. Initial section of the chapter gives details of deposition and characterisation of Cu_2S absorber layer employing spray pyrolysis method. For solar cell fabrication ITO/Cu_2S/In_2S_3/Ag structure was followed and the device having optimized thicknesses of absorber and buffer layer has efficiency of

4.11 %. Diffusion of Cu from Cu_2S to In_2S_3 converts some part of In_2S_3 to $CuInS_2$. Raman analysis of the solar cells (without the top electrode) was successfully employed to confirm the presence of both Cu_2S and $CuInS_2$ in the cell structure. In the final section of this chapter, aspects of deposition time required for entire solar cell fabrication is explained. Deposition time less than 45 minutes is only required for entire solar cell fabrication. Also, the electric energy consumed for depositing this solar cell was ~ 4.1 kWh, which will be still lower for one solar cell, as CSP is capable of fabricating large number of cells in a batch.

CHAPTER 6 summarises entire work along with scope for future work.

……..✷♦✷……..

Publications

Journal Publications

1) All sprayed ITO free $CuInS_2/In_2S_3$ solar cell.
   M.V. Santhosh, D. R. Deepu, K. Rajeev Kumar, C.Sudha Kartha, K. P. Vijayakumar.
   Solar Energy, 108 (2014) 508–514.

2) Spray pyrolysed microporous TiO_2 thin films by optimization of substrate temperature for all sprayed solar cells.
   M. V. Santhosh, D. R. Deepu, R. Geethu, K Rajeev kumar, C. Sudha Kartha and K. P. Vijayakumar.
   Semiconductor Science and Technology, 29 (2014) 115026 (7pp).

3) Thin film solar cells with extremely thin absorber layer having multiple absorption bands: A novel attempt.
   M. V. Santhosh, C. Sudha Kartha, K. Rajeev Kumar, K. P. Vijayakumar.
   Solar Energy (Under revision)

4) Improvement of device parameters of $CuInS_2/In_2S_3$ junction deposited using automated spray machine.
   M. V. Santhosh, C. Sudha Kartha, K. P. Vijayakumar.
   AIP CONF PROC, 1349 (2011), 673-674.

5) Ageing studies on $CuInS_2/In_2S_3$ junction (2.5×2 cm^2) deposited using automated spray machine.
   M. V. Santhosh, C. Sudha Kartha, K. P. Vijayakumar.
   AIP CONF PROC, 1591 (2014), 639-641.

6) Improvement in properties of window layer of sprayed $CuInS_2/In_2S_3$ solar cell by optimization of tin doping.
   M. V Santhosh, M. S. Sreejith, C. Sudha Kartha, K. P. Vijayakumar,
   AIP CONF PROC, 1576 (2014), 76-78.

Conference Papers

1) Sprayed TiO_2 Thin Films For Solar Cell Applications: **M. V. Santhosh**, K. Rajeev Kumar, C. Sudha Kartha, K. P. Vijayakumar, ICEEE- 2015, International conference conducted by Department of Physics CUSAT, Cochin, on Feb 5-7.

2) An Attempt to control the Cu diffusion in ITO/$CuInS_2$/In_2S_3/Ag solar cells: **M. V. Santhosh**, C.Sudha Kartha, K. P. Vijayakumar, T Abe, Y Kashiwaba, ICSET 2014, International conference conducted by PSG college Coimbatore, on Dec 12-14.

3) Preparation of $CuInS_2$/In_2S_3 Thin film Solar Cell Using Spray Pyrolysis: The effect of Cu concentration: **M. V. Santhosh**, C.Sudha Kartha and K. P. Vijayakumar, National Conference on Current Trends in Material Science (CTMS-2011), Christian College, Chengannur, Kerala, Aug 4-6.

4) The role of thickness of In_2S_3 buffer layer in $CuInS_2$/In_2S_3 junction deposited using automated spray machine: **M. V. Santhosh**, C.Sudha Kartha and K. P. Vijayakumar, Horizons in Thin Film Technology (HTFT-2011), TOC H Institute Of Science and Technology, Arakkunnam, Kerala, Jan 20-21.

……..✷ ♦ ✷……..

CONTENTS

……..✷♦✷……..

List of abbreviations

ALD	-	Atomic layer deposition
AFM	-	Atomic force microscopy
CPV	-	Concentrated photovoltaics
CSP	-	Chemical spray pyrolysis
CBD	-	Chemical bath deposition
CVD	-	Chemical vapor deposition
DSSC	-	Dye sensitized solar cell
ESAVD	-	Electrostatic spray assisted vapor deposition
EDAX	-	Energy dispersive X-ray analysis
ETA	-	Extremely thin absorber
FF	-	Fill factor
FTO	-	Fluorine doped tin oxide
GLAD	-	Glancing angle deposition
ILGAR	-	Ion layer gas reaction
ITO	-	Tin doped indium oxide
J_{sc}	-	Short circuit current density
MEG	-	Multiple exciton generation
MBE	-	Molecular beam epitaxy
MOCVD	-	Metalorganic chemical vapor deposition
PV	-	Photovoltaics
PECVD	-	Plasma enhanced chemical vapor deposition
PVD	-	Physical vapor deposition

PSD	-	Pressure spray deposition
QW	-	Quantum well
RMS	-	Root mean square
RTP	-	Rapid thermal process
R_s	-	Series resistance
R_{sh}	-	Shunt resistance
RBS	-	Rutherford back scattering spectrometry
SEM	-	Scanning electron microscopy
SILAR	-	Successive ionic layer adsorption and reaction
TCO	-	Transparent conducting oxide
TEM	-	Transmission electron microscopy
V_{oc}	-	Open circuit voltage
XPS	-	X-ray Photo electron spectroscopy
XRD	-	X-ray diffraction

……..✷♦✷……..

Chapter **1**

Photovoltaics: Basic concepts and developments

1.1 Introduction

Global power consumption of present civilized society is almost completely reliant upon non-renewable fossil fuels. Due to this, fossil fuels are depleting at a faster rate as the demand of energy is increasing day by day. Moreover, combustion of fossil fuels for energy production releases greenhouse gases that are responsible for disastrous effects on environment such as global warming and acid rain. We are in an irreversible, dangerous but avoidable circumstance that demands to replace the fossil fuel which hinders sustainable development of human civilization. While considering a suitable alternative to fossil fuels, it should be renewable, available in abundance, eco-friendly and capable of meeting growing energy demands. In this context, energy harvesting from sun is ultimate and perfect choice as it is ultra-clean, natural and sustainable source of energy. The energy supplied by sun on earth in one hour is equivalent to the amount of energy that is consumed by human beings in one year. Solar cells are the electrical device that directly converts sunlight into electricity based on photovoltaic (PV) effect. They have no moving parts and hence, after the initial installing cost, maintenance and repair costs are extremely low compared to existing technologies. Based on energy demand, they can be constructed to any size. For countries like India, the unused desert areas can be effectively used for installing solar cells. The concept of photovoltaic effect i.e., generation of electricity from light was discovered by Edmond Becquerel in 1839. At present, intensive researches are going on in this field. Now Si based solar cells are dominating this field with efficiency (at lab level) of 25.6 % [1]. But the higher cost for solar electricity, when comparing with existing technologies, still hinders the wide

spreading of this green technology. Thin film solar cells based on compound semiconductors are capable of overcoming the limitations of Si based technologies. Recent developments in this field are promising solutions for future energy demands.

1.2 Physics of solar cells

For most successful and versatile solar technologies, formation of a p-n junction using p-type and n-type semiconductors is essential. Nature and strength of internal built in electric field in a p-n junction is a critical factor in the operation of a solar cell. Light enters the solar cell through a window layer, which exhibits high electrical conductivity as well as transparency in the visible region of solar spectrum. Generally window layer is n-type material that ensures a low resistance contact to the device and transmits maximum amount of light to the absorber layer of the device. When light of suitable energy falls on the absorber layer of a solar cell, the electrons in the valence band get excited to the conduction band i.e., this results in excited electron in the conduction band and electron vacancy (hole) in the valence band. In effect, the electromagnetic energy in photon is now converted to the energy of electron-hole pairs. The built in electric field now comes into play and separates electrons to n side and holes to p side. If an external circuit is connected between this p and n-type region, the higher energy electron moves through this circuit. These electrons dissipate energy in the external circuit and finally return to the solar cell. For efficient solar cells, theoretically band gap of the light absorbing semiconductor material should be 1.4 to 1.6 eV [2]. Absorption coefficient of this absorber material should be very high to absorb maximum number of photons within a thin layer. Larger life time and diffusion length are preferable for minority carriers to enhance their better collection.

In practice, solar cells are connected in series to get the required voltage and in parallel to get required current. This arrangement of solar cells is

generally called a 'photovoltaic module' or 'photovoltaic panel'. These modules/panels can be interconnected to form an 'array' for getting required electrical output.

1.3 Equivalent circuit of a solar cell

Solar cells are current sources. As long as the intensity of incident solar radiation is constant, current obtained from a solar cell remains same. The voltage obtained from a given solar cell depends on the external load connected and it varies with the load. Hence solar cell can be represented as a current source. If no external circuit is connected across a solar cell, the incident light will produce excess electrons at n side and holes at p side i.e., a potential difference will be created at the ends of the solar cell. This potential forward biases the junction and a diode forward bias current (I_d) flows through the diode. This diode forward bias current (I_d) is opposite to the photocurrent (I_{ph}) produced in the solar cell. Hence the net current (I) from a solar cell (Figure 1.1) is

$$I = I_{ph} - I_d$$

$$I = I_{ph} - I_o\left[\exp\left(\frac{eV}{kT}\right) - 1\right] \quad \text{..... (1)}$$

Where 'I_o' is diode saturation current, 'e' is charge of an electron (1.6×10^{-19} Coulombs), 'V' is the voltage between the terminals, 'k' is the Boltzmann constant and 'T' is the temperature in Kelvin.

If an external load (R_L) is connected to the solar cell, then I_d can still exist and the rest of the current will pass through the external circuit. When the light generated electrons travel through the solar cell materials and external contacts, they will experience a resistance. This resistance appears in series with the external load and is represented as 'series resistance' (R_s). For an

ideal solar cell R_s should be zero so that there should be no voltage drop before the load. The equation for a solar cell in presence of series resistance is [3]

$$I = I_{ph} - I_o \exp\left[\frac{e\,(V+IR_s)}{kT}\right] \ldots\ldots\ldots\ldots (2)$$

The phenomenon of recombination of light generated carriers inside the solar cell material should also have to be considered. Due to recombination, these carriers cannot contribute electricity or it is shorted/shunted inside the device. A resistance corresponding to this process is represented as 'shunt resistance' (R_{sh}) in the circuit. For an ideal solar cell R_{sh} should be '∞' so that there is no alternate path for current to flow and equation for a solar cell in presence of shunt resistance is given below [3].

$$I = I_{ph} - I_o \exp\left[\frac{eV}{kT}\right] - \frac{V}{R_{sh}} \ldots\ldots (3)$$

Series and shunt resistances of a solar cell are called its 'parasitic resistances'. By dissipating power in these parasitic resistances efficiency of solar cells get reduced. Accurate determinations of these parasitic resistances have vital role in determining solar cell structure and hence its quality control. The equivalent circuit of a solar cell is shown in Figure 1.1.

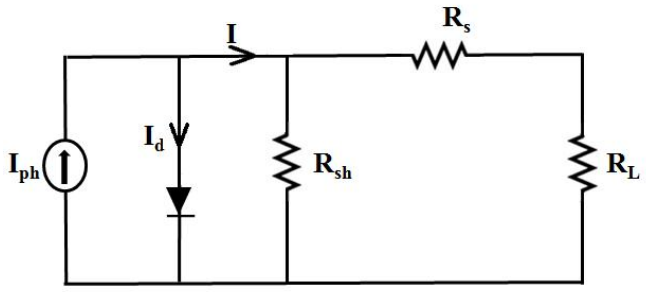

Figure. 1.1 Equivalent circuit of a solar cell.

1.4 Output parameters of a solar cell

The main output parameters of a solar cell that are used to compare its performance with other solar cells are (1) Open circuit voltage (V_{oc}) (2) Short circuit current (I_{sc}) (3) Fill factor (FF) (4) Efficiency (η).

1.4.1 Open circuit voltage (V_{oc})

Let us consider that no external load is connected to a solar cell or circuit is open. At this condition potential difference between the terminals of the device is maximum and the current through the external circuit is zero. The voltage across the output terminals of a solar cell in open circuit condition is termed as 'open circuit voltage' (V_{oc}). For an ideal solar cell ($R_{sh} = \infty$ and $R_s = 0$), equation for V_{oc} can be expressed from eqn.1 as

$$V_{oc} = \frac{kT}{e} \ln\left(\frac{I_{ph}}{I_0} + 1\right)$$

For higher V_{oc} from a solar cell, the diode saturation current (I_o) should be as small as possible. I_o decreases with increasing band gap of semiconductor material i.e., for higher value of V_{oc}, materials with higher band gap is required [2]. Bulk and surface recombination in semiconductor material are two fundamental factors that can limit V_{oc} from a solar cell. Lower the recombination rate, higher the V_{oc} [2].

1.4.2 Short circuit current (I_{sc})

Let us consider that external load is removed and circuit is shorted. At this condition, voltage across the solar cell is zero and maximum current will flow through the circuit. The maximum current that can be obtained from a solar cell in short circuit condition is termed as 'short circuit current' (I_{sc}). From eqn.1, I_{sc} for an ideal solar cell is

$$I_{sc} = I_{ph}$$

I_{sc} depends on area of solar cell. Hence while comparing the performance of solar cells with different areas; a term called short circuit current density (J_{sc}) is used. J_{sc} is generally expressed as mA/cm^2 of the device. At a particular value of light intensity (generally 1000 W/m^2), I_{sc} from a solar cell depends on band gap and diffusion length of minority carrier in the semiconductor material. Lower band gap and higher diffusion length for minority carriers are preferred for higher I_{sc}. Optical losses such as reflective nature of semiconductor, reflection from metal grid contact on the side of the cell exposed to sun light and inefficient absorption of light with suitable energy due to the low absorber layer thickness can also reduce the I_{sc} obtained from a solar cell [2].

1.4.3 Efficiency (η)

Solar cell efficiency is the ratio of output power obtained from a solarcell to the input power from the sun. The nature of general I-V characteristics of a solar cell is shown in Figure 1.2. At V_{oc}, voltage obtained from a solar cell is maximum, but current is zero, leading to zero output power at open circuit condition. At J_{sc}, current obtained is maximum but voltage is zero, leading to zero output power at short circuit condition also. Hence the maximum power point lies somewhere in the curve between J_{sc} and V_{oc}. Theoretically the maximum power is selected in such a way that area of the rectangle created with this point as one corner in the I-V curve has maximum area. Let P_m be the maximum power point with V_m and I_m corresponding to the voltage and current of the solar cell at that point (Figure 1.2). Then the maximum output power (P_m) from a solar cell is the product of this V_m and I_m.

$$\text{Maximum output power } (P_m) = V_m \times I_m$$

$$\text{Efficiency } (\eta) = \frac{\text{Output power } (P_m)}{\text{Input power } (P_{in})} \times 100$$

$$\eta = \frac{V_m \, X \, I_m}{P_{in}} \, X \, 100$$

Standard test conditions (STC) for solar cell specifies a temperature of 25 °C and an irradiance of 1000 W/m^2 with air mass ratio equal to 1.5 (AM1.5)**.** The Shockely Queisser limit calculations for solar cell efficiencies shows that only an efficiency of 34 % can be achieved for any type of single junction solar cells [4]. PV cells cannot respond efficiently to the entire spectrum of sunlight. As higher energy photons incident on the material, electrons are excited to higher levels in conduction band. These electrons quickly relax back to band edges and emit phonons. Thus a major portion of incident sunlight is wasted as heat. The photons with energy less than the band gap of the material are not absorbed, this process also wastes energy [2]. Recombination of electron-hole pairs can also waste a small portion of the incident energy depending on the semiconductor material. The efficiency limit of 34 % can be overcome by using multi junction solar cells.

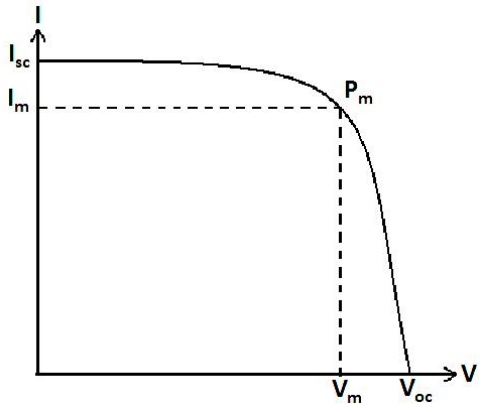

Figure. 1.2 I-V characteristics of a solar cell showing maximum power point.

1.4.4 Fill factor (FF)

Fill factor of a solar cell is defined as the ratio of maximum power (P_m) to the ideal power or theoretical power (P_I). Ideal power is the product of V_{oc} and I_{sc}.

$$\text{Fill factor} = \frac{V_m \cdot I_m}{V_{oc} \cdot I_{sc}} \text{ X } 100$$

For an ideal solar cell, theoretical power and the maximum power are the same. Then the I-V curve will be a perfect rectangle with fill factor of 100 %. Practically I-V curves are not in perfect square shape and fill factor values ranges from 50 % to 82 %. Thus fill factor is a measure of 'squareness' of I-V characteristics of a solar cell.

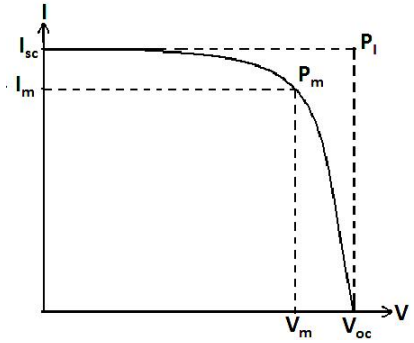

Figure. 1.3 I-V curve of a solar cell for illustrating fill factor.

1.5 Solar cell materials and technologies

Current PV industry is dominated by silicon (Si) based solar cells. Monocrystalline and polycrystalline Si solar cells are well developed and their efficiencies have almost reached theoretical maximum values. Due to the unaffordable cost of Si wafers, thin film solar cells based on compound semiconductors are now gaining paramount importance. Most of the thin film solar cells contain earth abundant elements and can be easily deposited by simple, cost effective techniques. Organic photovoltaics also show promising

signs as future PV technology mainly because of their flexibility and simpler deposition techniques. The fields of polymer solar cells and dye sensitized solar cells are undergoing steady development. In order to overcome the Shockley – Queisser limit, active researches are going on in the above mentioned solar cell materials mainly by employing technologies like tandem solar cells, hot carrier solar cells, concentrated solar cells, up conversion, defect level assisted/intermediate band photovoltaics and quantum dot solar cells.

1.5.1 Silicon solar cells

Silicon solar cells can be divided into different categories according to the crystallinity or crystal size of the Si used for its fabrication. All Si solar cells work by the photovoltaic action of a p-n junction.

1.5.1.1 Crystalline silicon solar cells

Crystalline Si solar cells are highly efficient, oldest and still the most popular solar cells. Due to the energy intensive and sophisticated deposition techniques, their cost is not competitive with traditional means of electricity production. Czochralski method is used for growing Si wafers for fabricating crystalline solar cells. The wafers should have thicknesses ~ 200 μm for efficient light absorption as Si has indirect band gap. Boron and phosphorous are the dopants for making the wafer p-type and n-type. To improve the light absorption, wafer surfaces are generally textured. Another important issue is that these solar cells lose their efficiency as the temperature increases about 25 °C. Hence air circulation must be provided to these panels to maintain the efficiency. An efficiency of 25.6 % has been reported for n-type crystalline Si solar cells by Panasonic for a large area of 144 cm^2. A thin p-type amorphous Si layer served as the cell emitter and a similar n-type layer as the rear contact. It is a rear-junction cell having both positive and negative contacts in the unilluminated rear cell surface [1, 5].

1.5.1.2 Multicrystalline silicon solar cells

Wafers of multicrystalline Si are easy to prepare when comparing with monocrystalline Si. They are less efficient, but more cost effective than monocrystalline Si solar cells. Grain boundaries in multicrystalline Si are passivated by incorporating hydrogen during the device fabrication. Maximum efficiency of 20.4 % was reported for multicrystalline Si solar cells [5, 6]. Ribbon Si is another type of polycrystalline Si formed by drawing flat thin films from molten Si. The process does not require sawing from ingots. Solar cells using ribbon technology possess lower efficiencies and are costlier than multi Si solar cells even though there is reduction in Si waste.

1.5.2 Thin film solar cells

Thin film solar cells using earth abundant elements are deposited by employing simple deposition techniques on comparing with Si photovoltaics. Hence both material and its processing are cost effective here. For solar cell fabrication only a smaller thickness of these materials are required due to their high absorption, small diffusion length and high recombination velocity. Hence very low weight per unit power is required here in comparison with crystalline Si technology. New concepts like tandem solar cell, hot carrier solar cells and multi junction concentrators are possible with thin film technology. A brief discussion about some important thin film solar cells are given below.

1.5.2.1 CdTe solar cells

CdTe is an ideal material for absorbing sunlight due to its direct band gap of 1.5 eV and high absorption coefficient. CdS was observed to be the suitable buffer layer for CdTe and CdTe/CdS is the only thin film solar cell so far to compete with crystalline Si in cost/watt. Major problem regarding this solar cell is the toxic nature of Cd and Te; again the limited supply of tellurium is another threat. Corrosion problem of the electrode was another major issue

in CdTe solar cells. Also for the formation of good junction, an activation process in the presence of $CdCl_2$ is required. A variety of deposition techniques such as vacuum evaporation, closed space sublimation, chemical bath deposition and screen printing are available for CdTe deposition [7]. For device fabrication, usually chemical bath deposition and closed space sublimation are preferred. The best reported efficiency for CdTe based device is 19.6 % by GE global research [5, 8] and an efficiency of 17.5 % was reported by 'First Solar' (who are the pioneers in this material) for CdTe solar cell modules with an area of 7021 cm^2 [9].

1.5.2.2 Cu chalcogenides based solar cells

Copper indium selenide ($CuInSe_2$) thin films having a band gap of ~ 1 eV and higher absorption coefficient was observed to be suitable absorber layer. $CuInSe_2$ thin films are less sensitive to impurities and grain size, making it a better absorber layer. Due to low band gap, the open circuit voltage for $CuInSe_2$ based device was less than 0.5 V. Devices with an efficiency of 15.4% were reported for $CuInSe_2$ [14].

Copper indium gallium selenide ($CuInGaSe_2$ or CIGS) has the highest efficiency among chalcogenide thin films. Direct band gap of ~ 1.3 eV and high absorption coefficient make it highly suitable as an absorber layer in thin film solar cells. Presence of sodium (Na) in CIGS is very essential for grain growth and grain boundary passivation [10, 11]. A variety of techniques like co-evaporation and homogenization, vacuum deposition, sputter deposition followed by selenization, chemical spray deposition, screen printing and electroplating are available for CIGS deposition. Highest reported efficiency for CIGS solar cells in lab scale is 20.5 % by Solibro and an efficiency of 15.7 % was obtained by 'Miasole' in modular form with an area of 9703 cm^2 [12, 13, 5]. Multiple binary phases, structural and electronic disorders are possible in CIGS thin films; hence sophisticated control is required during the

deposition [7]. Also the limited supplies as well as high costs of indium and Ga are serious issues for CIGS based solar cells.

Copper indium sulphide ($CuInS_2$) thin films are important solar cell materials mainly because of their optimum band gap of 1.5 eV and high absorption coefficient of 10^5 cm^{-1}, both are favorable for efficient light absorption. Moreover, it does not contain poisonous Se. A variety of deposition techniques like vacuum evaporation, sputtering, spray pyrolysis and atomic layer deposition can be successfully used for their deposition. CdS, In_2S_3, $In_x(OH,S)_y$ and ZnS are observed to be suitable buffer layers for $CuInS_2$ thin films. An efficiency of 12.5 % was reported for $CuInS_2$/CdS solar cell [15].

Cu_2S is another well studied absorber layer, mainly for Cu_2S/CdS solar cells. Cu_2S thin films are of particular interest because of their non-toxicity, earth abundance of constituents and simple production possibilities. An efficiency of 9.15 % was reported for Cu_2S/CdS solar cells way back in 1980's [16]. But the diffusion of Cu from Cu_2S to CdS makes these solar cells unstable and Cd in the buffer layer is toxic. These factors hindered the developments of Cu_2S/CdS solar cells.

Materials like $CuZnSnS_4$ (CZTS), CuZnS and Cu_2SnS_3 are some of the recently developed semiconductor chalcogenide materials for solar cell applications. The constituents of these compounds are earth abundant and non-toxic. Moreover simple deposition techniques can be employed for their deposition. An efficiency of around 12 % was already obtained for CZTS based solar cells [17].

1.5.2.3 III-V solar cells

GaAs and InP are the important III-V compound for solar cell applications. These materials possess optical and electrical properties that are highly suitable for an absorber layer in thin film solar cells. Since high purity is

mandatory for these compounds in solar cells, sophisticated and costly techniques like liquid encapsulated Czocharalski method, molecular beam epitaxy, liquid phase epitaxy, and chemical vapour deposition are used for deposition. These compounds are efficient but not cost effective when compared with other semiconductor materials used for thin film solar cells. Due to high power to mass ratio and radiation resistance, solar cells based on these compounds are excellent candidates for space applications. Highest efficiencies for GaAs and InP solar cells are 28.8 % and 22.1 % respectively [18, 19].

1.5.2.4 Amorphous silicon solar cells

Amorphous Si is the most well developed and widely accepted thin film technology to-date. Amorphous Si in thin film form possesses high absorption coefficient (> $10^5 cm^{-1}$) and band gap of 1.5 eV. For efficient light absorption only few microns of this material is required, leading to low material cost for device fabrication. Amorphous Si is usually deposited employing 'plasma enhanced chemical vapor deposition (PECVD)'of silane (SiH_4), over rigid as well as flexible substrates. Low temperature is required for deposition and by products of the techniques are environmentally benign. Due to the flexibility, amorphous Si is good choice for building integrated photovoltaics. Amorphous Si solar cells undergo degradation on exposure to strong sun light, these are not suitable for roof intallation. This is mainly due to light induced breakage of Si-H bonds(Staebler-Wronski effect), leading to enhancement of density of dangling bonds which leads to a degradation in efficiency. An efficiency of 10.1 % is reported for amorphous Si (lab scale) [20].

1.5.2.5 Polymer solar cells

Polymer based solar cell technology offers light weight, mechanically flexible and eco-friendly solar cells through inexpensive fabrication techniques. A variety of simple technologies like roll to roll, spin coating, screen printing, doctor blading, inkjet printing and spray deposition can be used to deposit polymer thin films. As polymer deposition through these techniques are at low temperature, device fabrication over plastic substrates are also possible [21]. In polymer solar cell light absorption and subsequent exciton formation occurs in an active layer which consists of an electron donor and an electron acceptor. These excitons are seperated at the interface of donor and acceptor. The resulting electrons and holes are selectively transported to the metal contacts by selecting suitable electron or hole blocking layers. Generally used materials for polymer photovoltaics are P3HT, MDMO-PPV and PCPDTBT. Low efficiency (~ 10 %) and stability problems due to photochemical degradations are major draw backs of polymer solar cells.

1.5.2.6 Dye sensitized solar cells

In dye sensitized solar cells (DSSC), a dye is the photoactive material that absorb sunlight. Basic element of a DSSC is nanostructured material deposited over transparent conducting oxide (TCO). Nanostructured material usually cosists of nanoparticles of TiO_2. Molecular sensitizers (dye molecules) then get attached to the semiconductor TiO_2 surface for absorbing sunlight. In the next step, a thin layer of iodide electrolyte is deposited over a separate conductive sheet (platinum metal). In the final stage of device fabrication, these two plates are joined and sealed together to prevent the electrolyte from leaking. Sunlight is absorbed by the dye layer and uses their energy to excite electrons, which is rapidly injected to the TiO_2 particles. The electrons flow towards the transparent electrode and later move through the external load. After that, they are re-introduced into the cell by a back metal electrode and

flows into the iodide electrolyte. The electrolyte then transports the electrons back to the dye molecules. In conventional solar cells, semiconductor assume both the task of light absorption and charge carrier transport. But in the case of DSSC, the two functions are separated. Light is absorbed by a dye molecule and the charge separation takes place at the interface between the dye and the semiconductor [22]**.** DSSC are semi-flexible, semi-transparent and simple to make using conventional roll-printing techniques. DSSC, which are the most efficient third generation solar cells, have major draw back of using of liquid electrolyte, which exhibits temperature stability problems. Moreover, the electrolyte is hazardous to human health and the environment. Higher cost of ruthenium dye, platinum catalyst and TCO still stands as major issues. An efficiency of 11.9 % was reported for DSSC (lab level) [23].

1.5.3 Tandem solar cells

Tandem solar cells are fabricated with multiple p-n junctions and each p-n junction responds to different energies in sunlight leading to an efficient absorption of sunlight. Here cells are deposited in the decreasing order of their band gap typically using metalorganic vapour phase epitaxy and the sunlight is illuminated from the sides of cell with higher band gap. Top junction absorbs the high energy photons. The lower-lying junctions then absorb consecutively lower photon energies. The individual junctions must be carefully connected via tunnel contacts [24]. In this way, the main energy loss mechanisms in single junction solar cells can be reduced. Maximum theoretical efficiency of 34 % for traditional single-junction solar cells can be overcome using this concept. Theoretically, infinite number of junctions would have limiting efficiency of 86.8 % under highly concentrated sunlight [25]. Tandem solar cells are now in commercial production (Natcore technology). An efficiency of 37.9 % was reported for InGaP/GaAs/InGaAs tandem solar cells [26]. Higher

'price-to-performance' ratio have limited their wide spread use. They are highly suitable for aerospace where high power-to-weight ratio is desirable. Concentrated photovoltaics (CPV) can be effectively used for these multi junction solar cells as it reduces cost/efficiency ratio. Here lenses and curved mirrors are used to focus sunlight onto multi-junction solar cells.

1.5.4 Hot carrier solar cells

Light generated carriers formed in conventional solar cells by absorbing photons of energy greater than the band gap lose their energy by cooling down from their initial energetic (''hot'') position to the band edges. Optical phonon emissions are also accompanied with this process. Hot carrier solar cells attempt to minimise this loss by extracting carriers at elevated energies in a narrow range. For extracting hot carriers, a substantial delay in carrier cooling in the hot carrier absorber and energy selective carrier extraction by an energy selective contact are essential [27]. At very high illumination intensities, significant reduction in cooling has been observed via a ''phonon bottleneck'' mechanism. This process has been demonstrated to be enhanced in quantum well (QW) nanostructures [28]. Recently, the concept of optical extraction was also developed for hot carrier cells. Optical extraction can be achieved with a layer consisting of silicon dioxide, Si nanocrystals and erbium ions (Er^{3+}). The Si nanocrystals transfer its excess energy to the erbium ions, before it is lost as heat. This leads to the emission of several low-energy infrared photons per absorbed photon, which can produce extra electricity [29]. The limiting value of efficiency for hot carrier cell is 65 % at 1 sun and 85 % at maximum concentration - very close to the limits for infinite number of energy levels. But a more realistic limit of efficiency by considering some real material properties is closer to 50–55 % [30].

1.5.5 Multiple carrier generation in solar cells

In conventional solar cells, high energy photons create just one electron-hole pair, even though their energies are sufficient to produce two or more pairs. Evidence for the creation of more than one pair by high-energy photons is observed in bulk semiconductors like Si, Ge, PbS, PbSe, PbTe and InSb. This is attributed to impact ionization by the photo-excited carriers. Impact ionization in bulk semiconductors is not an efficient process. Threshold photon energy required for impact ionization is many multiples of the threshold absorption energy [31]. In the case of quantum dots, generation of multiple electron-hole pairs from single photon becomes very efficient. Threshold photon energy for this process to generate two electron-hole pairs per photon can approach values as low as twice the threshold energy for absorption [31]. In quantum dot solar cells, the excited electron-hole pairs remain as exciton and this process is called 'multiple exciton generation' (MEG). The performance of nanocrystal based solar cells can be improved using MEG.

1.5.6 Up and down conversion for solar cells

In conventional solar cells, the photons having energy less than the band gap of the absorber are simply transmitted. In up-conversion, two or more these low energy photons are converted into one high energy photon, which has sufficient energy to be absorbed. High energy photons in conventional solar cells lead to thermalisation losses. In down-conversion, these high energy photons, which are inefficiently absorbed by solar cell is converted into two or more lower energy photons. The photons thus generated have sufficient energy to be absorbed by the photovoltaic cell, with negligible thermalisation loss. A significant challenge for up-conversion is that it is a non-linear optical process and a very high intensity of incident light is required to produce only a small intensity of up-converted light. In the solar cell structure, up-conversion layer lies between the photovoltaic material and the back reflector. The down-conversion layer lies on top of the photovoltaic material. It is desirable

that the down-conversion layer must not interact with the light from the sun that is normally absorbed by the device [32]. For up or down conversion of light, nanostructures like quantum dots, luminescent dye molecules, and lanthanide-doped glasses can be employed. These nanostructures are capable of absorbing photons at a particular wavelength and emitting photons at a different (shorter or longer) wavelength [33].

1.5.7 Quantum dot solar cells

A quantum dot is a semiconductor nanostructure that confines the motion of its excitons in all three spatial dimensions. In quantum dot solar cell, quantum dots are the light absorbing photovoltaic material. Bandgap of quantum dots are tunable across a wide range of energy levels by changing size of the dots. Both, expensive molecular beam epitaxy and cost effective wet chemistry processing techniques can be employed for quantum dot preparation. An efficiency of 8.55 % (9.2 % in lab scale) was reported for ZnO/PbS quantum dot solar cells. The performance of this device remains same even after more than 150 days storage in air [34].

1.5.8 Plasmonic solar cells

In plasmonic solar cells, metal nanoparticles are used to improve the light absorption. Generally metal nanoparticles are deposited on the top surface of the thin film solar cell. When light incident on plasmonic solar cells, due to plasmon resonance of metal nanoparticles at the surface, the light is scattered in many different directions. This allows light to travel along the solar cell and bounce between the substrate and the nanoparticles. These processes enabling the plasmonic solar cell to absorb more light [35]. Ag and Au nanoparticles are generally used for plasmonic solar cells.

1.5.9 Intermediate band photovoltaics

In this type of solar cells, an intermediate band (IB) energy level is purposefully introduced in between the valence and conduction bands. Theoretically, due to the presence of this IB, two photons with energy less than the bandgap can excite an electron from the valence band to the conduction band. This enhances the induced photocurrent and thereby efficiency of the device [36, 37]. These are theoretically highly efficient devices but they are hard to make. Intermediate bands are possible in single junction devices by introducing small, homogenous quantum dots in it. By changing the size and shape of quantum dot, the intermediate band can be tuned [38]. Chemical spray pyrolysis (CSP) method can be effectively used for the creation of defect bands and mixed phases (there by double band gap) of absorber material in thin film solar cells. Chapters 4 and 5 deal with the experimental and device fabrication using this idea.

1.6 Chemical spray pyrolysis for thin film deposition

Based on the nature of the deposition process, thin-film deposition methods can be divided into two group viz., physical or chemical. Physical deposition employs mechanical, electromechanical or thermodynamic means to produce a thin film of solid. Physical vapor deposition (PVD), molecular beam epitaxy (MBE), laser ablation and sputtering are the major physical deposition methods. In chemical methods of thin film deposition, fluid precursor undergoes a chemical change at a solid surface, leaving a solid layer. Chemical methods can be divided in to two i.e., gas-phase deposition methods and solution techniques. Important gas-phase deposition methods are chemical vapor deposition (CVD) and atomic layer epitaxy (ALE). In sol-gel, CSP, spin and dip-coating methods, precursor solutions are employed for thin film deposition [39]. Simplicity and inexpensiveness are the main advantages of solution based chemical techniques and they have been studied extensively for

the preparation of varieties of thin films. Another important aspect of solution based techniques is that they facilitate materials to be designed on a molecular level [40]. Among different chemical methods, CSP proved to be a suitable method for the deposition of large-area metal oxide, mixed oxides, spinel oxide, binary and ternary chalcogenides and super conducting compounds [41]. The process is already widely applied and is attractive for the deposition of low-cost thin film solar cells, sensor applications, anodes for lithium-ion batteries and optoelectronic devices [42]. In spray pyrolysis technique, a precursor solution containing soluble salts of the desired compound is sprayed using an atomizer on to preheated substrate. On reaching the hot substrate the droplets of precursor solution under goes a pyrolytic (endothermic) decomposition and the constituents react to form a chemical compound. The precursor solutions are prepared such that the products other than the desired compound are volatile at the temperature of deposition. The volatile by-products and solvents escape in the vapor phase. Typical spray pyrolysis equipment consists of an atomizer, atomizer control mechanism, precursor solution and its dispensing mechanism, substrate heater and temperature controller.

CSP offers many advantages over other thin film deposition techniques.

1) CSP represents a very simple, versatile, vacuum free, industrially viable, cost-effective (especially with regard to equipment costs) technique which is extremely easy technique for preparing dense and porous films of any composition on any area.

2) Deposition rate and hence the thickness of the films can be controlled easily over a wide range therefore eliminating the main drawbacks of chemical methods like sol-gel technique that produces films of restricted thickness. Even multilayered films can be easily prepared using this versatile technique.

3) Doping is extremely easy in CSP; it can be done just by adding the required proportion of dopant in the precursor solution. By changing composition of the spray solution during the spray process, even thin films having composition gradients throughout the thickness can be deposited.

4) A variety of substrates in any dimension and surface profile can be utilized in CSP as it operates at moderate temperatures (100 - 500 °C).

5) Solvent can be simple like water or alcohol which are very eco-friendly.

6) CSP does not require high-quality substrates or chemicals. Variety of chemicals can be used for a particular thin film deposition.

7) CSP is suited for large area deposition which offers industrial production of cost effective thin film solar cells.

1.6.1 Different steps involved in CSP

Various steps involved in spray pyrolysis are atomization of the precursor solution, aerosol transportation to the substrate and decomposition of the precursor (most probably on surface of substrate) to initiate film growth. Each step is very crucial in CSP and the properties of the deposited films can be easily tailored by optimizing various factors involved in each steps.

1.6.1.1 Atomization of precursor solution

Atomization is the first step in spray pyrolysis that involves the formation of fine droplets of precursor solution and send them, with some initial velocity, towards the substrate surface. CSP generally uses air blast,

ultrasonic and electrostatic techniques for atomization. In air blast type atomizer, fluid emerging from a nozzle at low speed is made to 'meet' a high speed stream of air (carrier gas). Friction between the liquid and air accelerates and disrupts the fluid stream leading to atomization. Here pressure of carrier gas is the energy source of atomization [43]. For ultrasonic atomization, the precursor solutions are vapourized with an ultrasonic nebulizer which is operated at a particular frequency (generally 2.56 MHz). The vapor generated is transported by the carrier gas through a pipe to the heated substrate [40]. In electrostatic atomization, precursor solution is exposed to a high electric field, which causes the atomization. Droplet size distribution, rate of atomization and initial velocity of the droplets are different for each type of atomizers. It is very important to understand basic atomization process of the device used. Selection of atomizer depends on the application of thin films to be prepared, liquid properties and operating conditions [39].

1.6.1.2 Aerosol transportation

The aerosol formed after the atomization is transported to the hot substrate. During this transportation there are four forces simultaneously acting on it, describing its path. The forces are gravitational, electrical, thermophoretic and the Stokes force. Gravitational force on a droplet depends on its mass and pulls the droplet downwards. Here the droplet transport is driven by the gravitational force and the initial velocity. This process do not has contribution from an electrical force. For ultrasonic and electrostatic atomizer, electrical force is the main component which drives the droplets downwards. Generally, the electrical force acting on a droplet is several orders of magnitude larger than the gravitational force. When the droplet travels through the air, Stokes force comes into play as the droplet experience a drag due to air resistance. As Stokes force is proportional to the

droplets velocity and size, large droplets which move with high velocity will experience the largest retarding force [42].

As the droplets of precursor solution move towards the hot substrate, thermophoretic force comes into play. Gas molecules from the hotter side of the droplet rebound with higher kinetic energy than those from the cooler side. Thus thermophoretic force pushes the droplets away from a hot surface [39]. Studies showed that thermophoretic force has no effect on the droplet movement when it is more than several (~ 5-7) mm away from the hot substrate. However, below this limit, thermophoretic force begins to dominate due to high thermal gradient. In pressure spray deposition systems gravitational force is the main driving force. As a result, thermophoretic force has significant influence here. But in electric spray deposition systems, electric force is often stronger than thermophoretic force [42].

During transportation towards the hot substrate, droplets experience evaporation of the solvent and a concentration gradient is developed within the droplet. When the surface concentration of the droplets exceeds the solubility limit, the precursor precipitates on the surface of the droplet. Rapid solvent evaporation and slow solute diffusion leads to this precipitation. As a result of these processes, droplets are converted to a porous crust and subsequently hollow particles, which are not desired because they increase the film roughness. In CSP, it is desired that most droplets fly to the substrate without forming particles [39].

1.6.1.3 Precursor decomposition

In CSP, the decomposition of precursor depends on the substrate temperature. At lowest substrate temperature, the droplet from atomizer splashes onto the substrate and decomposes. This process leads to rough or

non-adherent films. At higher temperatures, the solvent evaporates completely from the droplets during its flight from atomizer to the substrate. Finally dry precipitate hits the substrate and decomposition occurs. At even higher temperatures, this solid precipitate melts and vaporizes without decomposition and the vapor diffuses to the substrate to undergo a chemical vapor deposition (CVD) process [39]. It involves the diffusion of reactant molecule to the substrate surface and its adsorption, surface diffusion and a chemical reaction, incorporating the reactant into the lattice, desorption and diffusion of the product molecules from the surface [42]. This CVD-like deposition is desired to yield dense, high quality films but it rarely occur in most spray pyrolysis depositions. This is because either the deposition temperature is too low for the vaporization of a precursor or the precursor salt decomposes without melting and vaporization. At the highest temperatures, the precursor vaporizes before it reaches the substrate, and solid particles are deposited on the substrate as result of the chemical reaction in the vapor phase [39]. This process also leads to rough or non-adherent films.

1.7 Factors affecting CSP

Important factors that can affect nature of thin films deposited by CSP are composition of precursor solution, substrate temperature, spray rate of the precursor solution, deposition time, nozzle to substrate distance and pressure of carrier gas.

Composition of precursor solution: For spray pyrolysis, precursor solution is generally prepared by dissolving inexpensive metal salts like metal nitrate, chloride, acetate or sulfate in solvents like water or alcohol. Physical and chemical properties of the precursor solution have strong dependence on solvent, type of salt, concentration of salt and additives [39]. Nature of solvent

used in precursor solution determines its boiling point, solubility of salts and spreading behavior of droplets on the substrate. The salt must be easily available, non-toxic and should possess high solubility, which increases the yield of the process. Because of the possible by-reactions such as hydrolysis, polycondensation, etc. between the precursors, special care is required in handling the precursor solution. These by-reactions leading to solubility problems and phase segregation and the different components precipitate close to the working conditions [44].

Substrate temperature: Substrate surface temperature is the most important parameter in CSP that determines film morphology, electrical and optical properties. Except aerosol generation, deposition temperature plays vital role in all other thin film deposition steps in CSP. The properties of deposited films can be effectively manipulated by changing the deposition temperature. As substrate temperature increases, the film morphology can change from a cracked to a porous microstructure [39].

Spray rate: As spray rate increases, quantity of solution hitting the substrate surface in unit time increases which decreases the substrate temperature from a pre-set value. Since the drastic variation in spray rate affects the substrate temperature, spray rate can be a critical parameter in CSP. It was observed that by spraying same volume of precursor solution at different spray rates, thicknesses of the deposited films are increasing by increasing the spray rate. This may be due to re-evaporation in presence of higher temperature at lower spray rate.

Deposition time: In CSP, as deposition time increases, thickness of the deposited films increases. Thin films of many materials get peeled off as deposition time increases beyond a limit.

Nozzle to substrate distance: The sprayed droplets come out of the nozzle at a particular spraying angle. As substrate–nozzle distance decreases, the coverage of spray over the substrate decreases. Smaller is the distance of atomizer to the substrate higher the deposition rate. This also makes the coated area smaller.

***Pressure of carrier gas*:** In pressure spray deposition systems, pressure of carrier gas can manipulate the droplet size of the sprayed precursor solution. Generally as the pressure of carrier gas increases, droplet size decreases.

1.8 CSP deposition for the present study

An automated chemical spray pyrolysis machine was employed for thin film deposition in this study (Figure 1.4) [45]. The essential parts of this unit are

a) Atomizer and its controlling mechanism – An air blast type atomization was made possible using a surgical needle and ordinary compressed air. The atomizer is connected to a microprocessor so that it is made to move over the entire substrate surface to get uniform coverage over the substrate.

b) Substrate heater – The required temperature for the substrate is provided by a heater using which temperature can be varied from room temperature to 773 K. The heater can provide uniform temperature over an area of ~ 50 cm^2 and the temperature is measured using a K-type thermocouple attached with the heater. Temperature controller with feedback circuit was used for providing constant substrate temperature during the spray.

c) Solution dispenser – A container, made up of teflon, having motor controlled piston was used for dispensing precursor solution in to the

atomizer. The rotation of motor and hence the spray rate is controlled by the microprocessor.

d) Air compressor and gas controller – Atmospheric air was compressed using an air compressor (1HP, storage capacity = 45 litre). The pressure of air from the compressor to the atomizer is controlled and measured by a mechanical gauge.

Figure. 1.4 Photograph of the automated CSP machine for the present study.

1.9 Review on $CuInS_2$ and Cu_2S thin films

1.9.1 Deposition of $CuInS_2$ thin films

A variety of physical and chemical methods are available for the deposition of $CuInS_2$ thin films. Evaporation techniques are the most common deposition techniques for $CuInS_2$ thin films which yield good quality films. Scheer et al. reported deposition of $CuInS_2$ by co- evaporation on borosilicate glass substrate. Surface composition of the films is investigated by employing X-ray and ultraviolet photoelectron spectroscopy. A comparison of the front

and back surface, i.e., the interface between the Cu–In–S film and the Mo back contact, is done for films with different stoichiometry. Indium-rich films are covered at both surfaces by an indium-rich second phase, viz., $CuIn_3S_5$. The front surface of Cu-rich films shows aggregation of CuS and it was not found at the back surface [46]. The in-situ doping of N, P, Sn as well as the impact of these elements on electrical properties of co-evaporated $CuInS_2$ thin films was studied. On doping with Sn, n-type conductivity was not observed in $CuInS_2$. Phosphorous incorporation was possible only in the presence of Sn atoms (co-doping). Also Na, P co-doping leads to a decrease in conductivity of $CuInS_2$ films. It was observed that conductivity of the films decrease with increasing nitrogen concentration [47].

Two source evaporation (Cu and In) followed by a three source evaporation (Cu, In, and NaF) produced Na doped Cu-In precursor films having different Na concentrations. Sulfurization was performed immediately at the same evaporation chamber to form CIS thin films. The (112) preferred orientation in $CuInS_2$ was enhanced by the addition of Na but the grain sizes of the CIS films decreased with Na doping. It was observed that Na is distributed homogeneously in the deposited films. Also resistivity of the films decreased with Na doping. The phase transformation from $CuInS_2$–CuAu structure to $CuInS_2$–chalcopyrite structure was not altered during sulfurization even though Na is incorporated in the films [48]. Photoelectron spectroscopy studies on evaporated $CuInS_2$ shows that the Fermi level position is varying from $E_f - E_v$ = l.3 eV for In-rich to $E_f - E_v$ = 0.0 eV for the Cu-rich films [49]. The surfaces of evaporated $CuInS_2$ films were also investigated with the help of X-ray photoelectron spectroscopy (XPS). Surface properties of $CuInS_2$ films are highly sensitive to alterations in the bulk stoichiometry. For slightly indium rich films an enrichment of indium and depletion of Cu occur at the surface. Surface composition of these films corresponds to the stoichiometry of

$CuIn_3S_5$. Cu-rich films exhibit segregation of a CuS phase as indicated by an additional Cu-Auger structure in XPS analysis [50].

Hwang et al. reported deposition of single phase $CuInS_2$ thin films employing flash evaporation. Deposited films are analyzed using X-ray diffraction and atomic absorption studies. Source temperature was found to be the dominant factor for the formation of single phase $CuInS_2$ thin films. Flash deposition conditions are derived and they concluded that it would be very difficult to prepare single phase $CuInS_2$ thin films through flash evaporation [51]. Agarwal et al. reported the formation of single phase, n-type $CuInS_2$ thin films of thickness between 60 nm and 650 nm with the chalcopyrite structure on NaCI and glass substrates by flash evaporation. Influence of substrate temperature on the properties of the films were investigated and it was observed that molybdenum source temperature of 1873 K and a substrate temperature of 523 K were the upper limits for obtaining reproducible results and single phase n-type $CuInS_2$ thin films [52].

Abaab et al. reported the deposition of $CuInS_2$ thin films (single source vacuum thermal evaporation method) on substrates submitted to longitudinal thermal gradient. Cu, In and S elements having 99.999 % purity were used to prepare the initial ingot of $CuInS_2$. Some of these films were sulfurized to obtain homogenous $CuInS_2$ thin films. As-deposited and sulfurized films were characterized using X-ray diffraction, optical transmission and reflection measurements. As deposited $CuInS_2$ films deposited contain Cu_7In_4 and In aggregates. On annealing in S atmosphere, these secondary phases were converted into $CuInS_2$. After annealing in S atmosphere, film surfaces are covered by a segregated Cu_xS (x = 1.96 and 2) phase and optical band gap of these films were 1.50 eV which is the optimum value for photovoltaic energy conversion [53]. Glancing angle deposition (GLAD) was used for depositing

$CuInS_2$ films with highly orientated microstructure composed of slanted columns. In absence of the substrate rotation, as the incident angle was increased, nanocolumns are progressively inclined towards the evaporation source. When the substrate is rotated at an angle of 80 ° during film deposition, the nanocolumns become wire forms only for elevated rotational speeds. It was observed that island formation in the film was enhanced due to shadowing effect, introduces preferential growth on taller surface heights [54]. Rabeh et al. investigated the effect of post-growth treatments in air atmosphere on structural, morphological, optical and electrical properties of $CuInS_2$ thin films prepared employing vacuum thermal evaporation on non-heated glass substrates. It was observed that on annealing at temperature above 200 °C, the n-type conductivity is stable. The band gaps of the samples after annealing are in the range of 1.45–1.50 eV [55].

The effect of bismuth doping in $CuInS_2$ thin films prepared using single-source thermal evaporation method was investigated by Akaki et al.. Bi atoms enhances the growth of $CuInS_2$ single phase at lower temperature and the crystalline quality of doped films was higher compared with the non-doped ones [56]. Zribi et al. investigated the post-growth annealing treatment effects on properties of Na-doped $CuInS_2$ thin films grown by double source thermal evaporation method. Vacuum annealing was performed on the films from 250 to 500 °C. On annealing above 350 °C, traces of Cu and In_6S_7 in the films disappear. Good quality $CuInS_2$: Na 0.3 % films were obtained on annealing at 500 °C. The absorption coefficient of Na-doped $CuInS_2$ thin films reached 1.5 x 10^5 cm^{-1}. Band gap of the doped samples annealed in the temperatures from 250 to 500 °C was in the range 0.038–0.105 eV [57]. Rabeh et al. studied structural, optical and electrical properties of undoped and Sb-doped $CuInS_2$ thin films grown by single source thermal evaporation method on corning glass substrates heated at 100 °C. Quantity of the Sb source was determined to be in

the range 0-4 wt % molecular weight compared with the $CuInS_2$ alloy source. Effect of annealing atmospheres on the properties of the films was studied. Sb doped $CuInS_2$ possess relatively high absorption coefficient between 2 x 10^4 $cm^{-1}$and 10^5 cm^{-1} in the visible and near-IR spectral range. Sb-doped $CuInS_2$ thin films exhibit p-type conductivity and air annealing resulted n-type conductivity [58]. Structural and optical properties of non-doped and Sn-doped $CuInS_2$ thin films grown by using double source thermal evaporation method were studied by Rabeh et al.. Vacuum annealing was performed on these films at a temperature of 250 °C. After annealing polycrystalline $CuInS_2$ films were obtained and no Sn binary or ternary phases were observed for the deposition time of Sn (by evaporation from a thermal evaporator) less or equal to 5 min. The band gap of Sn-doped samples after annealing was in the range 1.45–1.49 eV and they exhibited n-type conductivity after annealing [59]. Zn-doping was also performed in $CuInS_2$ thin films grown with the help of double source thermal evaporation method. Vacuum annealing was performed on these films at 260 °C for 2 hours. The Zn-doped samples had band gap energy of 1.46-1.58 eV and they exhibited p-type conductivity. Zn species can be considered as suitable candidates, for use as doped acceptors to make $CuInS_2$-based solar cells [60].

Three- source evaporation technique is employed for depositing good quality $CuInS_2$ thin films. Both p and n-type films were prepared. By replacing sulphur source by an H_2S gas source equipped with mass flow control helped to improve the sulphur deposition further, which is regarded as the most critical factor in the stoichiometry control. Resistivity of the films was between 0.01 and 10 Ω.cm and the grain size was between 2 and 8 μm. Electron mobility (21.84 $cm^2V^{-1}s^{-1}$) and hole mobility (1.42 $cm^2V^{-1}s^{-1}$) of these samples are higher than those reported for samples prepared with other methods [61]. $CuInS_2$ thin films were also deposited using MBE type evaporation of the

elements on (100) Si and glass substrates. This three-stage source combines excellent focusing characteristics with the option of thermally cracking large sulphur molecules. Crystal quality of the films can be improved by depositing on heated substrates but these films show a pronounced island formation [62].

Guillen et al. prepared $CuInS_2$ thin films by 'rapid thermal annealing' at 350 °C. Binary sulfide precursors evaporated at a substrate temperature lower than 200 °C were compared with $CuInS_2$ layers prepared directly by evaporation on to 350 °C heated substrates. X-ray Diffraction (XRD) and XPS measurements on these films showed similar structure and chemical characteristics. Some morphological variations are observed in atomic force microscopy analyses of the two samples. Differences in the optical absorption for these samples can be co-related with atomic force microscopy (AFM) analyses. Fermi level for both samples were a little below the middle of the gap, as corresponds to almost ideal composition [63]. Akaki et al. annealed evaporated $CuInS_2$ films in H_2S atmosphere from 250 to 500 °C for 60 min. It was observed that all the films annealed above 350 °C were of $CuInS_2$ single phase, regardless of the Cu/In ratio of the source material. Carrier concentration, resistivity and carrier mobility of these films (Cu/In ratio-1.5) were approximately 1 x 10^{21} cm^{-3}, 0.1 Ω.cm and 0.1 cm^2/Vs respectively at room temperature. By using source material having Cu/In ratio 1.5, the films are Cu-rich and Cu/In ratio was 1.37 in the sample. Cu rich films i.e., Cu/In ratio of 1.5 shows larger grain size and roughness than those of the films prepared from the Cu/In ratio of 1.0 [64]. Neisser et al. studied effect of Ga incorporation in sequentially prepared $CuInS_2$ thin films. Thin films of $CuInS_2$: Ga was prepared by sequential evaporation of Cu-In-Ga precursors and sulfurization in sulfur vapor. The resulting compound was $CuGa_xIn_{1-x}S_2$, depending on overall Ga content and sulfurization temperature. This quaternary compound formed exhibited a change in absorber lattice constant

and band gap. Open-circuit voltages well above 800 mV and fill factor of 71 % could be achieved by using this absorber layer [65]. Akkari et al. used oblique angle deposition technique for depositing $CuInS_2$ films onto substrates submitted to a thermal gradient. Resulting films showed an improvement in the optical properties i.e., high absorption coefficient (10^5 – 3 x 10^5 cm^{-1}) in the visible range and near-IR spectral range. SEM analysis proved that the films had microstructure with columns that were progressively inclined as the incident angle was increased [66]. Akaki et al. doped Sb in $CuInS_2$ thin films grown by single source thermal evaporation method. The films were annealed from 100 to 500 °C in air after the evaporation. Polycrystalline films were formed on annealing Sb doped $CuInS_2$ films above 200 °C with band gap energy of 1.43–1.50 eV. Sb-doped $CuInS_2$ thin films are close to stoichiometry in comparison with undoped $CuInS_2$ thin films [67].

He et al. deposited $CuInS_2$ films on float glass substrates by a reactive radio frequency sputter process using Cu–In inlay target (Cu metal disc inlayed by indium) and H_2S gas in one step. The In/Cu ratio in films was much less than one although its ratio was nearly one in the target. Different sputter yield of indium and Cu, the presence of an additional layer covering the surface of the In inlay due to the reaction of H_2S and In inlay during sputtering are responsible for this. The sputtered film consisted of CuS, Cu_2S, and $CuInS_2$ phases. Hole concentration of the 'as deposited' Cu-rich 'CIS' films range between 3.55 x 10^{17} cm^{-3} and 1.58 x 10^{19} cm^{-3}, for temperatures between 77 and 350 K. Carrier concentration in the films could be tuned from 10^{19} to 10^{17} cm^{-3} by using Cu–In alloy target [68]. He et al. also reported the deposition of high quality $CuInS_2$ films with a fixed radio frequency power of 200 W on bare float glass substrates at a substrate temperature of 400 °C or above. H_2S flow was in the range of 20–30 sccm. As-sputtered films are highly (112) oriented with rougher surface, mainly due to incoherent top layer of Cu_xS precipitate.

The as-grown films sputtered at 500 °C have an optical bandgap of 1.44 eV. Resistivity, carrier concentration, Hall mobility of the films sputtered at 400 °C are approximately 2 x 10^3 –10 ^{4} Ω.cm, 3 x 10^{14} –10^{15} cm^{-3} and 2–20 cm^2/V s respectively [69].

Cayzac et al. reported deposition of crystalline chalcopyrite $CuInS_2$ thin films employing RF sputtering at room temperature using crystalline $CuInS_2$ target. The process does not involve any subsequent toxic gas, chemical or heat treatment. XRD studies indicated that until a critical thickness is reached the films are amorphous in nature and after that, they transform into crystalline chalcopyrite films with preferential (112) orientation with average grain size of 25–100 nm. At low deposition rates, smooth films were obtained. As the deposition rates increased by increasing RF power, rougher films covered with surface particles were formed. In order to avoid In_2S_3 and Cu_2S phases in the deposited films, the target preparation is essential. Hall measurements showed that the films were p-type with bulk carrier density about $10^{18}/cm^3$ [70]. Seeger et al. deposited good quality $CuInS_2$ absorber layers through reactive magnetron sputtering process from copper and indium targets in Ar/H_2S sputtering atmosphere. The intrinsic electronic quality of the films was excellent, allowing the preparation of $CuInS_2$ cells with efficiency of 11.4 % and open circuit voltage of 745 mV. However the reproducibility of the device is low. Deposition rate from the indium target decreased by about a factor of two, while that from the copper target only by about 20 %. This decreasing content of indium in the first deposition step lead to an open, 'porous' $CuInS_2$ film morphology which was responsible for shunting problems between back and front contact of the solar cell. For stable $CuInS_2$ film deposition process an in-situ control of the Cu/In ratio and the film morphology is advisable [71]. Liu et al. reported preparation of $CuInS_2$ films with the help of reactive sputtering together with vacuum rapid annealing. These films consisted of single

chalcopyrite phase with preferential crystalline orientation along (112). EDAX measurements showed the constituent ratio [Cu+In]/[S] and [Cu]/[Cu+In] of about 1 and 0.5 respectively. Fourier transform infrared spectrometer analysis revealed that all $CuInS_2$ films had good homogeneity in shape and size of the grains and in distribution of constituent and defects. The deposition method followed in this study is beneficial to promote genuine realization of the large-scale production of the ultra-high efficiency Cu-III-VI_2 thin film solar cells [72].

Ogawa et al. prepared chalcopyrite $CuInS_2$ by sulfurization of a layered metallic precursor at 550 °C in argon containing H_2S. The Cu/In ratio in the film was varied from 0.8 to 1.85. It was observed that the resistivity of the film decreased by aging in air and it can be attributed to gas absorption in the film which gives rise to an increase in the hole mobility. Also resistivity of the films increased by annealing in vacuum or in air and it is due to gas desorption. The hole concentration of the films was independent of aging and was in the order of 10^{20} cm^{-3}. The article discussed electrical conduction in the thin film in terms of hole transport crossing over an inter-granular potential barrier in the polycrystalline film [73]. Wada et al. developed a two-stage process for $CuInS_2$ deposition which comprised of a first process by which Cu-In-O films are prepared from $Cu_2In_2O_5$ target by pulsed laser deposition. The prepared Cu-In-O films were transformed into $CuInS_2$ films by applying an annealing in a H_2S gas. On annealing the films at a temperature higher than 400 °C, chalcopyrite $CuInS_2$ is obtained. This process is applicable to prepare $CuInSe_2$ thin films also by annealing Cu-In-O film in H_2Se atmosphere [74]. Antony et al. reported the deposition of single-phase $CuInS_2$ thin films with chalcopyrite structure by the two-stage processes which involved the preparation of $Cu_{11}In_9$ alloy by annealing the evaporated copper and indium bilayers followed by the sulphurisation. Sulphurisation temperature was optimized as 350 °C for three hours, which resulted in single-phase p-type chalcopyrite $CuInS_2$ films with a

band gap of 1.45 eV. These films were ideal for the application as absorber layer in solar cells [75].

Solvothermal route was also employed for the deposition of $CuInS_2$ thin films in ethylene glycol under the open-air condition. Copper chloride, indium chloride and thiourea were the starting materials. It was observed that the products were significantly affected by the reaction time, temperature and the diffusion of the reactors [76]. Tang et al. developed an in-situ growth strategy for preparing $CuInS_2$ films by solvothermally treating flexible Cu foil in an ethylene glycol solution containing $InCl_3.4H_2O$ and thioacetamide with a concentration ratio of 1:2. Higher solvothermal temperature is favorable for the growth of CIS films with higher crystallinity. Morphology of the deposited films was controlled by the reactant concentration. If $InCl_3.4H_2O$ concentration is relatively low ($\leq$ 0.042 M), single-layered CIS films composed of high ordered potato chips shaped nanosheets were formed; otherwise, it preferred to form a double layered film, for which the lower layer was similar to CIS ordered nanosheets while the upper layer was composed of flower shaped superstructures. All these CIS films possessed direct bandgap energy of 1.48 eV. Single-layered CIS films on Cu foil were employed for fabricating flexible solar cells with a structure of Cu foil/$CuInS_2$/CdS/i–ZnO/ITO/Ni–Al, which showed power conversion efficiency of 0.75 % [77].

Lee et al. employed sol–gel spin-coating method for depositing chalcopyrite $CuInS_2$ thin films, using copper acetate monohydrate ($Cu(CH_3COO)_2 \cdot H_2O$), dissolved in 2-propanol, and indium acetate ($In(CH_3COO)_3$) in 1-propanol. The two solutions were mixed to form the starting solution. Solution was dropped onto glass substrate, rotated at 1500 rpm and dried at 300 °C for Cu–In as-grown films. In the next step, the films were sulfurized inside a graphite container box. Raman spectra measurement confirmed that Cu–S or In–S compounds were not formed in the thin films [78].

Shi et al. reported deposition chalcopyrite $CuInS_2$ ternary films using successive ionic layer adsorption and reaction (SILAR) method on glass substrates at room temperature and heat-treated under Ar atmosphere at 500 °C for 1 h. Solution containing mixture of $CuCl_2$ and $InCl_3$ with different ionic ratios ([Cu]/[In]) were used as cation precursor and Na_2S as the anion precursor. Stoichiometric $CuInS_2$film was obtained by adjusting [Cu]/[In] ratios in solution. Nearly stoichiometric composition of CIS films was obtained from the solution with the [Cu]/[In] range from 1 to 1.25, while [S^{2-}] concentration kept at 0.05 mol/L and they possess a band gap of 1.45 eV. Resistivity of these films decreased with increase of [Cu]/[In] ratios. As the [Cu]/[In] increased from 1 to 2, the films showed wide range of resistivity down from 80.5 to 3.4 x 10^{-3} Ω.cm. This is due to the formation of high conductivity $Cu_{2-x}S$ phase in the grains [79]. Shi et al. also investigated the effect of hydrothermal annealing (at 200 °C) in Na_2S solution on $CuInS_2$ thin films deposited by SILAR method. Well-crystallized $CuInS_2$ films could be obtained after annealing in 0.1 mol/L Na_2S solution for 1.5 h. Annealing was carried out in a sealed teflon-lined autoclave. Sulfur rich films resulted after annealing and they showed direct band gap varied from 1.32 to 1.58 eV as the annealing time increased from 0.5 h to 2 h [80].

Penndorf et al. developed a new technique, "CISCuT", for the preparation of polycrystalline single-phase $CuInS_2$ thin films for solar applications in a continuous roll-to-roll process. In the first step, a copper tape is electrochemically plated with an indium layer. In the second step, this tape was made to undergo a rapid sulfurization process at a temperature (600 °C) and at an atmospheric pressure to form $CuInS_2$ thin films. Solar cells fabricated from this material showed efficiencies around 6 %. This low cost, continuous growth process without any vacuum set up is possibly a way to make solar cell and module production competitive with conventional energy generation [81].

Winkler et al. reported a consistent view of the compositional depth profile and phase content of CISCuT films produced under special conditions. $Cu_{2-x}S$ phase was removed by KCN etching. The $CuInS_2$ and $CuIn_5S_8$ layers in the films were under compressive and tensile stress respectively. Oxygen was observed to be a major contamination in the films [82].

Podder et al. reported deposition of $CuInS_2$ thin films on ITO glass substrate by a two-step process using a simple, low-cost, photochemical deposition and subsequent annealing. For InS thin films aqueous solution of $In_2(SO_4)_3$ and $Na_2S_2O_3$ were used. Cu_xS films were deposited on the InS films from $CuSO_4$ and $Na_2S_2O_3$ and the films were annealed at 300 °C for 30 min. Inter diffusion of Cu and In occurs during the annealing. Composition of the annealed films was determined by the deposition time of the binary layers. By optimizing the conditions, nearly stoichiometric CIS with band gap energy of about 2.2–2.3 eV was obtained [83].

'Paste coating' method was also reported for $CuInS_2$ absorber layers. Precursor powders i.e., $CuInS_2$ and CuS were synthesized by a solvothermal method. Ethyl cellulose and phosphate ester were used respectively as a resin and a dispersant and dihydroterpineol was used as solvent to dilute these. Screen printing method was used to distribute the paste on Mo-coated soda–lime glass substrate. It was difficult to obtain the densification of the CuS-doped $CuInS_2$ layer with only sulfurization. On introducing oxidation process before sulfurization led to quite dense $CuInS_2$ layer. On oxidation the chalcopyrite phase nearly broke down but the phase was restructured with the sulfurization [84].

Metzner et al. epitaxially grew $CuInS_2$ films with typical thickness of 100 nm on sulphur-terminated Si wafers of (001) and (111) orientation and on single-crystalline CaF_2 substrates using three-source molecular beam epitaxy

(MBE). Transmission electron microscopy (TEM) analyses shows that, metastable Cu-Au ordering on the cation sub lattice was found to be the dominating structure in the films deposited on Si (001) at medium temperature (300 °C). Electronic states deep in the $CuInS_2$ bandgap can be successfully removed by post deposition treatments in hydrogen and air at elevated temperatures up to 400 °C. Excess indium in the films leads to the formation of In_2S_3 and $CuIn_5S_8$ as minor phases. CuS segregates were formed at the surface of Cu-rich samples and could be removed by etching [85].

Qiu et al. deposited $CuInS_2$ thin films by 'ion layer gas reaction' (ILGAR) method using C_2H_5OH as solvent, CuCl and $InCl_3$ as reagents and H_2S gas as sulfuration source. The chalcopyrite $CuInS_2$ with near stoichiometry can be deposited with $[In^{3+}] \leq 0.05M$ and $[Cu^{+}] \leq 0.078M$. Further increase in cationic concentration resulted in Cu_xS segregation phase. $CuInS_2$ thin film deposited from lower cationic concentration was uniform, compact and good in adhesion to the substrates. With the increase in precursor concentrations the optical band gap decreased (1.40-1.30 eV) slightly along with dark resistivity (50 to 10 Ω.cm). The carrier concentration and hall mobility increased as the mixing precursor concentration increased [86]. Das et al. also reported the deposition of nanostructured $CuInS_2$ thin films using ILGAR process. Cu and In precursors were deposited on glass substrate through coating technique and annealed in H_2S atmosphere at different temperatures [87]. Camus et al. prepared $CuInS_2$ thin films employing spray ILGAR. Several post deposition treatments were applied to the deposited films. Composition and surface chemistry the ILGAR films were very similar to device grade reference samples prepared through rapid thermal processing [88].

Hou et al. deposited uniform $CuInS_2$ films employing electrostatic spray assisted vapor deposition (ESAVD) method. Copper nitrate and indium

nitrate salts were dissolved into a thiourea-based water/alcohol solution is the precursor solution. Film showed chalcopyrite crystalline structure with preferred (112) orientation. Depending on the precursor composition and processing parameters, bandgap varied from 1.40 to 1.49 eV. CdS/$CuInS_2$ heterojunction was also produced on an ITO glass substrate having good photovoltaic response [89].

Yukawa et al. prepared $CuInS_2$ thin films with the help of electrodeposition without usual heat treatment in H_2S atmosphere. Acidic aqueous solution containing $CuSO_4$, $In_2(SO_4)_3$and $Na_2S_2O_3$ at -0.9 V vs Ag/AgCI for 300-1200 s was used for film deposition. Single phase $CuInS_2$ films were obtained at pH about 1.5 by the proper adjustment of the Cu^{2+}/In^{3+} ratio, with the concentration of $Na_2S_2O_3$ fixed at 400 mM. Well-crystallized films were obtained by annealing in vacuum at 673 K. Films prepared were non-stoichiometric with tetragonal chalcopyrite type structure. Conduction type changed from p to n in the indium-rich region [90]. Asenjo et al. also reported $CuInS_2$ preparation by one-step electrodeposition using the same precursors. Electrochemical quartz crystal microbalance (EQCM) was used to study the growth of $CuInS_2$ films [91]. Martinez et al. reported preparation and characterization of Cu–In–S thin films on stainless steel by electrodeposition technique using an electrolytic bath consisting of metal salts dissolved in a buffer solution. Films were annealed in N_2 atmosphere to improve crystallinity. Band gap of the films is close to 1.5 eV [92]. $CuInS_2$ thin films for the application in solar cells were also grown on Ti substrates by electrodeposition and sulphurisation. Composition of the $CuInS_2$ films was mainly determined by the Cu/In atomic ratio of initial Cu–In precursor [93].

Hwang et al. reported growth of $CuInS_2$ layers on GaP substrates by the metalorganic chemical vapor deposition (MOCVD). Hydrogen sulfide gas

together with the vapors of $CuCl(NCCH_3)_n$ and $InCl_3(NCCH_3)$ were used as transport agents. X-ray analysis confirmed the formation of single phase $CuInS_2$ epitaxial layer on the substrate. Energy dispersive X-ray analysis (EDAX) and Rutherford back scattering (RBS) confirmed the existence of Cu and S in the films [94]. Harris et al. deposited copper indium disulfide films using spray chemical vapor deposition at atmospheric pressure. Temperature for deposition was 390 °C using $[(PPh_3)_2CuIn(SEt)_4]$ as a single source precursor in argon atmosphere. The films exhibited crystallographic gradient, with the leading edge having (220) preferred orientation and the trailing edge having (112) orientation. Films with the best electrical properties were annealed at 600 °C following deposition at 390 °C. It was observed that prolonged exposure of the films to the electrolyte decreased photo response. Solar cells were fabricated with $CuInS_2$ having the structure $Al/ZnO/CdS/CuInS_2/Mo/Glass$ and it showed an efficiency of 0.68 %, for a 0.5 cm^2 cell under simulated AM0 illumination [95].

Djessas et al. deposited copper indium disulfide thin films for photovoltaic applications by close-spaced vapor transport in a vertical reactor closed under vacuum. Solid iodine was used as reagent. Compared to other I-III-VI compounds the stoichiometry temperature range is relatively large: the lower limit (~ 370 °C) corresponds to the formation of CuI in the layers and the upper limit (~ 680 °C) is imposed by the glass substrate. Within this temperature range no phase change was observed. All the layers are p-type, with carrier densities of the order of 10^{16} cm^{-3} [96].

Cui et al. reported the deposition of non-crystalline $CuInS_2$thin films on ITO coated glass by one step chemical bath deposition (CBD) in acidic conditions. For the deposition of $CuInS_2$ thin films, solutions of $CuSO_4$, $InCl_3$ and $Na_3C_6H_5O_7$ were used. With the addition of HCl, pH of the solution was maintained at approximately 3.5–4.5. Deposition temperature was 45 °C and

deposition time was 2 hour. Under continuous stirring thioacetamide was also added in the solution. Polycrystalline $CuInS_2$ films were obtained after sulfuration of the films in sulfur atmosphere at 450 °C for 1.5 h. These films were p-type and the carrier concentration was 1.68 x 10^{16} $cm^{-3}$and band gap was about 1.45 eV [97].

Nanu et al. deposited $CuInS_2$ thin films employing atomic layer deposition (ALD) over glass, TCO glass, and TiO_2 substrates using CuCl, $InCl_3$ and H_2S as reactants. For the deposition, pressure was in the range 2-10 mbar and temperature was between 350 °C and 500 °C. It was observed that composition of the films depended on the length of CuCl pulse. Microstructure and homogeneity of the films improved on increasing reaction temperature. Depending on deposition conditions single phase, Cu-poor and Cu-rich $CuInS_2$ films are formed. Also, no chloride impurity was detected in the films which indicated the complete reaction between the metal chloride and H_2S [98]. Lin et al. employed electrochemical atomic layer deposition (EC-ALD) for depositing $CuInS_2$ on gold substrate at room temperature. Optimum deposition potentials for each element were determined using cyclic voltammetry (CV) technique. Amperometric I–t method was employed to prepare the semiconductor compound. Films had (112) preferred orientation and Cu, In, S are present in an atomic ratio of approximately 1:1:2. Also these films were composed of particles with uniform grain size fell into nano-range. Band gap of this film was 1.50 eV as measured using FT-IR [99].

Chemical spray pyrolysis is already proved to be a simple, low cost chemical deposition technique for device quality $CuInS_2$ thin films. Generally used precursors for $CuInS_2$ deposition contain $CuCl_2$, $InCl_3$ and thiourea [100-102]. Instead of chloride based precursors, deposition of $CuInS_2$ by nitrate based precursors are also reported [103]. Cu/In ratio in the precursor solution and substrate temperature are the two important factors that controls the

structural, optical and electrical properties of $CuInS_2$ thin films [45, 104, 105]. Generally Cu rich films are suitable for photovoltaic applications [106]. Deposition temperature was between 300 to 350 °C for good quality $CuInS_2$ films [102,103]. A variety of substrates like glass, alumina, metal oxide and polymer substrates can be used to deposit $CuInS_2$ by spray pyrolysis [107-110]. Nature of substrate can affect the growth and structure of as deposited films. The crystal structure of $CuInS_2$ films deposited using CSP technique are either sphalerite or chalcopyrite structures and sphalerite structure changes to chalcopyrite on annealing [111]. It was observed that on post deposition annealing of $CuInS_2$ films in H_2S atmosphere, crystallinity and stoichiometry of the films improved. Optical band gap increased and there was an adverse effect on electrical properties of the films [112]. On incorporating Na in sprayed $CuInS_2$ crystallinity, band gap, conductivity and photosensitivity of the films improved. Na_2S can be added in the precursor solution as dopant [113]. Incorporation of Al and Mn in sprayed $CuInS_2$ had also been reported. On Mn doping in sprayed $CuInS_2$ band gap increases [114].

1.9.2 Review on $CuInS_2$ based solar cells

The maximum reported efficiency for $CuInS_2$ based thin film solar cell is 12.5 % by Klaer et al.. Molybdenum was the back contact and $CuInS_2$ absorber was deposited using dc magnetron sputtering and sulphurization. Heterojunctions were then prepared by chemical bath deposition of 50 nm CdS and sputtered transparent conducting ZnO window layer. Aluminium grid was used for contacting and MgF_2 was the antireflection coating over the cell. They observed that solar cell performance decreased only slowly for small deviations of the Cu/In ratio from the optimum value [15]. Goto et al. reported 13 % efficient thin film solar cell by following TCO/CdS/$CuInS_2$/$CuGaS_2$ structure. For absorber layer deposition, vacuum evaporation and sulphurization was employed. Buffer layer was chemical bath deposited CdS

and for TCO, RF sputtered In_2O_3 layer was used. They concluded that the improved characteristics of the cell arise due to high crystallinity and electron barrier of the hetero-structure consisting of $CuInS_2$ absorber layer and thin $CuGaS_2$ base layer [115]. Hengel observed improvement in open circuit voltage (V_{oc} > 800 mV) in $CuInS_2$ thin film solar cells by incorporating Ga in $CuInS_2$. They employed sequential technique for the preparation of $CuInS_2$: Ga/CdS/ZnO cells having efficiency of 11.6 % [116].

Seimer et al. reported 11.4 % total area efficiency (A = 0.5 cm^2) $CuInS_2$ solar cells from rapid thermal process (RTP). They followed glass/Mo/$CuInS_2$/CdS/ZnO cell structure. Vapor pressure of sulfur and its constancy during the process has an important influence on device quality [117]. Braunger et al. reported 11.4 % efficient polycrystalline $CuInS_2$ thin film solar cell having Cd-free buffer layer [$In_x(OH,S)_y$]. $CuInS_2$ was deposited by thermal evaporation. They concluded that the choice of the buffer layer strongly influences the electrical characteristics of the heterojunction through light induced secondary transport paths [118]. $CuInS_2$ thin films, prepared through sulfurization of a metallic precursor, is used to form thin film solar cell with CdS which exhibits efficiency of 10.5 % deposited either on a Pt sheet or a Mo-coated soda lime glass substrate. Adhesion of $CuInS_2$ was significantly improved by introducing very thin Ga layer between the Mo surfaces and stacked Cu/In precursor layer [119]. Scheer et al. reported 10.2 % efficiency for solar cell prepared with copper-rich p-type $CuInS_2$ absorber prepared by thermal co-evaporation. The cell structure was glass/Mo/p-$CuInS_2$/n-CdS/n^+-ZnO/Al. For this configuration copper to indium ratio between 1.0 and 1.8 can be tolerated with small (< 10 %) solar-to-electrical conversion losses [120]. Lewerenz et al. fabricated new heterogeneous poly crystalline n-$CuInS_2$ based semiconductor which has yielded conversion efficiencies of 9.7 % in an electrochemical cell. Origin of the improved efficiency is attributed to impurity

scavenging by In spheres resulting from modified vapour/liquid/solid (VLS) growth process and the influence of the acidic iodine iodide electrolyte on the cell performances [121]. Using spray deposited $CuInS_2/In_2S_3$ heterojunction Teny et al. fabricated 9.5 % solar cell on ITO substrates. Manual spray was used to deposit the cell. They were able to avoid the usual cyanide etching and CdS buffer layer, both toxic, for the fabrication of the cell [101]. Asenjo et al. fabricated $CuInS_2/In_2S_3/ZnO$ type solar cells and the influence of CBD deposited In_2S_3 film properties on the behavior of the device was investigated. Maximum efficiency of 8.6 % was reported. $CuInS_2$ films were grown on Mo substrate through sequential sputtering-evaporation process [122]. Sandino et al. analyzed $Mo/CuInS_2/ZnS$ stacked layers, using high resolution transmission electron microscopy (HRTEM) and used it for the fabrication of solar cells with $Mo/CuInS_2/ZnS/TCO$ structure. $CuInS_2$ was prepared by co-evaporation and efficiencies of 7.8 % and 5.4 % were attained using evaporated and CBD deposited ZnS buffer layers [123]. One dimensional $CuInS_2$–ZnS hetero-structured nanomaterials synthesized by 'seed-assisted' synthetic route were used as the counter electrodes of dye sensitized solar cells. Shapes of hetero-structured nanorods could be tuned from burning torch-like to longer rod-like by varying the concentration of added indium. Dye-sensitized solar cells (DSSCs) using these hetero-structured nanocrystals exhibited power conversion efficiency (7.5 %) superior to DSSCs made with conventional platinum electrode (7.1 %) under the same device configuration [124].

An efficiency of 7% was reported by Goossens et al. for spray deposited $CuInS_2$ solar cells. Here spray deposited TiO_2 was used as the nanoporous electron conductor and sprayed In_2S_3 was the buffer layer. Transient absorption spectroscopy was employed to make an accurate assessment of the fundamental electronic processes that are involved in $CuInS_2$ absorber layer and electronic states in the band gap related to the presence of

anti-site defects. The population lifetime of electrons in deep states was large and these states acted as electron traps rather than recombination centers. Upon irradiation, electrons were stored, leading to space–charge formation. The low open circuit voltage (V_{oc}) of $CuInS_2$ cells as well as the crossover of the current–voltage curves is due to this temporal storage of charge [125]. Luo et al. reported simple aqueous solution route to prepare mercaptoacetic acid attached $CuInS_2$ quantum dots. Using this material, core–shell $CuInS_2$–Mn doped CdS quantum dot sensitized solar cells were assembled and it showed power conversion efficiency of 5.38 % [126].

Okuda et al. reported fabrication of buffer-free $CuInS_2$ solar cells having 5.5 % efficient with transparent conducting $Zn_{1-x}Mg_xO$:Al films. They eliminated CdS buffer layer from typical ZnO:Al/CdS/$CuInS_2$/Mo/glass type solar cells. ZnO:Al was replaced with (Zn,Mg)O:Al layer prepared by co-sputtering ZnO:Al and MgO:Al for conduction band offset matching. The junction quality, deteriorated by sputtering damage during (Zn,Mg)O:Al deposition; this was recovered by post annealing after cell fabrication. Low V_{oc} of as-fabricated cells of 0.25 V was improved to 0.52 V by annealing at 250 °C for 10 min, leading to an improvement in efficiency from 1.9 to 5.5 % [127]. 3D solar cell concept was used by Nanu et al. for fabricating solar cells with TiO_2/$CuInS_2$ nanocomposites with efficiency of 4 %. Here nanometer scale inter penetrating network was formed by infiltrating $CuInS_2$ inside the pores of n-type TiO_2 by atomic layer chemical vapor deposition. Al_2O_3 inter layer was used for suppressing Cu diffusion and In_2S_3 was used as the buffer layer. It was also observed that during deposition process, the stoichiometry of $CuInS_2$ and TiO_2 were modified and the stoichiometry was restored by thermal annealing in sulfur and oxygen [128]. Li et al. reported quantum dot-sensitized solar cell (QDSSC) with 4.2 % efficiency which consisted of TiO_2/$CuInS_2$-QDs/CdS/ZnS photo anode, polysulfide electrolyte, and CuS counter electrode

[129]. $CuInS_2$ deposited by spin coating method was also used to fabricate solar cells with 3.99 % efficiency. Post deposition treatment was also carried out at 250 °C in inert atmosphere [130].

Kazmerski et al. reported $CulnS_2$ thin-film homojunction solar cells having an efficiency of 3.62 %. $CulnS_2$ films were grown employing dual-source deposition technique. Forward dark J-V characteristics indicated that recombination-generation mechanism at the junction dominated device operation. The devices had stability but materials-related problems limited the device performance of this solar cell [131]. Rath et al. fabricated nanocomposite $CuInS_2$/PSiF-DBT solar cells with conversion efficiency of 2.8 %. Spin coating was used for solar cell fabrication [132]. Chang et al. fabricated Cu_2S–$CuInS_2$–ZnSe quantum dot (QD)-sensitized solar cell having efficiency of 2.52 %. $CuInS_2$ sensitizer, Cu_2S buffer layer and ZnSe passivation layer were fabricated through SILAR process. The band edges of the Cu_2S–$CuInS_2$–ZnSe in the QD-sensitized solar cell generated stepwise cascade, which promoted the separation of excited electrons and holes across the interfacial region [133].

Krunks et al. deposited extremely thin absorber layer (ETA) solar cells through spray pyrolysis method. Spray deposited ZnO nanorod layer (ZnO_R) was used for ITO/ZnO_R/'InS'/In_2S_3/$CuInS_2$ solar cells having an efficiency of 2.5 %. In this type of ETA solar cells, p-n junction area is increased very much when comparing with flat structure and this increased short-circuit current density. Preparation technology is simple, fast and operates at low or moderate temperature; hence it could be possible to fabricate efficient solar cells with large area at low cost using this structure [134]. Weil et al. reported the fabrication of $CuInS_2$ solar cells by air-stable ink rolling. The ink for $CuInS_2$ consists of elemental sulfur, $Cu(acac)_2$, and $In(acac)_3$ (acac = acetylacetonate)

dissolved in pyridine. CdS was the buffer layer used and it was deposited through chemical bath deposition. ZnO (TCO) layer was deposited using reactive DC magnetron sputtering. Power conversion efficiency of the fabricated device was 2.15 % [135]. Tiwari et al. fabricated all-sprayed $CuInS_2$/ZnO solar cells with an efficiency of 2 %. Indium-doped ZnO films are essential for better photovoltaic response and [In]/[Zn] atomic concentration ratio was 0.03 for the best device. Deposition of an interlayer of $CuInS_2$ and post-deposition annealing of junctions are essential for obtaining good quality solar cells. Multistep tunneling and recombination is the most likely mode of carrier transport in $CuInS_2$/ZnO heterojunctions [111].

Cho et al. synthesized monodispersed CIS nanocrystals by colloidal synthetic route and re-dispersed in toluene to form 'ink'. CuCl, $InCl_3$, sulfur dissolved oleylamine (OLA) were used in the preparation of ink. This ink was applied to thin film solar cell devices with superstrate configuration by spray coating method. Device structure followed for the study was ITO/TiO_2/CdS/CIS/Au. TiO_2 and CdS were used as blocking layer and buffer layer respectively. Power conversion efficiency of 1.45 % was achieved by this device [136]. Ryo et al. fabricated superstrate type $CuInS_2$ solar cells by spray pyrolysis method. Glass/FTO/TiO_2/In_2S_3/$CuInS_2$ structure was followed for device fabrication. Crystallinity of the spray-deposited $CuInS_2$ films was generally good and its band gap value of was ~ 1.3 eV. For $CuInS_2$ films with thickness < 2 μm there was only one layer and had good adhesion. But $CuInS_2$ films with thickness > 3 μm were having several layers, and were easily peeled off during deposition. The best cell obtained had efficiency of 1.7 % [137]. Polymer/$CuInS_2$ hybrid solar cells and modules on flexible plastic substrate were also reported. Device fabrication was based on the metal xanthate route and low temperature annealing. These hybrid solar cells were deposited on flexible PET foils, which showed efficiency of 1.6 % [138].

1.9.3 Deposition of Cu_2S thin film

A variety of deposition techniques like chemical spray pyrolysis, electrodeposition, chemical bath deposition, sputtering, SILAR, chemical vapor deposition and solvothermal technique were already reported for Cu_2S thin films. Wang et al. employed asynchronous-pulse ultrasonic spray pyrolysis technique for the deposition of Cu_xS (x = 1, 2) thin films on glass from $CuCl_2$ and thiourea. Film deposition was at relatively low temperature without any complexing agent. The deposited Cu_2S films were a mixture of amorphous and polycrystalline phases. The crystalline phases of the films were highly depended on the molar ratio of thiourea to $CuCl_2$ and the pyrolysis temperature. Presence of both "covellite CuS" and "chalcolite Cu_2S" were confirmed by XRD and XPS analysis. Raman shifts for CuS phase was at 474 cm^{-1} and that of Cu_2S phase was at 472 cm^{-1} [139].

Isac et al. deposited copper sulfide (Cu_xS, x = 1.8–2) thin films through spray pyrolysis method. Aqueous and alcoholic solutions, containing $CuCl_2$ and thiourea were used as precursors. Deposition temperature was maintained at 285 °C. By controlling precursor solution composition and deposition parameters, dense, relative homogenous and uniform films of Cu_2S were obtained. Deposited films were chemically close to chalcocite (Cu_2S) or to mixtures of copper-rich phases (Cu_2S, $Cu_{1.8}S$, $Cu_{1.9375}S$) in which chalcocite or digenite ($Cu_{1.8}S$) were predominant. By optimizing spray time and modifying precursor solution concentration, using mixtures of water: ethanol: glycerin as solvents, morphology of the deposited films can be tailored. For the deposition of Cu_2S, the optimum precursor solution has Cu:S molar ratio of 1:3 in a water: ethanol: glycerin solvent with the volume ratio of 7: 2: 1. Spray time of more than 40 min at 285 °C are also preferred [140]. Davis et al. synthesized Cu_2S nanocrystals using single precursor by employing aerosol spray pyrolysis.

Copper diethyldithiocarbamate in toluene was used as the precursor solution. The precursor is aerosolized and aerodynamically dragged through a tube furnace. Inside the tube furnace, the droplets are dried and nanocrystals are formed. Particle size was smaller than 20 nm. These particles were preferentially formed as digenite ($Cu_{1.8}S$); but at low furnace temperature, it was possible to produce chalcocite (Cu_2S, p-type) nanocrystals, promising candidates for the development of low-cost, printable photovoltaic devices [141].

Grozdanov et al. employed electroless chemical deposition to deposit thin films of Cu_2S, $Cu_{1.8}S$, $Cu_{1.4}S$, and CuS on glass, polyester or metal substrates. Aqueous copper thiosulfate bath in acidic media was used for deposition. Deposited films differ in the optical transmission in the near infrared region, with Cu_2S being highly transmissive and CuS highly absorptive in the microwave radiation (i.e., in spectral range 0.8- 2.5 μm). All films were p-type and highly conductive in nature. Conductivity increased from Cu_2S towards CuS [142]. A modified chemical deposition method was employed by Pathan et al. for the deposition of stoichiometric copper sulphide (Cu_2S) thin films. In this method the substrate was immersed into separate cation and anion precursor solutions and rinsing between every immersion with ion exchange water to avoid homogeneous precipitation. The cationic precursor was copper(II)sulphate pentahydrate ($CuSO_4.5H_2O$) solution complexed with mixture of 2N triethanolamine (TEA) and 2N hydrazine hydrate (HH). The pH of this solution was adjusted to ~ 5. Anionic precursor was sodium sulphide ($Na_2S.H_2O$) solution with pH ~ 12. For the preparation of stoichiometric, nanocrystalline Cu_2S, the preparative conditions such as concentration, pH of cationic and anionic precursors, adsorption, reaction and rinsing time durations, complexing agent, etc. were optimized. Absorbance of the film was 10^4 cm^{-1} with direct optical band gap of 2.35 eV. Deposited films showed p-type conductivity and room temperature electrical resistivity was of the order of 10^{-2} Ω.cm [143].

Podder et al. deposited Cu_xS thin films(x from 2.3 to 1.3) on ITO coated glass substrates by photochemical deposition from an aqueous solution of $CuSO_4$ and $Na_2S_2O_3$. pH was kept at 3 and photo irradiation was for the duration of 1–2 h. Thickness of the films was in the range of 0.15–0.35 μm. XRD studies showed polycrystallinity of the Cu_xS thin films and the energy band gap of the films were estimated in the range of 2.15–2.53 eV [144]. Bagul et al. deposited thin films of Cu_xS (x=1.0, 1.76, and 2.0) by solution growth technique (SGT) using thiosulfate, which acted as both complexing and sulfiding agent. The deposition parameters of Cu_xS such as pH of solution, deposition time, and deposition temperature were optimized. As the deposited films were amorphous, annealing was carried out in Ar atmosphere at 250 °C. Annealed films were polycrystalline in nature. Absorption coefficient varied in the range of $1x10^5$– $6x10^5$ cm^{-1}. The optical band gap of Cu_2S was 2.48 eV [145].

Schimmel et al. reported the combined use of voltammetry and electrode illumination during anodic growth of Cu_2S and $CuInS_2$ films on copper substrates in KOH medium containing sulfur [146]. Anuar et al. employed cathodic electrodeposition for the preparation of Cu_2S thin film on Ti substrate. The process was carried out in presence of EDTA in aqueous solution. For Cu_2S films, they reported optimum deposition potential to be -0.40 V. In order to elucidate the electrodic processes that occur while potentials for electrodeposition were applied to determine the optimum potential for electrodeposition, cyclic voltammetry was carried out. The deposition bath consisted of $CuSO_4$ and $Na_2S_2O_3$ solution. Better photo activity was observed for samples prepared using higher concentrations of $CuSO_4$ compared to a fixed concentration of $Na_2S_2O_3$. For better films, the deposition period was 60 min and above. The band gap energy of these films was 1.50 eV [147].

Nair et al. deposited Cu_xS thin films using CBD on SnO_2/glass substrates. Chemical bath is constituted from copper(II)chloride, triethanolamine and thiourea at appropriate pH (10-12). These films were stable with respect to electrical and optical properties on storage under ambient conditions [148]. Allouche et al. deposited copper sulphide (Cu_2S) thin films through CBD technique. Depositions were carried out during deposition time of about 32.5 min in the pH range of 9.4 to 11. X-ray diffraction study showed that Cu_2S films exhibited the best crystallinity for pH = 10.2 and films grown on an SnO_2/glass substrate exhibited stoichiometric composition with [Cu]/[S] concentrations ratio equal to 2.02. The work function difference for the Cu_2S films deposited on SnO_2/glass substrates at the optimum pH value was found to be equal to 145 meV. Hall measurements confirmed the p-type electrical conductivity and electrical resistivity was of the order of 3.85 x 10^4 Ω.cm. Band gap energy of the films is about 2.37 eV. Refractive index (n) and extinction coefficient (k) of the films varied in the range of 1.7–2.1 and 0.02–0.09 respectively. The optical properties of these films made them suitable for solar control coatings and photovoltaic devices [149].

Nomura reported preparation of copper sulfide thin layers by a single-source metal-organic chemical vapor deposition (MOCVD). This work deals with growth of high quality copper-deficient $Cu_{1.96}S$ layers by low pressure MOCVD process using copper(II)bis(diethyldithiocarbamate). Films were grown on Si (III), quartz, or glass substrates in horizontal hot-wall reactor made of quartz [150].

Pathan et al. employed (SILAR) method for depositing single phase of Cu_2S with hexagonal crystal structure using $CuSO_4$ and Na_2S. These films exhibited maximum transmittance ~ 53.4 % for λ = 630 nm. Absorption coefficient of the film was 10^4 cm^{-1}. Film showed p-type conductivity with

band gap of 2.33 eV. Growth rate of the film was estimated to be 7 nm/cycle [151].

Das et al. prepared Cu_2S thin films of well-controlled thickness and stoichiometry by solid state reaction between CdS and CuCl films. Temperature range for this reaction was 200-250 °C. These films existed in the orthorhombic chalcocite phase and were utilized to fabricate Cu_2S/CdS solar cells. CdS films were prepared employing vacuum evaporation of pellets of CdS powder. Cu_2S films were deposited over CdS films by evaporating freshly prepared pure CuCl powder from a molybdenum boat. Growth of Cu_2S on CdS is topotactial. Chalcocite Cu_2S phase is obtained on reaction with both wurtzite and sphalerite structures of CdS [152].

Gorai et al. synthesized a series of stoichiometric and non-stoichiometric copper sulphides (Cu_2S, $Cu_{31}S_{16}$, $Cu_{1.81}S$, Cu_7S_4, $Cu_{39}S_{28}$) via solvothermal route. Both ethylenediamine (En) and water were used as the solvent system at 130 °C. Solvothermal system consists of solvent, bivalent copper nitrate and thiourea. When the solvent was pure En, six-petal dendritic Cu_2S with central mid-ribs supporting each petal was observed. As the solvent was changed from pure En to (En + H_2O), dendrites were progressively broke to individual rods. For pure water as the solvent, spherical particles with a part of the surface covered with thin spaghetti-like form was observed. When pure En was used as the solvent, bidentate ligands En has connectivity with Cu ions, to which thiourea molecule also get attached. Partial reduction of Cu^{2+} and breakdown of thiourea then occurs due to the elevated temperature and pressure of the solvothermal system, which resulted in dendritic or rod-like copper sulphides [153].

Cu_2S and CuS films were deposited by He et al. on float glass substrates using reactive RF sputter process with optimized sputter parameters,

such as power, temperature of the substrate, and the gas flow of the H_2S. XRD spectra showed that the Cu_2S films had (002) preferential orientation and both compounds had hexagonal structure. Hall-effect measurements indicated two activation energies related to the intrinsic defects in the Cu_2S films. CuS has relatively high carrier concentration around 10^{22} cm^{-3}, hence a much lower resistivity of about 10^{-4} Ω.cm, and slightly lower Hall mobility of about 3 $cm^2V^{-1}s^{-1}$ compared with the semiconducting phase Cu_2S [154].

1.9.4 Review on Cu_2S based solar cells

Cu_2S possesses extremely favorable material characteristics for absorber layer in thin film solar cells. Cu_2S/CdS solar cell gained paramount promises and its history spans more than a half century, beginning in 1954, when Reynolds et al. first discovered photovoltaic response in heat treated Cu contacts on CdS at photon energies less than the CdS band edge [155]. Highest efficiency for Cu_2S based solar cell is 10.2 %, reported by Hall et al. for $Cu_2S/Cd_{(1-x)}Zn_xS$ heterojunction. Here $Cd_{1-x}Zn_xS$ film was deposited using thermal co-evaporation of CdS and ZnS from two-chamber concentric source onto a zinc-plated copper substrate at 210 °C. The zinc concentrations of the films were in the range of $0.1 < x < 0.2$. Before depositing Cu_2S over $Cd_{(1-x)}$ Zn_xS surface, texturing of $Cd_{(1-x)}Zn_xS$ film was done to improve light trapping characteristics of the device. Cu_2S layer was formed by reaction in a cuprous chloride solution. Gold was used as the front contact and Ta_2O_5 as the antireflection coating. Heat treatment at 170 °C in a flowing hydrogen atmosphere was also performed to improve light generated current and junction characteristics [156].

Bragagnolo et al. fabricated thin film CdS/Cu_2S cells having 9.15 % conversion efficiency. For cell fabrication, CdS was vapor deposited over Zn plated electroformed copper substrate. Heavily textured light-trapping Cu_2S

layer was topotaxially grown over CdS by reaction in a cuprous-ion solution. Very interestingly, a new technology to deposit the top grid and anti-reflection coating onto the Cu_2S and new analysis and processing techniques to separately measure and minimize fill factor losses have been developed in this work. Top electrical contact was formed by evaporating highly transmitting Au grid onto the Cu_2S surface. Finally an anti-reflecting SiO_2 quarter-wave coating was vapor deposited over the structure [16].

Saraf et al. synthesised Cu_2S and CdS nanoparticles through wet chemical method and Cu_2S/CdS solar cell was fabricated using spin coating technique. For solar cell fabrication, thin film of CdS nanoparticle approximately 100 nm in thickness was created using spin-coating technique on top of glass substrate and then thin film of Cu_2S nanoparticle (approximately 10 μm in thickness) was created on CdS thin film using the same technique. Silver was the back electrode. Efficiency of the fabricated cell approached around 10.9 % and fill factor around 73 % [157]. Cu_2S/CdS solar cells having efficiency of 7.6 % was fabricated by combining spray pyrolysis and evaporation. For device fabrication, solution containing cadmium was sprayed onto heated electrically conductive transparent substrate to form cadmium containing sulfide. Cuprous chloride powder was then vacuum evaporated onto the CdS crystals. By heating this Cu coated CdS layer during a time-temperature controlled cycle, a portion of the surface of the CdS crystals was converted to Cu_xS [158].

Ashour et al. fabricated glass/Ag/CdS/Cu_2S/Au solar cells having 7.2 % efficiency. The CdS layer was deposited using vacuum evaporation of pure CdS powder. The Cu_2S layer was produced by vacuum evaporation of thin layer of CuCl powder onto the CdS film at room temperature. Then the structure was heated at 170 °C for 5 min in the same vacuum chamber at pressure of 10^{-3} Pa. Here a layer of Cu_2S is formed by the topotaxial

conversion of some portion of CdS by CuCl. The major limitations for the present device were poor design of grid and high resistivity of CdS films [159]. Goldenblum et al. reported fabrication of large-area Cu_2S/CdS solar cells using vacuum evaporation technology alone. Successive vacuum deposition of chromium and silver over ordinary window glass at 200 °C served as the back contact. CdS layer was then vacuum evaporated over this using CdS powder. In the next step CuCl was vacuum evaporated over CdS and the samples were heated at 140 °C for 4 minutes. A solid state reaction take place and a layer of Cu_2S was grown topotaxially on the CdS surface. Methyl alcohol was used to wash off cadmium chloride produced by the reaction. High surface roughness of these films ensured high absorbance in the Cu_2S layer without any etching. The maximum efficiency of the device was 6.49 % at 100 mW/cm^2 [160]. Aperathitis et al. reported all vacuum evaporated Cu_xS/CdS solar cells having efficiency in excess of 7 %. Copper sulphide layer was prepared by employing vacuum evaporation from single Cu_xS source, as an alternative to the chemiplating technique for fabricating Cu_xS layer in Cu_xS/CdS solar cells. Deposition rate less than 150 Å/min produced Cu_xS layers with chalcocite as major phase. Layers free from excess copper have chalcocite-related phase transition between 75 and 80 °C. Also they exhibited room temperature resistivity between 10^{-2} and 10^{-3} Ω.cm. and showed direct and indirect band gaps of 2.25 and 1.25 eV respectively. For solar cell fabrication Cu_2S layer with well controlled evaporation conditions was deposited on hot CdS thin film substrates [161].

Low cost Cu_2S/CdS thin film solar cells having efficiency of 4.5 % were also prepared through chemical spraying. For solar cell fabrication thin transparent tin oxide transparent electrode was sprayed over glass substrate. Over this CdS layer was spray deposited. A very thin film of Cu_xS was then formed by spraying, dipping, or electrolytic ion exchange. Finally for top

contact copper/lead electrode was evaporated over the Cu_xS layer [162]. Islam et al. prepared thin film CdS/Cu_2S heterojunction solar cells on gold grid plated glass substrates by first depositing Cu_2S employing elemental evaporation of copper and sulphur and then evaporating CdS. Here the cells were prepared with Cu_2S layer sandwiched between the glass substrate and the CdS layer and was found to be stable. The maximum efficiency was 5 % for these solar cells [163].

Vanhoecke prepared Cu_2S/CdS solar cell by sputtering thin chalcocite (Cu_2S) films using pure copper target in an H_2S-Ar atmosphere onto evaporated CdS layer. For active area of 3.6 cm^2, efficiency of up to 4.9 % was attained. On large area cells (21cm^2) efficiency of 2.4 % was attained. They were able to reduce the thickness of CdS layers to 10 μm for obtaining good quality solar cells [164]. Wu et al. prepared colloidal Cu_2S nanocrystals by injection reaction between copper (II) acetylacetonate and ammonium diethyl dithiocarbamate in mixed solvent of dodecanethiol and oleic acid. Cu_2S nanocrystal was used as active light absorbing component in combination with CdS nanorods to make solution-processed solar cell with 1.6 % power conversion efficiency on both conventional glass substrates and flexible plastic substrates. The device showed stability over 4 month testing period [165].

1.10 Significance of the present work

For thin film preparation, present study followed simple, cost effective and versatile CSP method. As cost effectiveness is the primary necessity prevailing in photovoltaic industry, CSP method is a suitable candidate capable of fulfilling this demand. Moreover, feasibility of large area deposition offers special recognition for CSP among industrially viable thin film solar cell techniques. $CuInS_2$ and Cu_2S are the absorber materials for the present study.

Optical absorption coefficients and band gaps of these materials are ideal as an absorber in thin film solar cells. Comparing with CdTe and $CuInSe_2$, these materials are non-toxic, earth-abundant and simple CSP method can be effectively used to deposit device quality films using these two materials. Buffer layer used for the present study is In_2S_3, which is also non-toxic when comparing with CdS buffer layer. Spray pyrolysed In_2S_3 is a well-studied and proven buffer layer for solar cell application. The main issue that limits the performance of solar cells based on thick absorber layer is the reduced collection probability of light generated carriers at the contacts due to recombination in thick absorber layer. In this context, the concept of ETA solar cell was also introduced for both $CuInS_2$ and Cu_2S based solar cells. The main idea was to reduce the thickness of the absorber layer in which light-generated electron-hole pairs travel to reach the electrical contacts before recombining. As the absorber layer thickness was reduced, light absorption will reduce considerably. In order to compensate this, multiple band gaps of $CuInS_2$ and Cu_2S was introduced by CSP in this extremely thin absorber layer so that device can absorb photons of two different energies.

References

[1] Panasonic Press Release, **10 April 2014**, Panasonic HIT® solar cell achieves world's highest energy conversion efficiency of 25.6 % at research level.

[2] Green M A, Solar Cells: Operating Principles, Technology and System Applications, University of New South Wales (1992).

[3] http://pveducation.org/pvcdrom.

[4] Shockley W, Queisser H, Journal of Applied Physics, 1961**,** **32**, 510-519.

[5] Green M A, Emery K, Hishikawa Y, Warta W, Dunlop E D, Progress in photovoltaics: Research and applications, 2014, **22**, 701-710.

[6] Schultz O, Glunz S W, Willeke G P, Progress in Photovoltaics: Research and Applications, 2004, **12**, 553-558.

[7] Chopra K L, Thin Film Solar Cells- A Status Review, http://www2.kfupm.edu.sa/cent/img/kfupm-tfsc-dec20.pdf.

[8] www.ge-energy.com/products and services/products/solar power/CdTe thin film solar module78.jsp (accessed 13 November 2012).

[9] First Solar press release, 19 March **2014**. First Solar Sets Thin-Film Module Efficiency World Record of 17.0 Percent.

[10] Rudmann D, Brémaud D, da Cunha A F, Bilger G, Strohm A, Kaelin M, Zogg H, Tiwari A N, Thin Solid Films, 2005, **480-481**, 55.

[11] Granata J.E. et al, Proceedings of 2nd World Conference on Photovoltaic Solar Energy Conversion, Vienna (1998).

[12] Osborne, M. Hanergy's solibro, 20.5 % CIGS solar cell verified by NREL, 8 April 2014.

[13] http://www.miasole.com.

[14] Hedstrom J, Ohlsen H, Proc. 23rd IEEE Photovoltaic Specialists Conference, 1993, **364**.

[15] Klaer J, Bruns J, Henninger R, Siemer K, Klenk R, Ellmer K, Braunig D, Semiconductor Science and Technology, 1998, **13**,1456–1458.

[16] Bragagnolo J A, Barnett A M, Phillips J E,Hall R B, Rothwarf A, Meakin J D, IEEE transactions on electron devices, 1980, **ED-27**, 645-650.

[17] Wang W, Winkler M T, Gunawan O, Gokmen T, Todorov T K, Zhu Y, Mitzi D B. Advanced Energy Materials, 2013, **4**, 1301465.

[18] Kayes B M, Nie H, Twist R, Spruytte S G, Reinhardt F, Kizilyalli I C, Higashi G S. Proceedings of the 37th IEEE Photovoltaic Specialists Conference, 2011.

[19] Keavney C J, Haven V E, Vernon S M., 21st IEEE Photovoltaic Specialists Conference, Kissimimee, May, 1990, 141–144**.**

[20] Benagli S, Borrello D, Vallat-Sauvain E, Meier J, Kroll U, Hötzel J, Spitznagel J, Steinhauser J, Castens L, Djeridane Y, 24th European Photovoltaic Solar Energy Conference, Hamburg, September 2009.

[21] Mayer A C, Scully S R, Hardin B E, Rowell M W, McGehe M D, Materials Today, 2009, **10**, 28-33.

[22] Grätzel M, Journal of Photochemistry and Photobiology C: Photochemistry Reviews, 2003, **4**, 145–153.

[23] Komiya R, Fukui A, Murofushi N, Koide N, Yamanaka R, Katayama H, 21st International Photovoltaic Science and Engineering Conference, Fukuoka, November 2011.

[24] Queisser H J, Solar Energy Materials and Solar Cells, 2010, **94**, 1927–1930.

[25] Green M A, (2003), Third Generation Photovoltaics: Advanced Solar Energy Conversion, Springer. p. 65.

[26] Sasaki K, Agui T, Nakaido K, Takahashi N, Onitsuka R, Takamoto T, Proceedings of 9th international conference on concentrating photovoltaics systems, Miyazaki, Japan**,** 2013.

[27] Konig D, Casalenuovo K, Takeda Y, Conibeer G, Guillemoles J F, Patterson R, Huang L M, Green M A, Physica E, 2010, **42**, 2862-2866.

[28] Conibeer G, Ekins-Daukes N, Guillemoles J, Konig D, Cho E, Jiang C, Shrestha S, Green M A, Solar Energy Materials and Solar Cells, 2009, **93**, 713-719.

[29] Saeed S, de Jong E M L D, Dohnalova K, Gregorkiewicz T, Nature Communications, 2014, **5**.

[30] Conibeer G, Patterson R, Huang L, Guillemoles J, Konig D, Shrestha S, Green M A, Solar Energy Materials and Solar Cells, 2010, **94**, 1516–1521.

[31] Nozik A J, Chemical Physics Letters, 2008, **457**, 3–11.

[32] http://siser.eps.hw.ac.uk .

[33] Van Sark W G, de Wild J, Rath J K, Meijerink A, Schropp R E, Nanoscale Research Letters, 2013, **81**.

[34] Jeffrey, Colin , "New record efficiency for quantum-dot photovoltaics", May 27, 2014.

[35] Catchpole K R, Polman A, Optics Express, 2008, **16**, 21793-21800.

[36] Luque, Antonio, Martí A. Physical Review Letters, 1997, **78.26**, 5014-017.

[37] Okada.Y, Ekins-Daukes N J, Kita T, Tamaki R, Yoshida M, Pusch A, Hess O, Phillips C C, Farrell D J, Yoshida K, Ahsan N, Shoji Y, Sogabe T, Guillemoles J F, Applied Physics Reviews, 2015, **2**, 021302-48.

[38] Ramiro, Inigo, Martí A, Antolin E, Luque A, IEEE Xplore. N.p, n.d**,** 2014.

[39] Perednis D, Gauckler L J, Journal of Electroceramics, 2005, **14**, 103-111.

[40] Patil P S, Materials Chemistry and Physics, 1999, **59**, 185-198.

[41] Sabnis S M, Bhadane P A, Kulkarni P G, IOSR Journal of Applied Physics, 2013, **4**, 2013, 7-11.

[42] Filipovic L, Selberherr S, Mutinati G C, Brunet E, Steinhauer S, Kock A, Teva J, Kraft J, Siegert J, Schrank F, Proceedings of the World Congress on Engineering, Vol II, 2013.

[43] GracoInc, Atomization Concept and Theory, 1995.

[44] Duminica F D, Maury F, Abisset S, Thin Solid Films, 2007, **515**, 7732-7739.

[45] Sebastian T, PhD thesis, Cochin University of Science And Technology, 2009.

[46] Scheer R, Lewerenz H J, Journal of Vacuum Science and Technology, 1995, **A 13**, 1924.

[47] Scheer R, Luck I, Kanis M, Matsui M, Watanabe T, Yamamoto T, Thin Solid Films, 2001, **392**, 1-10.

[48] Tsai W, Tsai C, Chang C, Ting J, Wang R, Thin Solid Films, 2010, **519**, 1712-1716.

[49] Scheer R, Lewerenz H J, Journal of Vacuum Science and Technology, 1994, **A12**, 56.

[50] Scheer R, Lewerenz H J, Journal of Vacuum Science and Technology, 1994, **A12**, 51.

[51] Hwang H L, Solar Energy Materials, 1980**, 2**, 433–446.

[52] Agarwal M K, Patel P D, Chaki S H, Lakshminarayana D, Bulletin of Material Science, 1998, **21**, 291-295.

[53] Abaab M, Kanzari M, Rezig B, Brunel M, Solar Energy Materials and Solar Cells, 1999, **59**, 299-307.

[54] Akkari F C, Kanzari M, Rezig B, Physica E, 2008, **40**, 2577-2582.

[55] Rabeh M B, Kanzari M, Rezig B, Thin Solid Films, 2007, **515**, 5943-5948.

[56] Akaki Y, Matsuo H, Yoshino K, Physica status solidi (c), 2006, **3**, 2597-2600.

[57] Zribi M, Kanzari M, Rezig B, Materials Science and Engineering B, 2008, **149**,1-6.

[58] Rabeh M B, Chaglabou N, Kanzari M, Chalcogenide Letters, 2009, **6**, 83-89.

[59] Rabeh M B, Zribi M, Kanzari M, Rezig B, Materials Letters, 2005, **59**, 3164-3168.

[60] Rabeh M B, Kanzari M, Rezig B, Journal of Optoelectronic and Biomedical Materials, 2009**, 1**, 70-78.

[61] Wu Y L, Lin H Y, Sun C Y, Yang M H, Hwang H L, Thin Solid Films, 1989, **168**, 113-122.

[62] Gossla M, Hahn T, MetznerH , Conrad J, Geyer U, Thin Solid Films, 1995, **268**, 39-44.

[63] Guillen C, Semiconductor Science and Technology, 2006, **21,** 709-712.

[64] Akaki Y, Nakamura S, Nomoto K, Yoshitake T,Yoshino K, Physica Status Solidi C, 2009**, 6,** 1030-1033.

[65] Neisser A, Hengel I, Klenk R, Matthes T W, Alvarez-Garcia J, Perez-Rodriguez A, Romano-RodrIguez A, Lux-Steiner M C, Solar Energy Materials and Solar Cells, 2001, **67,** 97-104.

[66] Akkari F C, Brini R, Kanzari M, Rezig B, Journal of materials science , 2005, **40**, 5751- 5755.

[67] Akaki Y, Komaki H, Yokoyama H, Yoshino K, Maeda K, Ikari T, Journal of Physics and Chemistry of Solids , 2003, **64**,1863-1867.

[68] He Y B, Polity A, Gregor R, Pfisterer D, Osterreicher I, Hasselkamp D, Meyer B K, Physica B, 2001, **308-310**, 1074-1077.

[69] He Y B, Kramer T, Polity A, Gregor R, Kriegseis W, Osterreicher I, Hasselkamp D, Meyer B K, Thin Solid Films, 2003, **431 – 432**, 231-236.

[70] Cayzac R, Boulc'h F, Bendahan M , Lauque P, Knauth P, Materials Science and Engineering B, 2009, **157**, 66-71.

[71] Seeger S, Ellmer K, Thin Solid Films, 2009, **517**, 3143-3147.

[72] Liu X, Shao L, Surface and Coatings Technology, 2007, **201**, 5340-5343.

[73] Ogawa Y, Uenishi S, Tohyama K, Ito K, Solar Energy Materials and Solar Cells, 1994, **35**,157-163.

[74] Wada T, Negami T, Nishitani M, Applied Physics Letters, 1993, **62**, 1943-1945.

[75] Antony A, Asha A S, Yoosuf R, Manoj R, Jayaraj M K, Solar Energy Materials & Solar Cells, 2004, **81**, 407-417.

[76] Long F, Wang W, Tao H, Jia T, Li X, Zou Z, Fu Z, Materials Letters, 2010, **64**, 195-198.

[77] Tang M, Tian Q, Hu X, Peng Y, Xue Y, Chen Z, Yang J, Xu X, Hu J, CrystEngComm, 2012, **14**, 1825–1832.

[78] Lee S, Park B, Thin Solid Films, 2008, **516**, 3862-3864.

[79] Shi Y, Jin Z, Li C, An H, Qiu J, Applied Surface Science, 2006, **252**, 3737-3743.

[80] Shi Y, Xue F, Li C, Zhao Q, Qu Z, Li X, Applied Surface Science, 2012, **258**, 7465-7469.

[81] Penndorf J, Winkler M, Tober O, Roser D, Jacobs K, Solar Energy Materials and Solar Cells, 1998, **53**, 285-298.

[82] Winkler M, Tober O, Penndorf J, Szulzewsky K, Roser D, Lippold G, Otte K, Thin Solid Films, 200, **361-362**, 273-277.

[83] Podder J, Miyawaki T, Ichimura M, Journal of Crystal Growth, 2005, **275**, e937- e942.

[84] Lee S, Kim K, Park B, Thin Solid Films, 2008, **516**, 4709-4712.

[85] Metzner H, Hahn T, Bremer J H, Seibt M, Plikat B, Dirnstorfer I, Meyer B K, Thin Solid Films, 2000, **361-362**, 504-508.

[86] Qiu J, Jin Z, Qian J, Shi Y, Wu W, Materials Letters, 2005, **59**, 2735-2740.

[87] Das K, Panda S K, Chaudhuri S, Applied Surface Science, 2007, **253**, 5166-5172.

[88] Camus C, Allsop N A, Gledhill S E, Bohne W, Rohrich J, Lauermann I, Lux-Steiner M C, Fischer C, Thin Solid Films, 2008, **516**, 7026-7030.

[89] Hou X, Choy K, Thin Solid Films, 2005, **480–481**, 13-18.

[90] Yukawa T, Kuwabara K, Koumoto K, Thin Solid Films, 1996, **286**, 151-153.

[91] Asenjo B, Chaparro A M, Gutierrez M T, Herrero J, Thin Solid Films, 2006, **511–512**, 117-120.

[92] Martinez A M, Fernandez A M, Arriaga L G, Cano U, Materials Chemistry and Physics, 2006, **95**, 270-274.

[93] Wijesundera R P, Siripala W, Solar Energy Materials and Solar Cells, 2004, **81**,147-154.

[94] Hwang H L, Sun C Y, Fang C S, Chang S D, Cheng C H, Yang M H, Lin H H, Tuwan-Mu H, Journal of crystal growth, 1981, **55**, 116-124.

[95] Harris J D, Banger K K, Scheiman D A, Smith M A, Jin M H, Hepp A F, Materials Science and Engineering B, 2003, **98** ,150-155.

[96] Djessas K , Masse G, Ibannaim M, Journal of Electrochemical Society, 2000, **147**, 235-239.

[97] Cui F, Wang L, Xi Z, Sun Y, Yang D, Journal of Material Science: Mater Electron, 2009, **20**, 609-613.

[98] Nanu M, Reijnen L, Meester B, Schoonman J, Goossens A, Chemical Vapor Deposition, 2004, **10**, 45-49.

[99] Lin S, Shi X, Zhang X, Kou H, Wang C, Applied Surface Science, 2010, **256**, 4365-4369.

[100] Cherian A S, Abe T, Kashiwaba Y, Sudha Kartha C, Vijayakumar K P, Energy Procedia, 2012, **15**, 283-290.

[101] John T T, Mathew M, Kartha C S, Vijayakumar K P, Abe T, Kashiwaba Y, Solar Energy Materials & Solar cells, 2005, **89**, 27-36.

[102] Santhosh M V, Deepu D R, Kartha C S, Rajeev Kumar K, Vijayakumar K P, Solar Energy, 2014, **108**, 508-514.

[103] Teny Theresa John, Ph.D Thesis, Cochin University of Science and Technology, India (2004).

[104] Mere A, Kijatkina O, Rebane H, Krustok J, Krunks M, Journal of Physics and Chemistry of Solids, 2003, **64**, 2025-2029.

[105] Kim J, Yun B S, Journal of the Korean Physical Society, 2008, **53**, 2453-2457.

[106] Krunks M, Kijatkina O, Mere A, Varema T, Oja I, Mikli V, Solar Energy Materials and Solar Cells, 2005, **87**, 207-214.

[107] John T T, Wilson K. C, Ratheesh Kumar P. M, Sudha Kartha C, Vijayakumar K P, Kashiwaba Y, Abe T, Yasuhiro Y, Physica Status Solidi (A), 2005, **202**, 79.

[108] Gorska M, Beaulieu R, Loferski J J, Roessler B, Solar Energy Materials, 1979,**1**, 313.

[109] Kijatkina O, Krunks M, A. Mere, Mahrov B, Dlozik L, Thin Solid films, 2003, **431-432**, 105-109.

[110] Jin Michael H. et al., Proceedings of the 3rd World Conference on Photovoltaic Energy Conversion, Osaka, Japan (2003).

[111] Tiwari A N, Pandya D K, Chopra K L, Thin Solid Films, 1985, **130**, 217.

[112] Krunks M, Mere A, Katerski A, Mikli V, Krustok J, Thin Solid Films, 2006, **511-512**, 434-438.

[113] John T T, Sebastian T, Sudha Kartha C, Vijayakumar K P, Abe T, Kashiwaba Y, Physica B: Condensed Matter, 2007, **388**,1-9.

[114] Vijayalakshmi R P, Venugopal R, Reddy D R, Reddy B K, Solid State Communications, 1992, **82**, 997-1000.

[115] Goto H, Hashimoto Y, Ito K, Thin Solid Films 2004, **451-452**, 552-555.

[116] Hengel I, Neisser A, Klenk R, Lux-Steiner M C, Thin Solid Films, 2000, **361-362**, 458-462.

[117] Siemer K, Klaer J, Luck I, Bruns J, Klenk R, Braunig D, Solar Energy Materials and Solar Cells, 2001, **67**, 159-166.

[118] Braunger D, Hariskos D, Walter T, Schock H W, Solar Energy Materials and Solar Cells, 1996, **40**, 97-102.

[119] Nakabayashi T, Miyazawa T, Hashimoto Y, Ito K, Solar Energy Materials and Solar Cells, 1997, **49**, 375-381.

[120] Scheer R, Walter T, Schock H W, Fearheiley M L, Lewerenz H J, Applied Physics Letters, 1993, **63**, 3294-3296.

[121] Lewerenz H J, Goslowsky H, Husemann K D,Fiechter S, Nature, 1986, **321**, 687-688.

[122] Asenjo B, Chaparro A M, Gutierrez M T, Herrero J, Klaer J, Solar Energy Materials and Solar Cells, 2004, **87**, 647–656.

[123] Sandino J, Romero E, Oyola J S, Gordillo G, Lichte H, Solar Energy Materials and Solar Cells, 2011, **95**, 2006-2009 .

[124] Yi L, Liu Y, Yang N, Tang Z, Zhao H, Ma G, Su Z, Wang D, Energy and Environmental Science, 2013, **6**, 835-840.

[125] Goossens A, Hofhuis J, Nanotechnology, 2008, **19**, 424018 (8pp).

[126] Luo G, Wei H, Huang Q,Hu X, Zhao H, Yu R, Li D, Luo Y, Meng Q, Chem Communication, 2013, **49**, 3881- 3883.

[127] Okuda K, Chantana J, Fujita Y, Hironiwa D, and Minemoto T, Japanese Journal of Applied Physics, 2014, **53**, 05FW04-(1-5) .

[128] Nanu M, Schoonman J, Goossens A, Advanced functional materials, 2005, **15**, 95-100.

[129] Li T, Lee Y, Teng H, Energy and Environmental Science, 2012, **5**, 5315-5324.

[130] Li L, Coates N, Moses D, Journal of American Chemical Society, 2010,**132,** 22.

[131] Kazmerski L L, Sanborn G A, Journal of Applied Physics, 1977, **48**, 3178-3180.

[132] Rath T, Edler M, Haas W, Fischereder A, Moscher S, Schenk A, Trattnig R, Sezen M, Mauthner G, Pein A, Meischler D, Bartl K, Saf R, Bansal N, Haque S, Hofer F, List E J W, Trimmel G, Advanced Energy Materials, 2011, **1**, 1046.

[133] Chang J, Su L, Li C, Chang C, Lin J, Chem. Communication, 2012, **48**, 4848-4850.

[134] Krunks M, Katerski A, Dedova T, Acik I O, Mere A, Solar Energy Materials and Solar Cells, 2008, **92**, 1016-1019.

[135] Weil B D, Connor S T, Cui Y, Journal of American Chemical Society, 2010, **132**, 6642-6643.

[136] Cho J W, Park S J, Kim W, Min B K, Nanotechnology, 2012, **23**, 265401.

[137] Ryo T, Nguyen D, Nakagiri M, Toyoda N, Matsuyoshi H, Ito S, Thin Solid Films, 2011, **519**, 7184-7188.

[138] Fradler C, Rath T, Dunst S, Letofsky-Papst I, Saf R, Kunert B, Hofer F, Resel R, Trimmel G, Solar Energy Materials and Solar Cells, 2014, **124**, 117-125.

[139] Wang S, Wang W, Lu Z, Materials Science and Engineering B, 2003, **103**, 184-188.

[140] Isac L, Duta A, Kriza A, Manolache S, Nanu M, Thin Solid Films, 2007, **515**, 5755- 5758.

[141] Davis P, Mangolini L, MRS Communications, 2013, **3**, 57–60.

[142] Grozdanov I, Najdoski M, Journal of solid state chemistry, 1995, **114**, 469-475.

[143] Pathan H M, Desai J D, Lokhande C D, Applied Surface Science, 2002, **202**,47-56.

[144] Podder J, Kobayashi R, Ichimura M, Thin Solid Films, 2005, **472**, 71-75.

[145] Bagul S V, Chavhan S D, Sharma R, Journal of Physics and Chemistry of Solids, 2007, **68**, 1623-1629.

[146] Schimmel M I, Tacconi N R, Rajeshwar K, Journal of Electroanalytical Chemistry, 1998, **453**, 187-195.

[147] Anuar K, Zainal Z, Hussein M Z, Saravanan N, Haslina I, Solar Energy Materials and Solar Cells, 2002, **73**, 351-365.

[148] Nair M T S, Nair P K, Semiconductor Science and Technology, 1989, **4**, 191-199.

[149] Allouche N K, Nasr T B, Guasch C, Turki N K, ComptesRendusChimie, 2010, **13**, 1364-1369.

[150] Nomura R, Miyawaki K, Toyosaki T, Matsuda H, Chemical Vapor Deposition, 1996, **2**, 174-178.

[151] Pathan H M, Lokhande C D, Bulletin of Material Science, 2004, **27**, 85-111.

[152] Das S R, Vankar V D, Nath P, Chopra K L,Thin solid films, 1978, **51**, 257-264.

[153] Gorai S, Ganguli D, Chaudhuri S, Materials Science and Engineering B, 2005, **116**, 221-225.

[154] He Y B, Polity A, Osterreicher I, Pfisterer D, Gregor R, Meyer B K, Hardt M, Physica B, 2001, **308-310**, 1069-1073.

[155] Chopra K L, Das S R, Thin Film Solar Cells, Springer Science and Business Media, 1983.

[156] Hall R B, Birkmire R W, Phillips J E, Meakin J D, Applied Physics Letters, 1981, **38**, 925-926.

[157] IOSR Journal of Electrical and Electronics Engineering, 2012, **2**, 47-51.

[158] Singh V P, United States Patent 4404734, 1983.

[159] Ashour A, Journal of optoelectronics and advanced materials, 2006, **8**, 1447-1451.

[160] Goldenblum A, Popovici G, Elena E, Oprea A, Nae C, Thin solid films, 1986, **141**, 215-221.

[161] Aperathitis E, Bryant F J, Scott C G, Solar Energy Materials,1990, **20**,15–28.

[162] Jordan J F, Samara G A, National solar photovoltaic program review meeting, 1975, Los Angeles, California.

[163] Islam M N, Haque M A, Thin solid films, 1982, **94**, 15-22.

[164] Vanhoecke E, Burgelman M, Anaf L, Thin solid films, 1986, **144**, 223-228.

[165] Wu Y, Wadia C, Ma W, Sadtler B, Alivisatos A P, Nano letters, 2008, **8**, 2551-2555.

……..✷ ♦ ✷……..

Chapter 2

$CuInS_2/In_2S_3$ solar cell in superstrate configuration using microporous TiO_2 thin films as electron conducting layer

2.1 Introduction

In superstrate configuration, the entire solar cell structure is deposited over a transparent conducting oxide (TCO) coated glass substrate and illumination is given from substrate side. Here glass substrate functions not only as a supporting structure but also as a window for illumination. 'Glass/TCO/buffer layer/absorber layer/metal' configuration is followed for these types of solar cells. Generally a micro or nanoporous electron conducting layer is deposited over TCO layer prior to the buffer layer deposition. Due to infiltration of both absorber and buffer layer over these structures, effective path length of light in the absorber material increases as multiple scattering occurs in the internal interfaces. Hence the absorber layer thickness can be reduced to a few nanometers and still it is capable of maintaining excellent light trapping capacity. Extension of interface increases for these configurations, which can promote effective charge carrier separation [1, 2]. For $CuInS_2$ absorber layer, TiO_2 or ZnO are the generally used micro/nanoporous electron conducting layer [3, 2]. Due to large inter facial junction area between the micro or nanoporous electron conducting layer and the absorber layer; probability of recombination of light generated carriers is very high. The role of buffer layer such as In_2S_3 or CdS is to suppress this recombination. Here the light generated electrons are transferred to the conduction band of large band gap buffer layer before recombination in the

absorber. From buffer layer electrons are injected to the conduction band of TiO_2 or ZnO [4].

2.2 $CuInS_2$ in superstrate configuration: A brief review

$CuInS_2$ was already utilized as an excellent absorber layer in superstrate configuration [1-4]. Direct band gap of 1.5 eV and high absorption coefficient (10^5 cm^{-1}) are the exceptional qualities that attribute paramount importance for this absorber material. Using a suitable micro or nanoporous electron conducting layer, $CuInS_2$ becomes ideal candidate for 'Extremely Thin Absorber (ETA)' layer solar cells in superstrate configuration [1-4].

Lensmann et al. reported the fabrication of $TiO_2/Al_2O_3/In_2S_3/CuInS_2$ solar cell having efficiency of 2.9 % [5]. Here nanostructured TiO_2 films were deposited by combining spray and 'doctor-blade' techniques. Al_2O_3 layer (as recombination barrier), In_2S_3 buffer layer and $CuInS_2$ absorber layer were deposited using atomic layer deposition (ALD). Results shows that Al_2O_3 recombination barrier and In_2S_3 buffer layer play crucial role in the better performance of $TiO_2/CuInS_2$ interface.

Nanu et al. also reported the fabrication of $TiO_2/Al_2O_3/In_2S_3/CuInS_2$ 3D solar cell having better performance with 4 % efficiency [3]. In this case, TiO_2 was prepared with the help of spray pyrolysis; but all other layers were prepared through atomic layer chemical vapor deposition (ALCVD). They observed that during deposition process, the stoichiometry of TiO_2 and $CuInS_2$ are modified and the stoichiometry is retained by thermal annealing in sulfur and oxygen.

CSP was employed by Goossens et al. to incorporate $CuInS_2$ nanocrystals into the matrix of In_2S_3/TiO_2. The device showed efficiency of about 5 % [6]. Ryan O'Hayre et al. reported fabrication of $TiO_2/In_2S_3/CuInS_2$

solar cells with efficiency of 2.8 % [7]. Here TiO_2 layer was deposited by employing spray and 'doctor-blade' technique. Both absorber and buffer layers were deposited using CSP. They suggested that by optimizing electron transport and reducing recombination in TiO_2, device performance can be improved.

Goossens et al. reported fabrication of 7 % efficient solar cells by following $TiO_2/In_2S_3/CuInS_2$ cell structure [8]. All the component layers were deposited employing spray pyrolysis. Transient absorption spectroscopy was used to study the deep electronic states in $CuInS_2$ and concluded that these states act as electron traps rather than as recombination centers. Temporal storage of charge in these traps reduces the V_{oc} of the device.

Krunks et al. reported fabrication of $ITO/ZnO/InS/In_2S_3/CuInS_2$ solar cells using CSP and the device shows an efficiency of 2.5 % [2]. Solar cells were also fabricated with ZnO layer without nanostructure and the cell parameters are low. Improvement in current density for structured solar cell is mainly due to the increase in p-n junction area.

Ryo et al. employed CSP for fabricating superstrate type $CuInS_2$ solar cells by following the structure $FTO/TiO_2/In_2S_3/CuInS_2$ [9]. Role of spray rate in the quality of $CuInS_2$ absorber layer was also studied and they observed that films deposited at high spray rate contain large quantity of carbon and oxygen. Presence of these two detoriorates the PV responses of the device. The best device fabricated under this study showed an efficiency of 1.7 %.

2.3 Device structure selected for the present study

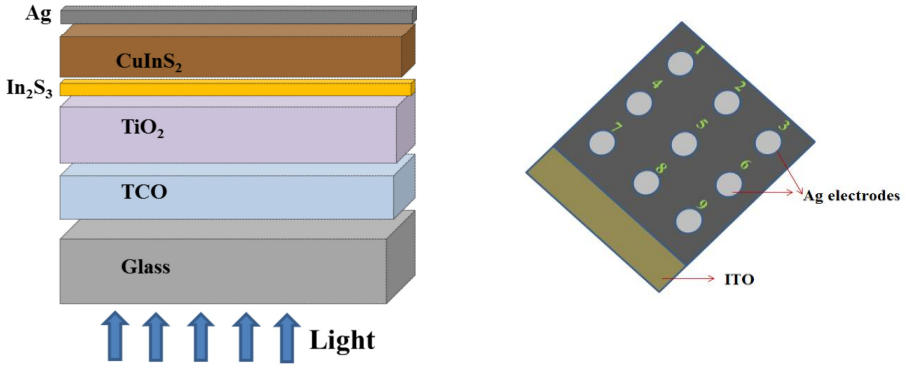

(a) (b)

Figure. 2.1(a) Schematic diagram of the fabricated device (b) Top view of the device.

A schematic diagram of the fabricated device for the present study is shown in Figure 2.1(a). TCO coated glass plate was used as the substrate. Two types of TCOs were used. Tin doped indium oxide (ITO) (sheet resistance ~ 12 Ω/□; Geomatec, Japan; prepared through sputtering) was used for the initial studies. As this material is costly, flourine doped tin oxide (FTO) was (prepared through CSP technique in our lab) used as TCO in the cell structure. Over the TCO layer microporous elctron conducting layer was spray deposited using commercially available TiO_2 powder (Degussa p25). Spraying helped the In_2S_3 buffer layer and $CuInS_2$ absorber layer to infiltrate into the micropores of TiO_2. Regarding the absorber layer, $CuInS_2$ is a best choice because of its direct band gap of 1.5 eV and high absorption coefficient of 10^5 cm^{-1} [10, 11]. In_2S_3 buffer layer has a critical role in the performance of the device. Large number of electronic interface states exists at $TiO_2/CuInS_2$ junction, which lies in the band gap of $CuInS_2$ and promotes the back flow of electrons [8]. A buffer layer between $CuInS_2$ and TiO_2 can be used to avoid this process. CdS

and In_2S_3 are good choices for buffer layers with $CuInS_2$ [12, 3]. Due to the toxicity of CdS, In_2S_3 was preferred for the present study. Moreover, the conduction bands of In_2S_3 and $CuInS_2$ have approximately same energy and hence electrons can cross the interface of $CuInS_2$ and In_2S_3 without enegy loss [3]. Finally, for top contact, silver was vacuum evaporated over the cell structure. Here silver was deposited as an array of 9 electrodes each having area of 0.03 cm^2 and thickness of 50 nm (Figure 2.1(b)), taking care to isolate each electrode using edge of doctor-blade. Dark and illuminated J-V characteristics of the heterojunctions were recorded employing Source Measure Unit (SMU; NI PXI-1033). For illumination purpose 'Class AAA' solar simulator (PET, model SS50AAA) was used.

2.4 Deposition of $CuInS_2$ absorber layer by optimising the spray rate

For spray deposition of $CuInS_2$, Cu/In ratio (in the precursor solution) and substrate temperature are the critical parameters that can affect structural, electrical, morphological and optical properties of the deposited films [13, 14]. For the present study, $CuInS_2$ thin films were deposited using precursor solution containg $CuCl_2$, $InCl_3$ and thiourea $[CS(NH_2)_2]$. Sebastian et al. observed that as Cu/In ratio increases the crystallinity of the sample improves [15]. They varied Cu/In ratio as 0.5, 1, 1.5 keeping S/Cu ratio as 5. Cu rich samples (Cu/In = 1.5) showed better crystallinity with enhanced electrical transport properties of the absorber layer. Band gap of ~ 1.35 eV for these sample is ideal for PV conversion. For precursor solution with Cu/In ratio 1.5, there is a chance of precipitation of the solution when it is kept for some time (above 45 minutes). Hence as a safer limit, Cu/In ratio was fixed as 1.4 and S/In as 5 for the deposition of $CuInS_2$ absorber layer in the present study. The variations in structural, electrical and optical properties of $CuInS_2$ thin films

with substrate temperature was also studied by Sebastian et al. [15]. Substrate temperature was varied as 300 °C, 350 °C and 400 °C. It was observed that as substrate temperature increases crystallinity improves; but at higher temperature, thickness of the samples decreases drastically due to re-evaporation of the precursor solution. As deposition rate was very low, at higher temperature, it takes long time to deposit a particular thickness of the absorber. Hence for the present study, intermediate substrate temperature of 350 °C was selected for $CuInS_2$ deposition. At 350 °C, samples possess good crystallinity and band gap of ~ 1.4 eV, favorable for a good quality absorber layer.

For $CuInS_2$ deposition, Cu/In ratio was fixed at 1.4 and substrate temperature was maintained at 350 °C. It was observed that spray rate can also play a crucial role in the deposition of $CuInS_2$. In spray pyrolysis, spray rate is generally measured as the milli liters of precursor solution sprayed on the substrate in a minute (ml/min). In order to analyse effect of spray rate on $CuInS_2$ films, it was varied as 2 ml/min, 4 ml/min, 6 ml/min and 8 ml/min; correspondingly the samples were named as S-2, S-4, S-6 and S-8 respectively. Ultrasonically cleaned soda lime glass plates were used as the substrates. Spray volume of precursors for all samples was fixed as 80 ml. Thickness of the samples were measured using stylus depth profiler (Dektak 6M). Here diamond tipped stylus is mechanically coupled to the core of a linear variable differential transformer (LVDT). As stylus rides over the sample surface, core position of LVDT changes and eletrical signals are produced which is converted to digital format. Thicknesses of S-2, S-4, S-6 and S-8 samples were 254±16 nm, 320±17 nm, 365±20 nm and 432±23 nm respectively.

2.4.1 Structural analysis

X-ray diffraction (XRD) technique was used for the structural analysis of $CuInS_2$ samples deposited at different spray rates. XRD analysis was done using Rigaku (D. Max. C) X- ray diffractometer, employing CuK_α line and Ni filter, operated at 30 kV and 20 mA. When the incident X-ray beam on the samples satisfies the Braggs condition ($n\lambda = 2d\sin\theta$, where n is the order of the spectrum, λ is the wave length of X-ray, θ is the Bragg angle and d is the inter planar spacing), it gets diffracted to the detector and an XRD pattern is recorded. Figure 2.2 depicts the XRD patterns of $CuInS_2$ samples deposited with different spray rates. In order to get information about different crystallographic phases and preferred orientations, the data is compared with Joint Council Powder Diffraction (JCPDS) data for standards.

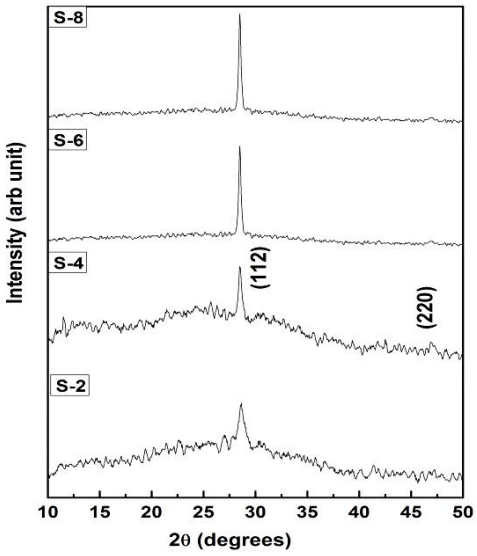

Figure. 2.2 XRD patterns of $CuInS_2$ samples prepared at different spray rates.

All samples show preferential orientation along (112) plane which is the characteristic peak of tetragonal $CuInS_2$ (JCPDS data card 270159) [11]. Intensity of XRD peaks increases as the spray rate increases. This is mainly because of the increase in thickness of the deposited samples as spray rate

increases. At lower spray rate, quantity of the solution hitting the substrate in a minute is very small and hence the deviation in substrate temperature from the preset value is negligible. As a result, re-evaporation is predominent leading to low thickness. But at higher spray rate, the deviation in substrate temperature is significant and possibility of re-evaporation is low. Deposition rate is high at higher spray rate and the samples are thicker when compared to those prepared at lower spray rate for the same volume of the precursor solution.

2.4.2 Optical studies

Optical absorption spectra of the $CuInS_2$ samples with different spray rates were recorded using UV-VIS-NIR spectrophotometer (JASCO, V-570 model). Absorption coefficient (α) is related to the energy gap (E_g) according to the equation

$$\alpha h\nu = A\,(h\nu - E_g)^n$$

where A is a constant, h the Plank's constant, ν the frequency of incident beam and n is equal to ½ for direct allowed band gap [15]. E_g can be obtained from the graph of $(\alpha h\nu)^2$ versus $h\nu$ which is illustrated in Figure 2.3. It was observed that there is not much change in the band gap (E_g) of the material with spray rate and it was around 1.4 eV. Due to high thickness of S-8 sample, it exhibits higher slope at absorption edge. Similar trend was observed for S-6 sample also.

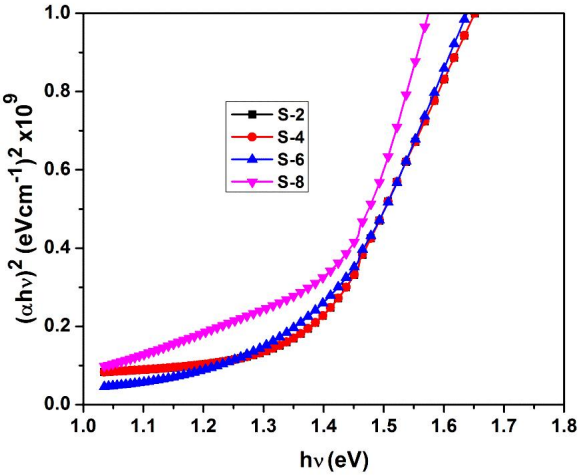

Figure. 2.3 $(\alpha h\nu)^2$ vs hν graph of $CuInS_2$ samples prepared at different spray rates.

2.4.3 Electrical studies

Electrical studies were conducted at room temperature using Hall measurement system (HMS 5300, Ecopia). Hall effect measurements in semiconductor materials give valuable information about its resistivity, carrier concentration, conductivity type and mobility of carriers. When magnetic field is applied to a semiconductor perpendicular to the current flow direction, an electric field is developed perpendicular to the direction of magnetic field and current. This phenomenon is known as Hall effect and the developed voltage perpendicular to the current flow in the sample is known as Hall voltage (V_H). V_H is proportional to carrier mobility in the sample and its sign depends on the type of the (majority) charge carrier (electrons or holes) in the sample. From the measured Hall voltage, the carrier concentration (n) of the semiconductor can be determined. In combination with conductivity (σ) measurement, the Hall mobility (μ_H) of the sample can be calculated using the equation $\mu_H = \sigma/(qn)$, where q is the charge of the carrier. The results of Hall measurements performed on the samples were tabulated in Table.1. Bulk concentration of

majority carrier is not much affected by the variations in spray rate. But as spray rate decreases resistivity of the samples increases and this may be due to the evaporation of volatile sulfur at low spray rates. This is expected because at lower spray rate substrate temperature deviation is negligible and the higher temperature allows escaping of sulfur from the sample. The sulfur vacancies create donor levels, which reduces the p-type conductivity [8, 16]. Variations in mobility values for the samples are not in order and the reason for this is not clearly understood. All samples shows p-type conductivity.

Sample	Bulk concentration (cm^{-3})	Resistivity (Ω.cm)	Mobility (cm^2/VS)	Conductivity type
S-2	$3.29x10^{19}$	10.68	$1.7x10^{-2}$	p-type
S-4	$1.87x10^{19}$	2.49	$1.34x10^{-1}$	p-type
S-6	$8.59x10^{19}$	4.84	$1.5x10^{-2}$	p-type
S-8	$6.45x10^{19}$	0.27	$3.5x10^{-1}$	p-type

Table. 2.1 Electrical studies on $CuInS_2$ samples deposited at different spray rates.

2.4.4 Atomic force microscopy (AFM) studies

For gathering a clear picture of the surface of $CuInS_2$ samples prepared at different spray rates, AFM studies were performed. A sharp tip having a diameter of less than 100 Å, fixed to a cantilever beam, scans the selected area of the sample surface. Due to the presence of inter atomic force between sample surface and the probe tip, the cantilever deflects with respect to the nature of the surface. This deflection is measured by the reflection of a laser beam from the back of the cantilever. These data are processed by computer to generate map of the topography. For the present study 'Nanosurf easyScan 2' AFM system was used. AFM studies revealed significant variations in surface

morphology of the samples deposited at different spray rates. Figure 2.4 shows AFM analysis of $CuInS_2$ samples prepared at different spray rates [10].

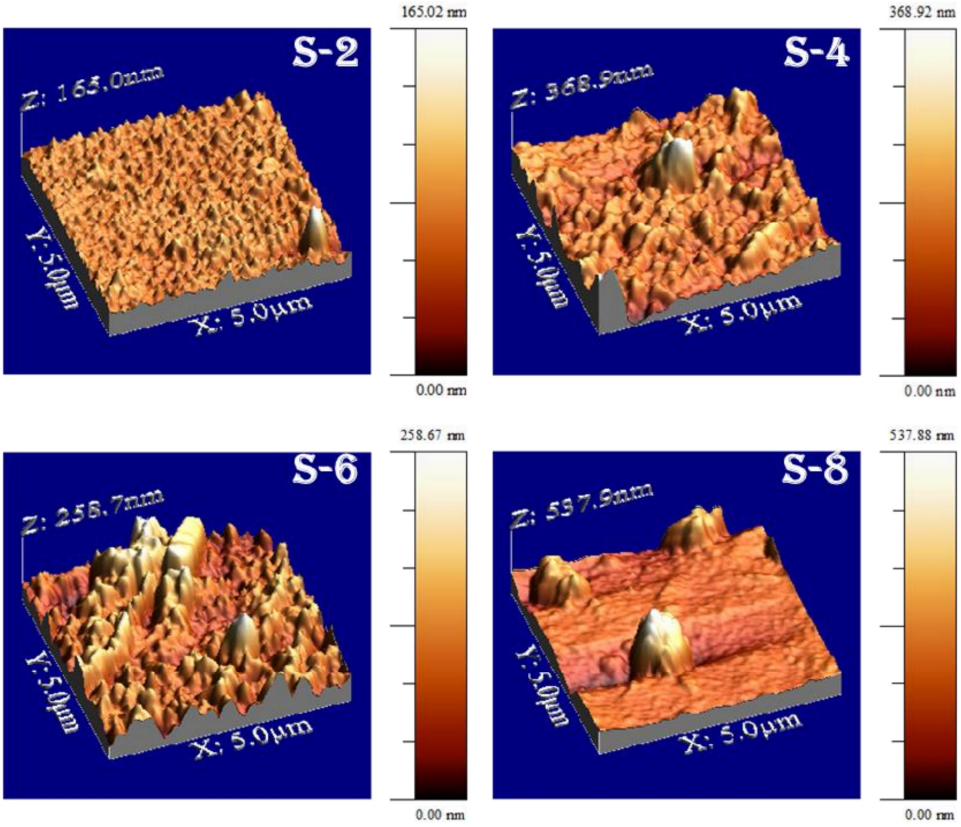

Figure. 2.4 AFM analysis of $CuInS_2$ samples deposited at different spray rates.

From AFM studies, it was observed that the root mean square (RMS) value of surface roughness of $CuInS_2$ samples increases drastically as spray rate increases. RMS surface roughness of samples sprayed at 2 ml/min was 11 nm and it increases to 61 nm for samples sprayed at 8 ml/min. Moreover, it is like a large 'hillock' and this will be present in the window layer deposited over the absorber, which is not good for the cell. For device fabrication rougher $CuInS_2$ sprayed at higher spray rate is not preferred because the probability of shorting of the device increases [10]. Moreover, at higher spray rate, time is not enough for the reaction between thiourea in the solution and oxygen in the

atmosphere to liberate gases such as NO, CO_2, SO_2 or H_2O. It was already reported that the existence of carbon and oxygen in the films will reduce the photovoltaic properties of the solar cell [9]. Hence the samples prepared at lower spray rate are expected to be good for device fabrication. However, in this case, the deposition rate is too low so that too much time is consuming for depositing a particular thickness of the absorber. Hence an intermediate spray rate of 4 ml/min having average surface roughness of 40 nm and reasonably good deposition rate was selected for device fabrication. Thus from these studies, we could conclude that optimum values for spray parameters such as Cu/In ratio, substrate temperature and spray rate were 1.4, 350 °C and 4 ml/min respectively for a good quality $CuInS_2$ absorber layer.

2.5 Deposition of In_2S_3 buffer layer

Spray deposition technique can be effectively used for the deposition of In_2S_3 buffer layer for solar cell applications [8, 10, 11]. In_2S_3 is an excellent alternative to toxic CdS buffer layer and is capable of improving the spectral response in blue wave length region. Moreover, spray deposited In_2S_3 is well-studied buffer material in our lab [10, 11, 15, 17]. For the present study In_2S_3 is prepared using $InCl_3$ and thiourea [$CS(NH_2)_2$] precursors. In/S ratio was fixed as 1.2/12. The spray rate and substrate temperature were 4 ml/min and 350 °C respectively [10, 17].

2.5.1 Structural analysis

XRD analysis shows that In_2S_3 film [Figure 2.5] has preferential orientation along (220) plane which is the characteristics of tetragonal β-In_2S_3 thin films [15]. $CuInS_2$ is also tetragonal crystal structure; hence the lattice mismatch during junction fabrication is not a big problem here.

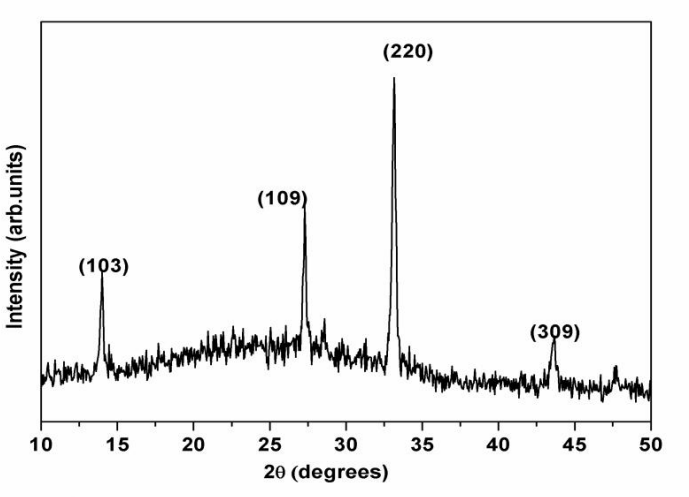

Figure. 2.5 XRD pattern of sprayed In_2S_3 thin film.

2.5.2 Optical studies

By plotting (hν) vs $(\alpha h\nu)^2$ graphs, band gap (E_g) of In_2S_3 films were calculated (Figure 2.6). Band gap was around 2.6 eV for In_2S_3 samples.

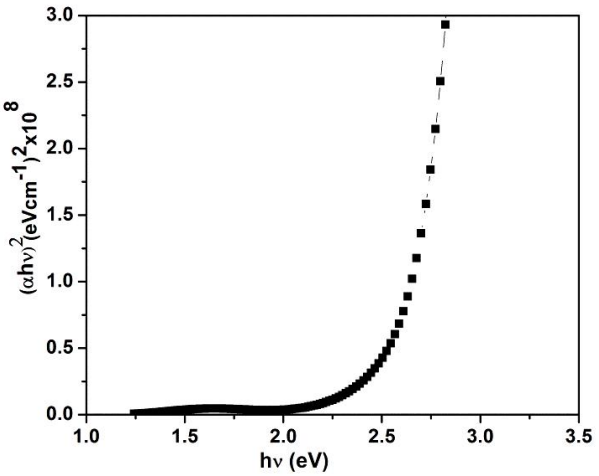

Figure. 2.6 $(\alpha h\nu)^2$ vs hν graph of In_2S_3 thin film.

2.6 Deposition of microporous TiO_2 electron conducting layer

For spray pyrolysis, most works deal with organo-metallic Ti compound precursors such as Ti tetra-ethoxide, Ti iso-propoxide, Ti acetyl acetonate and Ti isobutoxide [18]. Besides organometallic Ti compound precursors, peroxo-polytitanic acid prepared from Ti-metal powder was also used as precursor for spray deposition [19, 20]. In our case, commercially available TiO_2 powder Degussa P25 (DP25, supplied by Evonik industries, Japan with TiO_2 weight percentage 99.5) having high chemical purity was used for TiO_2 film deposition. DP25 is a mixture of anatase and rutile crystallites and was generally used as a photo catalyst [21, 22]. Initially a precursor solution of 0.125 M peroxo-titanic acid was prepared by dissolving the powder in a solution of hydrogen peroxide (H_2O_2) and ammonium hydroxide (NH_4OH) taken in the ratio 8:2. The precursor solution was then diluted to 0.025 M using distilled water and sprayed on ultrasonically cleaned soda lime glass substrate. The spray rate was maintained at 6 ml/min and substrate temperature was varied from 300 °C to 500 °C in steps of 50 °C. Samples prepared at 300 °C, 350 °C, 400 °C, 450 °C and 500 °C were named as Ti-300, Ti-350, Ti-400, Ti-450 and Ti-500 respectively [17].

2.6.1 SEM and EDAX analysis

Changes on film surfaces with deposition temperature were studied using scanning electron microscopy (SEM). SU6600 variable pressure field emission scanning electron microscope (FESEM) (Hitachi, Japan) was used for SEM analysis. At lower temperature it was observed that the adhesion of TiO_2 over the substrate was very poor and hence the films were non-uniform. From 300 ºC onwards the films had adhesion and were continuous. Samples deposited at 300 ºC composed of non-uniformly arranged aggregates (Figure

2.7(a)). As temperature was increased to 350 ºC, the aggregates arranged themselves into open porous structures [size in the range 2-6 microns] as can be seen in the Figure 2.7(b). SEM analysis of samples prepared at higher substrate temperatures 400 ºC, 450 ºC and 500 ºC (Figure 2.7(c) -2.7(e)) were not microporous in nature; instead these samples had good adhesion and homogeneity over the substrate [17].

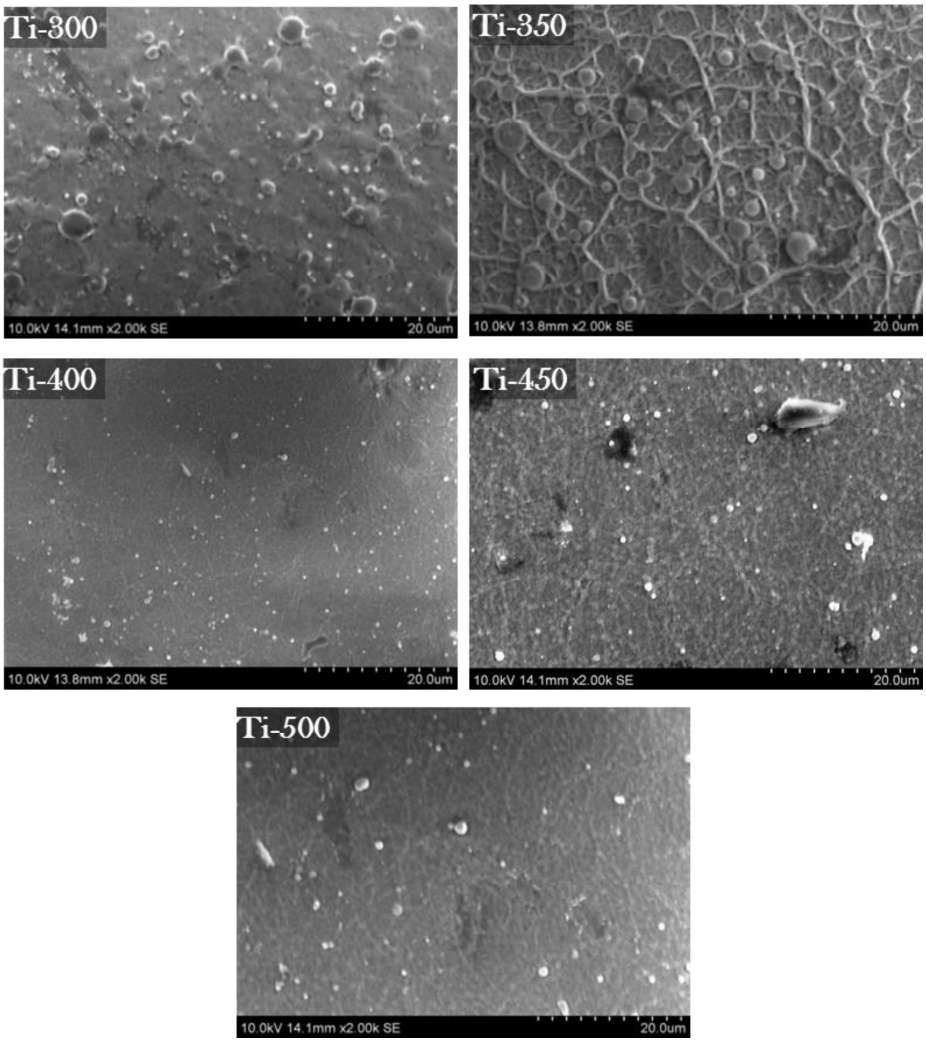

Figure. 2.7 SEM pictures of TiO_2 samples; Ti-350 [microporous].

As substrate temperature increases evaporation rate of constituents in the precursor solution also increases. Hence the composition of the deposited films has strong dependence on substrate temperature [23]. EDAX measurements showed that atomic concentration of Ti decreases on increasing the substrate temperature. As a result, thickness of the films decreased drastically. Ti-300, Ti-350, Ti-400, Ti-450 and Ti-500 samples had thicknesses of around 510 nm, 500 nm, 480 nm, 450 nm and 380 nm respectively. Above 500 °C the film surface seems to be discontinuous. Atomic concentrations of Ti and O with substrate temperature were depicted in Figure 2.8 [17].

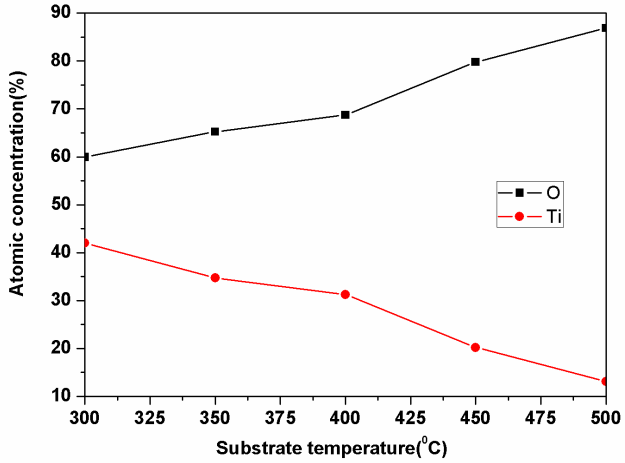

Figure. 2.8 Atomic concentration of titanium and oxygen in TiO_2 films vs substrate temperature [obtained from EDAX analysis].

2.6.2 AFM analysis

AFM analysis indicates that RMS surface roughness of the samples decreases with increase in substrate temperature (Figure 2.9). For Ti-300 samples RMS roughness was 321 nm which decreases to 55 nm for Ti-500 samples. The highly inter connected microporous structure at 350 °C is also evident from 2D AFM images of Ti-350 samples (Figure 2.10). The open

microporous structure is unique to the samples prepared at substrate temperature 350 ºC and hence the study reveals that porosity of the films strongly depends on substrate temperature [17].

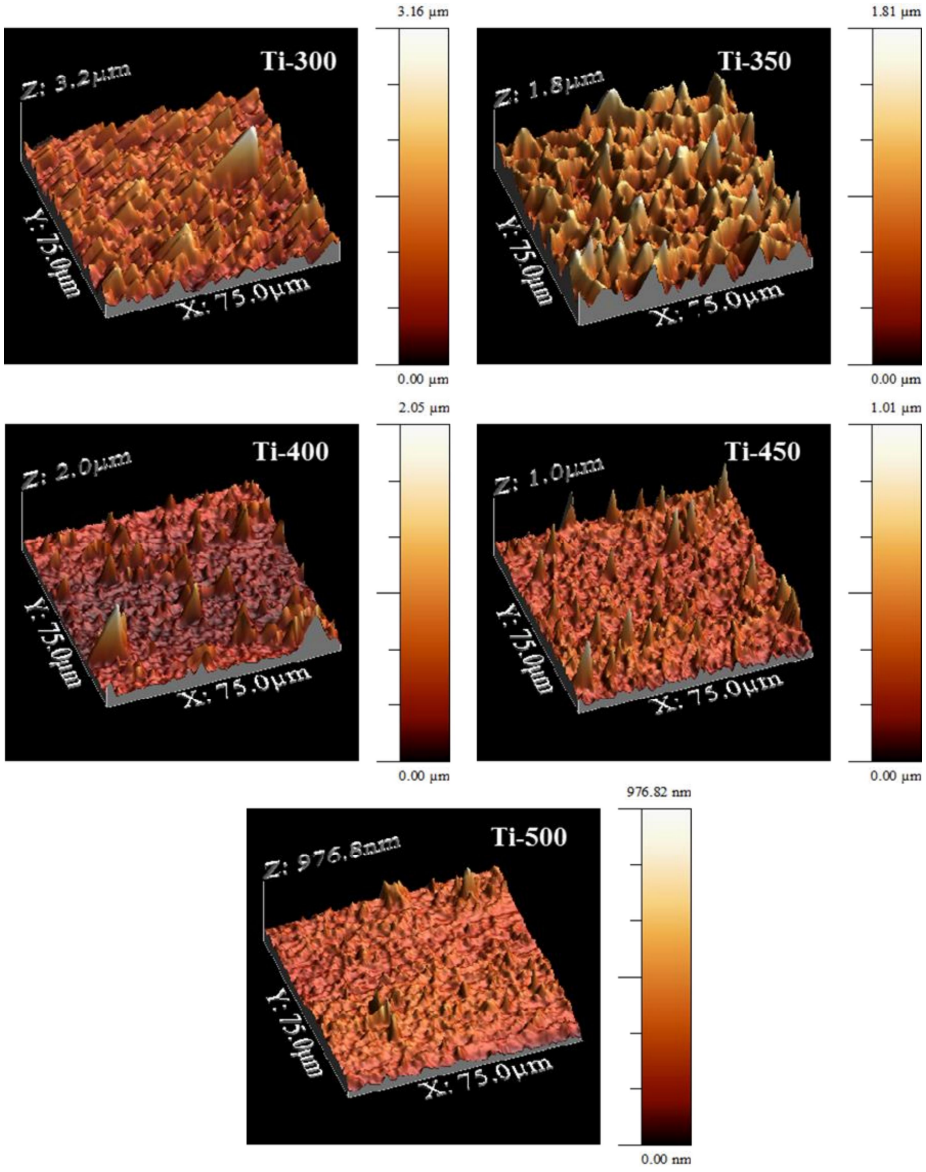

Figure. 2.9 AFM analysis of TiO_2 samples deposited at different substrate temperatures.

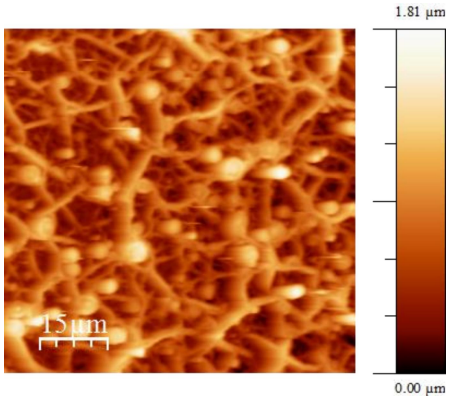

Figure. 2.10 2D AFM image of Ti-350 sample.

SEM analysis clearly indicated the microporous nature of TiO_2 films at 350 °C and EDAX analysis shows that the films are nearly stoichiometric. Results of both SEM and EDAX indicate that Ti-350 samples can be good candidates for solar cell application. Moreover, In_2S_3 buffer layer and $CuInS_2$ absorber layer were also prepared at 350 ºC. This is very important as far as device fabrication at industrial level is concerned since there is no need to change the substrate temperature for each layer fabrication [17]. Thus cell fabrication in this study was very fast and can be completed in one stretch process. For the remaining studies, only Ti-350 samples were selected. But it was almost amorphous in nature as revealed by XRD analysis. In order to improve crystallinity of the samples for device application, air annealing was carried out at 400 °C for 1 hour (Ti-1), 2 hour (Ti-2) and 3 hour (Ti-3). 'Ti-p' represents the sample before annealing. Even after annealing the films are microporous in nature with no significant changes in the pore size.

2.6.3 XRD analysis

XRD analyses of TiO_2 samples with and without annealing are shown in Figure 2.11. After annealing, samples exhibit strong XRD peaks along (101), (112), (200) and (105) planes. In all cases, preferential orientation is

along (101) plane, which is the characteristics of tetragonal anatase phase TiO_2 [24]. Also after 1 hour of annealing grain size of the sample is 30 nm. On increasing annealing time further by 1 hour, grain size improves to 40 nm. Thereafter, further improvement in grain size is not observed.

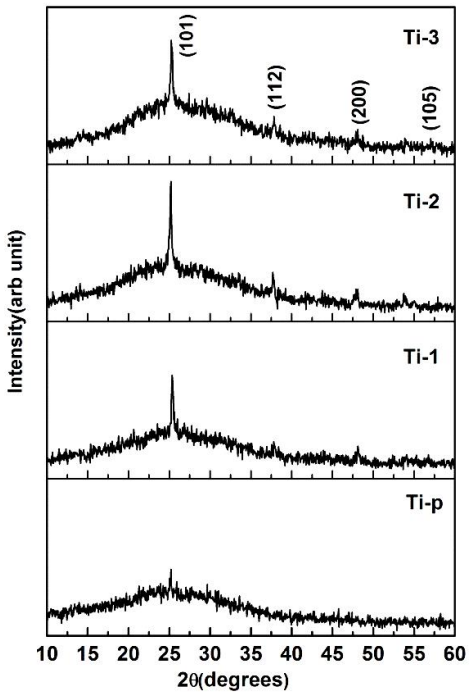

Figure. 2.11 XRD analysis of as-prepared and annealed TiO_2 samples.

2.6.4 Raman analysis

Raman spectroscopy can be used as an effective tool for structural characterization of semiconductors. Here samples are illuminated with a laser in the visible, near infrared, or near ultraviolet range. As the laser light interacts with atomic/molecular vibrations (phonons) or other excitations in the samples, energy of the laser photons is shifted up or down. This shift in energy of monochromatic light due to the inelastic scattering or Raman scattering in the sample gives information about the vibrational modes in the system. Here

Raman analyses of the prepared samples were recorded using Horiba Jobin Yvon Lab Ram HRsystem at spatial resolution of 2 mm in a 'back scattering' configuration. The 514.5 nm line of argon ion laser was used for excitation. Raman scattering spectrum of the as-prepared and annealed TiO_2 samples is shown in Figure 2.12. Before annealing, low frequency E_g mode at 144 cm^{-1} only existed. This indicates the existence of anatase TiO_2 phase [2]. On annealing, intensity of E_g mode at 144 cm^{-1} increased, indicating structural improvement. This result is in good agreement with XRD analysis. Besides E_g mode at 144 cm^{-1}, annealed samples clearly shows four other modes i.e., E_g mode at 196 cm^{-1}, B_{1g} mode at 397 cm^{-1}, A_{1g} mode at 518 cm^{-1} and E_g mode at 638 cm^{-1}.

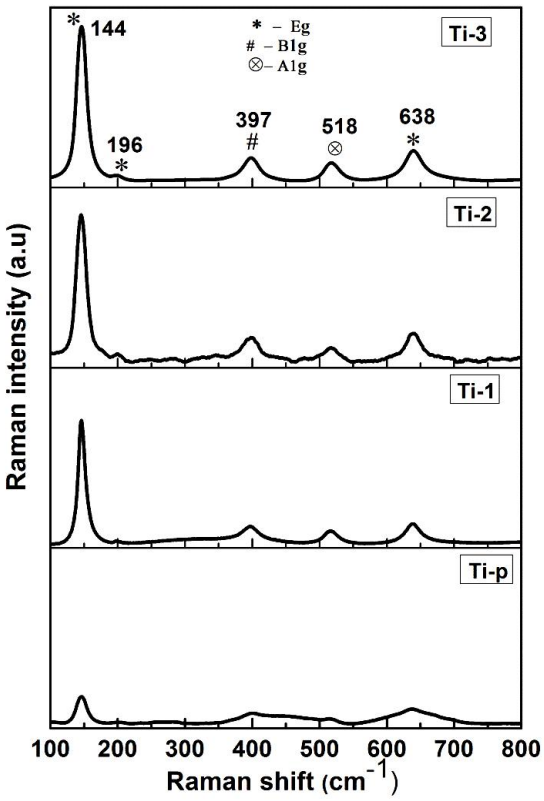

Figure. 2.12 Raman analysis of as-prepared and annealed TiO_2 samples.

2.6.5 Optical studies

Optical response of the as-prepared and annealed samples were investigated by plotting $(\alpha h\nu)^2$ vs hν graphs (Figure 2.13). On annealing, there was not much variation in the band gap of the samples. It was always around 3.4 eV.

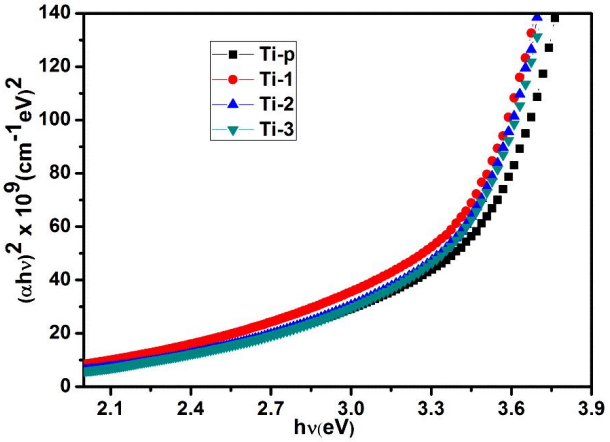

Figure. 2.13 $(\alpha h\nu)^2$ vs hν graph of as-prepared and annealed TiO_2 sample.

2.6.6 AFM analysis

Figure 2.14 shows AFM analysis of the as-prepared and annealed samples. It was observed that the RMS value of roughness of as-prepared samples (261 nm) increases to 309 nm as annealing time increased by 1 hour. It was increased to 322 nm for Ti-2 samples, thereafter it starts decreasing to 268 nm for samples Ti-3. It was further observed that even after 3 hours of annealing at 400 °C, sample is microporous in nature. Therefore annealing of spray pyrolysed TiO_2 samples for 1 hour and 2 hour results in increase of the crystallinity as well as surface roughness. TiO_2 samples with higher surface roughness can provide higher surface area. These samples are good candidates as highly rough electron conducting layer for solar cell applications.

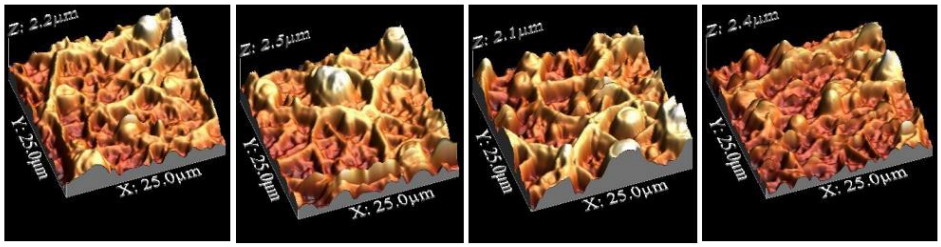

(a) (b) (c) (d)

Figure. 2.14 AFM analysis of (a) as-prepared (b) Ti-1 (c) Ti-2 (d) Ti-3 samples.

2.6.7 XPS analysis

Ti-2 samples are finally selected for device fabrication. To analyse the chemical state and concentration of each element across the thickness of the sample, depth profile measurements were carried out using 'X-ray Photoelectron Spectroscopy (XPS)'. For the present study, Shimadzu XPS unit (model: AMICUS) was used for XPS analysis. 10 cycle of argon ion etching was carried out in these films. Figure 2.15 represents binding energy vs intensity spectra for Ti 2p and O 1s states in the samples after etching (50 seconds). Presence of Ti $2p_{3/2}$ peak at 460.46 eV indicates the presence of Ti^{4+} oxidation states. Binding energy peak at 466.44 eV indicates Ti $2p_{½}$ peak. The doublet separation between the $2p_{3/2}$ peak and Ti $2p_{½}$ was 5.92 eV which is in good agreement with reported value of 5.7 eV for anatase phase TiO_2 thin films deposited using MOCVD [25]. The O1s binding energy is at 532.15 eV and this indicates bonding of oxygen to tetravalent Ti ions [26, 17].

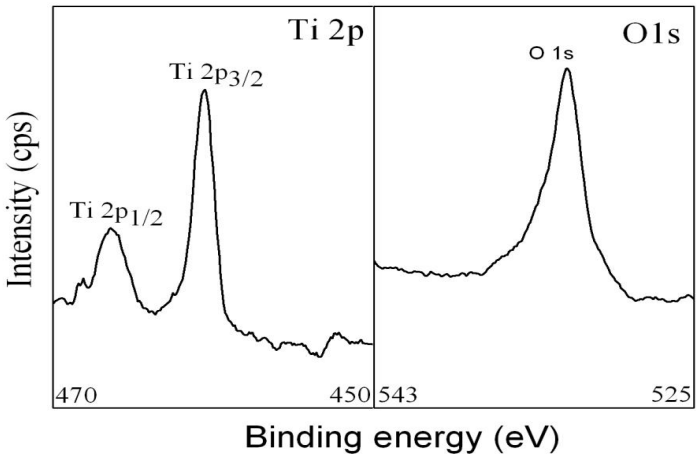

Figure. 2.15 XPS analysis of Ti 2p and O1s states in Ti-2 film.

Atomic concentration of titanium and oxygen across the thickness of Ti-2 sample were recorded using XPS depth profile analysis is shown in Figure 2.16. The sample maintains almost same stoichiometry across the thickness. Atomic concentration of titanium is ~ 75 % and that of oxygen is ~ 25 %. This was also supporting the chemical nature of TiO_2 films prepared were good for device application.

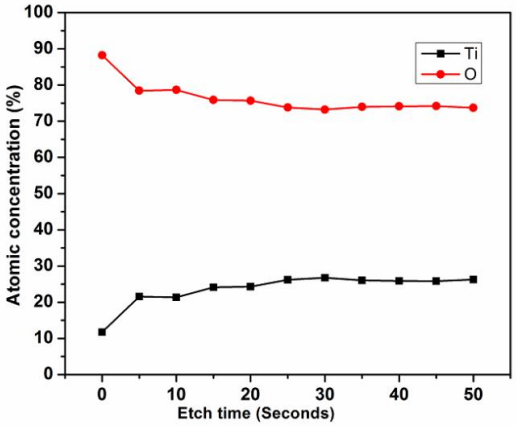

Figure. 2.16 Atomic concentration of titanium and oxygen across the thickness of Ti-2 sample.

2.7 Fabrication of FTO/TiO_2/In_2S_3/$CuInS_2$/Ag solar cells

Fluorine doped tin oxide (FTO) deposited on glass substrate (sheet resistance ~ 20 Ω/□) employing CSP is used for back contact. Microporous TiO_2 electron conducting layer, In_2S_3 buffer layer and $CuInS_2$ absorber layer as optimized in previous sections were spray deposited in a sequence over FTO layer to realise an 'all sprayed' solar cell. Finally for top contact silver was deposited (area = 0.03 cm^2) over the entire solar cell structure (see Figure 2.1(b)) using vacuum evaporation. In order to explore the effect of microporous structure on the cell performance, solar cells were fabricated using both the microporous (Ti-2) and flat structured (Ti-400 samples annealed for 2 hour at 400 °C) TiO_2 thin films and they were named as S-350 and S-400. In both cases thickness of $CuInS_2$ absorber layer and In_2S_3 buffer layer were kept constant. Thicknesses of FTO, TiO_2, $CuInS_2$, In_2S_3, Ag layers were around 300 nm, 350 nm, 200 nm, 50 nm and 50 nm respectively for both configurations [17]. Schematic diagram of the fabricated device is shown in Figure 2.17.

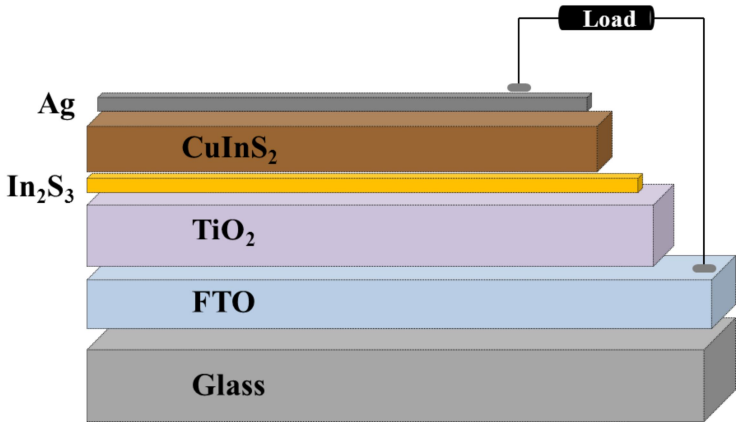

Figure. 2.17 Schematic diagram of the fabricated device.

S-400 cells showed an open circuit voltage (V_{oc}) of 350 mV and short circuit current density (J_{sc}) of 3.22 mA/cm^2. Efficiency (η) and fill factor (FF) were 0.35 % and 31 %. On the other hand, S-350 cells exhibited an improvement in device parameters with V_{oc} = 409 mV, J_{sc} = 3.90 mA/cm^2, η = 0.61 % and FF = 38 % (Figure 2.18). In this case, thin absorber layer was sprayed over microporous structured TiO_2 thin films having enhanced surface area compared to flat structured samples. Hence this configuration exhibits better light absorption due to multiple scattering in the absorber [1, 17].

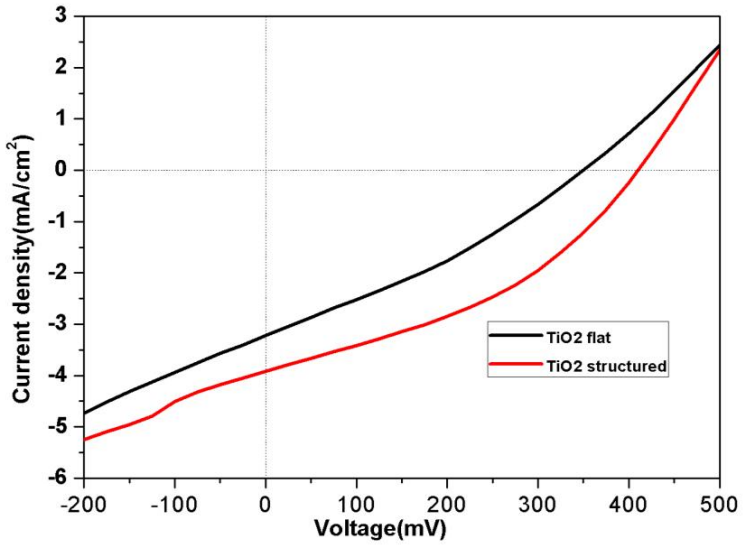

Figure. 2.18 J-V characteristics of solar cells fabricated using structured and flat TiO_2 films.

Performance parameter of the devices can also be explained on the basis of its parasitic resistances [series (R_s) and shunt (R_{sh})]. R_s and R_{sh} were calculated from the slope of the illuminated J-V characteristics at V = 0 (for R_s) and J = 0 (for R_{sh}) [27]. While comparing the performance parameters

(shown in Table 2.2) of two cells on the basis of R_s and R_{sh}, better one should have a low value for R_s and a high value for R_{sh}. For S-400 cells R_{sh} was 141 $\Omega.cm^2$ and it increased to 196 $\Omega.cm^2$ for S-350. This increase in R_{sh} may be responsible for effective charge carrier separation there by reducing alternate path for light generated carriers [28]. As a consequence of this process, V_{oc} for S-350 was 409 mV which is better value compared to that of 350 mV for S-400 cells. The series resistance value for S-350 was 45 $\Omega.cm^2$ and that of S-400 was 72 $\Omega.cm^2$. The increase in the value of J_{sc} for S-350 cells can be attributed to the decrease in series resistance. Since V_{oc} and J_{sc} enhances for S-350 cells, its efficiency and fill factor also improves [17].

Cell name	V_{oc} (mV)	J_{sc} (mA/cm^2)	FF (%)	η (%)	R_s ($\Omega.cm^2$)	R_{sh} ($\Omega.cm^2$)
S-400 (Flat)	350	3.22	31	0.35	75	141
S-350 (Microporous)	409	3.90	38	0.61	45	196

Table. 2.2 Photovoltaic parameters of S-400 and S-350 cells.

2.8 Fabrication of ITO/TiO_2/In_2S_3/$CuInS_2$/Ag solar cells

Solar cells were also fabricated by replacing FTO back contact in S-350 cells with tin doped indium oxide (ITO) contacts (sheet resistance ~ 12 Ω/□; Geomatec, Japan) prepared through sputtering. Here also the procedure for fabrication was the same. It has V_{oc} of 428 mV and J_{sc} of 7.97 mA/cm^2. The fill factor and efficiency were 34 % and 1.17 % respectively. The device exhibits better PV parameters when comparing with devices having FTO back contacts because of the lower sheet resistance of ITO films. Dark and illuminated J-V characteristics of the device are shown in Figure 2.19.

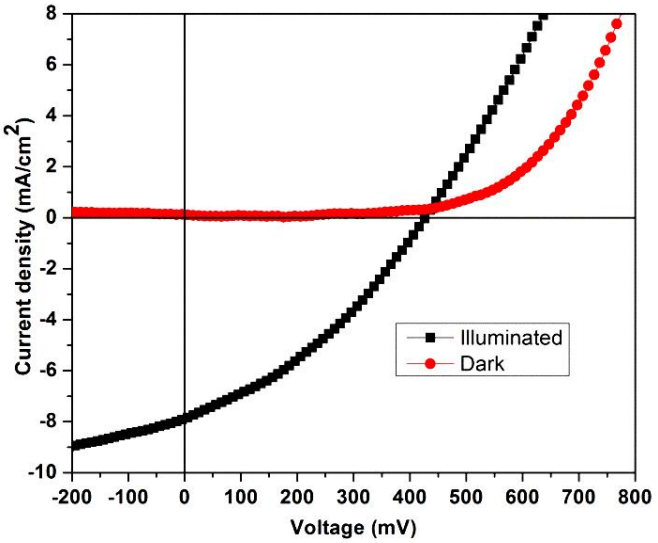

Figure. 2.19 J-V characteristics of ITO/TiO_2/In_2S_3/$CuInS_2$/Ag solar cell.
For top contact, silver was vacuum evaporated over the cell structure as an array of 9 electrodes each having an area of 0.03 cm^2, taking care to isolate each electrode using edge of doctor-blade.

2.9 Conclusions

Sprayed $CuInS_2/In_2S_3$ solar cell in superstrate configuration fabricated using spray deposited microporous TiO_2 as 'electron conducting layer'. Effect of spray rate on $CuInS_2$ absorber layer was investigated and spray rate of 4 ml/min was chosen for solar cell fabrication. For TiO_2 deposition, commercially available TiO_2 powder (Degussa p25) was used. Microporous nature of TiO_2 films was observed for a substrate temperature of 350 °C and to improve the crystallinity of this films air annealing was carried out at temperature of 400 °C. The device structure followed was FTO/TiO_2/In_2S_3/$CuInS_2$/Ag. Here FTO is also deposited employing spray pyrolysis to realize an 'all sprayed solar cells' and the device shows an efficiency of 0.61 %. Solar cells are also fabricated by replacing FTO by ITO back contact and an efficiency of 1.17 % was obtained for this configuration.

The performance of $CuInS_2/In_2S_3$ cells in superstrate configuration was not up to our expectation. Highly resistive nature of as deposited TiO_2 thin films may be the problem with this configuration. Possibilities are there to decrease the resistivity of this layer either by the further modifications in spray parameters or by doping. Since all these processes make the cell fabrication process more complex, hereafter we are restricting our studies on superstrate configurations up to this much.

References

[1] Kaiser I, Ernst K, Fischer Ch- H, Konenkamp R, Rost C, Sieber I, Luxsteiner M. Ch, Solar Energy Materials & Solar Cells, 2001, **67**, 89-96.

[2] Krunks M, Katerski A, Dedova T, Oja A I and Mere A, Solar Energy Materials & Solar Cells, 2008, **92**, 1016-1019.

[3] Nanu M, Schoonman J and Goossens A, Advanced Functional Materials, 2005, **15**, 95-100.

[4] O'Hayre R, Nanu M, Schoonman J, Goossens A, Nanotechnology, 2007, **18**, 055702 (7pp).

[5] Lenzmann F, Nanu M, Kijatkina O, Belaidi A, Thin Solid Films, 2004, **451–452**, 639-643.

[6] Nanu M, Schoonman J, Goossens A, Nano Letters, 2005, **5**, 1716.

[7] O'Hayre R, Nanu M, Schoonman J, Goossens A, Wang Q, Grätzel M, Advanced Functional Materials, 2006, **16**, 1566-1576.

[8] Goossens A, Hofhuis J, Nanotechnology, 2008, **19**, 424018.

[9] Ryo T, Nguyen D, Nakagiri M, Toyoda N, Matsuyoshi H, Ito S, Thin Solid Films,2011, **519**, 7184-7188.

[10] Santhosh M V, Deepu D R, Kartha C S, Rajeev Kumar K, Vijayakumar K P, Solar Energy, 2014, **108**, 508-514.

[11] Cherian A S, Abe T, Kashiwaba Y, Kartha C S, Vijayakumar K P, Energy Procedia, 2012, **15**, 283-290.

[12] Cho J W, Park S J, Kim W, Min B K, Nanotechnology, 2012, **23**, 265401 (6pp).

[13] Krunks M, Kijatkina O, Mere A, Varema T, Oja I, Mikli V, Solar Energy Materials & Solar Cells, 2005, **87**, 207-214.

[14] Kim J H, Yun B S, Journal of the Korean Physical Society, 2008, **53**, 2453-2457.

[15] Sebastian T, Ph.D. Thesis, Cochin University of Science and Technology, India (2009).

[16] Lewerenz H J, Solar Energy Materials & Solar Cells, 2004, **83**, 395-407.

[17] Santhosh M V, Deepu D R, Geethu R, Kartha C S, Rajeev Kumar K, Vijayakumar K P, Semiconductor Science and Technology, 2014, **29**, 115026.

[18] Natarajan C, Fukunaga N, Nogami G, Thin Solid Films, 1998, **322**, 6-8.

[19] Aoki A, Nogami G, Journal of the Electrochemical society, 1996, **143**, L191-L193.

[20] Rogers K D, Lane D W, Painter J D, Chapman A, Thin Solid Films, 2004, **446**, 97-102.

[21] Zhao C, Krall A, Zhao H, Zhang Q, Li Y, International Journal of Hydrogen Energy, 2012, **37**, 9967-9976.

[22] Hurum D C, Agrios A G, Gray K A, Journal of Physical Chemistry B, 2003, **107**, 4545-4549.

[23] Deshmukh H P, Shinde P S, Patil P S, Material Science and Engineering B, 2006, **130**, 220-227.

[24] Tang H, Prasad K, Sanjines R, Schmid P E, Levy F, Journal of Applied Physics., 1994, **75**, 2042-2047.

[25] Babelon P, Dequiedt A S, Mostefa-Sba H, Bourgeois S, Sibillot P , Sacilotti M, Thin Solid Films, 1998, **322**, 63-67.

[26] Stefanov P, Shipochka M, Stefchev P, Raicheva Z, Lazarova V, Spassov L, Journal of Physics: Conference Series, 2008, **100**, 012039.

[27] Moritake N, Fukui Y, Oonuki M, Tanaka K, Uchiki H, Physica Status Solidi. C, 2009, **6**, 1233-1236.

[28] Priyanka, Lal M, Singh S N, Solar Energy Materials & Solar Cells, 2007, **91**, 137-142.

……..✷♦✷……..

Chapter **3**

Fabrication of TCO/$CuInS_2$/In_2S_3/Ag heterojunction solar cells using single and double layer structure for the absorber layer

3.1 Introduction

The superstrate configuration of $CuInS_2$ (i.e., TCO/TiO_2/In_2S_3/ $CuInS_2$/ Ag) does not work up to our expectation, as explained in detail in last chapter. Hence trials were also conducted to fabricate solar cells without using TiO_2 thin films and followed TCO/In_2S_3/$CuInS_2$/Ag configuration with light from TCO side. Thickness of In_2S_3 was kept as low as possible to ensure that maximum light is transmitted to the $CuInS_2$ absorber layer. As we are depositing $CuInS_2$ layer over thin In_2S_3 layer it gets peeled off. On increasing buffer layer thickness, junction is formed between $CuInS_2$ and In_2S_3, but it shows feeble light activity. This is because light is not reaching up to the absorber due to the absorption in thick In_2S_3. It is to be specifically noted that here the entire device fabrication was done using automated spray pyrolysis machine having facilities to control precisely the spray parameters like spray rate, substrate temperature and spray head movement [1]. Still a working device with TCO/In_2S_3/$CuInS_2$/Ag configuration could not be fabricated. Similar observations were also made by John et al. while fabricating $CuInS_2$/In_2S_3 heterojunction using manual spray technique; this may be due to specialty of spray technique [2]. Devices are hence fabricated hereafter with TCO/$CuInS_2$/In_2S_3/Ag structure and it shows photo activity. This structure is used for further studies in this chapter.

3.2 ITO/$CuInS_2$/In_2S_3/Ag solar cell fabrication and characterization

A schematic diagram of the fabricated device is shown in Figure 3.1(a). ITO films coated glass (sheet resistance ~ 12 Ω/□, Geomatec, Japan; deposited employing sputtering) was used as the substrate in this work. Over ITO, $CuInS_2$ absorber and In_2S_3 buffer layer were spray deposited using the optimized spray conditions as explained in chapter 2. Finally, for top contact, silver is vacuum evaporated over the cell structure. Silver is a good choice for top electrode in $CuInS_2$/In_2S_3 heterojunction solar cells as it improves the crystallinity of In_2S_3 thin films [3]. Dark and illuminated J-V characteristics of the heterojunctions were recorded using source measure unit (NI PXI-1033). For illumination purpose 'Class AAA' solar simulator (PET, model SS50AAA) was used.

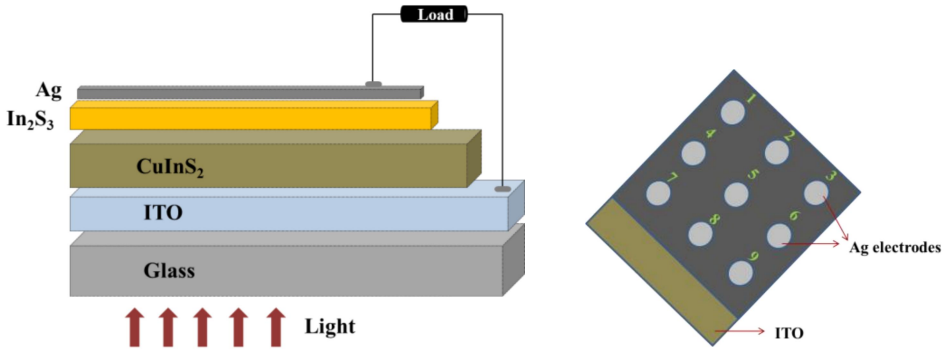

(a) (b)

Figure. 3.1(a) Schematic diagram of the fabricated device (b) Top view of the device.

3.2.1 Effect of $CuInS_2$ absorber layer thickness on solar cell performance

Absorber layer in a solar cell absorbs sunlight and coverts the electromagnetic energy of sunlight to the energy of electron hole pairs. Hence

thickness of the absorber layer is crucial parameter that can influence the overall performance of the device. The absorber layer should possess enough thickness to absorb maximum amount of light. At the same time, thickness of the absorber should be comparable with minority carrier diffusion length to ensure effective charge carrier collection [4, 5]. Hence there should be an optimum thickness for the absorber layer. In this study absorber layer thickness was varied simply by adjusting the spray volume of the precursor solution. Buffer layer thickness (~ 300 nm) was kept constant for all trials. Top contact silver was deposited as an array of 9 electrodes, each having area of 0.03 cm^2 and thickness of 50 nm (Figure 3.1(b)) for all devices, which were isolated by curving around each electrode, using doctor-blade. Five samples were prepared for each thickness of the absorber layer (i.e. total of 45 cells were considered for each thickness in this study). The photovoltaic (PV) parameters like V_{oc}, J_{sc}, fill factor and efficiency were measured for each sample. Average value, (along with upper and lower limit values) of these parameters for each thickness of the absorber is tabulated in Table 3.1.

Spray volume(ml)	Thickness of $CuInS_2$ (nm)	V_{oc} (mV)	J_{sc} (mA/cm^2)	Fill factor (%)	Efficiency (%)
48	150±10	408±30	6.52±1.98	37±4	1.02±0.28
60	210±14	448±26	9.74±0.89	42±2	1.84±0.30
72	**320±18**	**481±11**	**11.13±1**	**44±3**	**2.33±0.26**
84	370±20	467±17	7.66±1.64	45±5	1.61±0.25
96	440±25	393±50	6.45±1	31±6	0.78±0.31

Table. 3.1 Performance parameters of the device with different absorber layer thickness.

As absorber layer thickness increases from ~ 150 nm to 320 nm, an overall improvement in performance parameters can be observed. Average values of V_{oc} improves from 408 to 481 mV, J_{sc} improves from 6.52 to 11.13 mA/cm^2, fill factor improves from 37 to 44 % and efficiency improves from

1.02 to 2.33 %. But for devices with thickness of absorber layer above ~ 320 nm, the PV parameters start decreasing. In our case, light reaches the junction through absorber side and hence more absorption will be naturally near ITO-absorber interface. If thickness of the absorber was very high (above 320 nm), light generated carriers far away from the junction will find it difficult to reach the junction due to losses because of recombination and/or other losses. This may be the reason for poor functioning of the devices with absorber layer thickness above 320 nm. Best efficiency range (2.33 ± 0.26 %) was observed for device with an absorber layer thickness of 320 ± 18 nm. Out of the measurements from 45 cells (five different trials) of this configuration, 25 cells (55 % of total cells) exhibited this efficiency range.

3.2.2 Effect of buffer layer thickness on solar cell performance

In $CuInS_2/In_2S_3$ heterojunction, diffusion of Cu from $CuInS_2$ to In_2S_3 buffer layer was an easy process due to the high mobility of Cu ions [6, 7]. As a result of this diffusion, a portion of In_2S_3 buffer layer, near to $CuInS_2$ layer, gets converted to $CuInS_2$. Hence, if the buffer layer thickness is too low, Cu diffusion becomes significant reaching top of the buffer layer and the device gets shorted. For higher thickness of the resistive buffer layer (~ 10^3 Ω.cm), series resistance of the device increases which adversely affect the current obtained from the device [8, 9]. Hence there should be an optimum thickness of buffer layer for better performance of $CuInS_2/In_2S_3$ heterojunction. In the next step, In_2S_3 buffer layer thickness was varied above and below 300 nm by adjusting the spray volume of the precursor solution. Here absorber layer thickness was kept constant around 320 nm, which is fixed from the above studies. Five samples were prepared for each thickness of the buffer layer. Average value (along with upper and lower limit values) of PV parameters for each thickness of the buffer layer is tabulated in Table 3.2.

Spray volume (ml)	Thickness of In_2S_3 (nm)	V_{oc} (mV)	J_{sc} (mA/cm^2)	Fill factor (%)	Efficiency (%)
16	230±15	413±39	8.76±0.99	38±4	1.46±0.23
24	**300±10**	**481±11**	**11.13±1**	**44±3**	**2.33±0.26**
32	410±25	498±8	7.83±1.16	40±2	1.58±0.31

Table. 3.2 Performance parameters of the device with different buffer layer thickness.

By varying buffer layer thickness above or below 300 nm, there is no improvement in the efficiency of the device. At lower thickness (~ 230 nm) of the buffer layer, Cu diffusion may be prominent which can reduce the PV parameters. At higher thickness, due to the resistive nature of In_2S_3 buffer layer, series resistance of the device increases [8]. As a result, the average value of current decreases from 11.13 to 7.83 mA/cm^2.

One can conclude from the studies that the absorber layer thickness should be ~ 320 nm and buffer layer thickness should be ~ 300 nm for the better performance of ITO/$CuInS_2$/In_2S_3/Ag heterojunction solar cells. The best device under this study has V_{oc} = 478 mV, J_{sc} = 12.13 mA/cm^2. Fill factor and efficiency are 45 % and 2.59 % respectively. The illuminated J-V characteristics of the best device fabricated is shown in Figure 3.2.

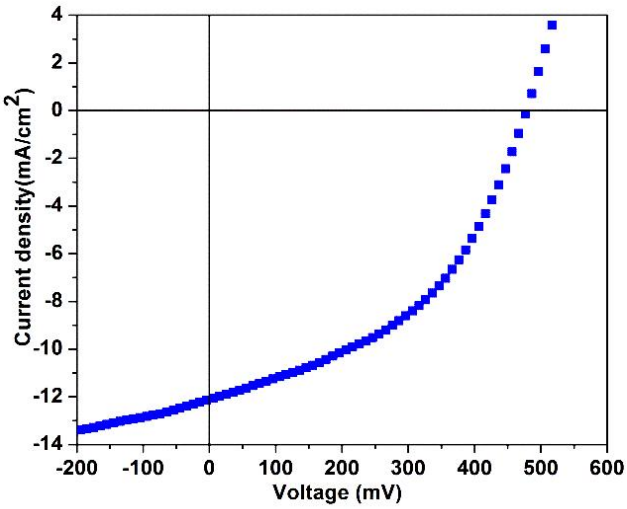

Figure. 3.2 J-V characteristics of ITO/$CuInS_2$/In_2S_3/Ag solar cell.

3.2.3 XPS depth profile analysis of the device

XPS depth profile analysis of the fabricated solar cell was carried out to determine chemical state of elements across the thickness of the cell. Here argon ion sputtering was employed for layer by layer etching of the solar cell. The information collected from each layer is represented as series of peaks corresponding to binding energies of valence electrons of each element; one such graph is denoted as an 'etching cycle' in Figure 3.3. The lowest value/beginning of Y-axis represents the surface of the solar cell (In_2S_3 portion) and top represents the substrate.

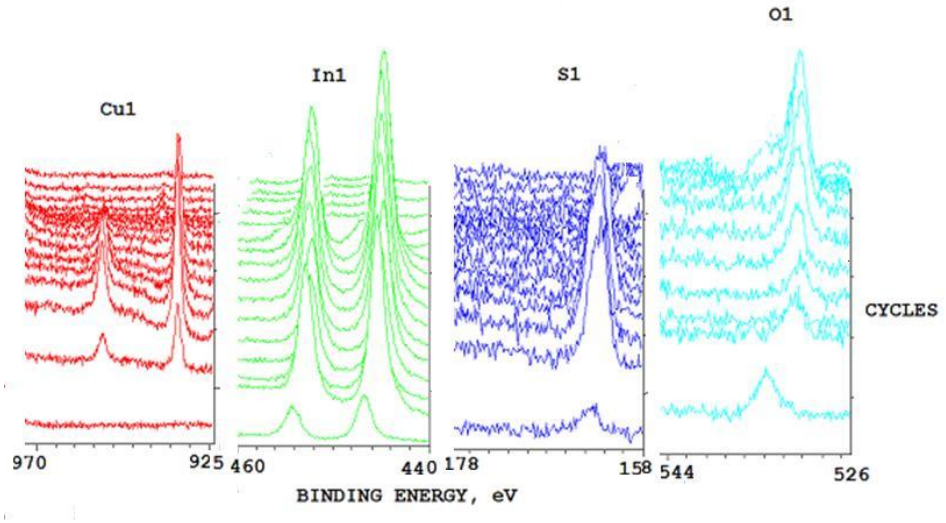

Figure. 3.3 XPS depth profile analysis of ITO/$CuInS_2$/In_2S_3/Ag solar cells.

In order to collect information about the chemical states of copper, indium, sulfur and oxygen across the thickness of the device, 250 cycles of Ar ion sputtering was done. Binding energy (B.E) peaks at 932 eV ($2p_{3/2}$) and 952 eV ($2p_{1/2}$) correspond to that of copper [10]. Presence of indium is confirmed by the B.E peaks at 445.2 eV ($3d_{5/2}$) and at 454 eV ($3d_{3/2}$). B.E peak at 162.32 eV corresponds to S $2p_{3/2}$ [11]. Presence of oxygen is also observed inside the device. B.E of oxygen at the surface of the sample was 534 eV and that in the sample was 531 eV. This shift in B.E of oxygen is due to the substitution of sulfur in the surface of the device by oxygen to form sulfate [2]. This process can be inferred by the decrease in peak height of sulfur and increase in peak height of oxygen at the surface of the device.

Lower portion of the graph (beginning of Y-axis) represents In_2S_3 portion. For device fabrication thicker (~ 300 nm) In_2S_3 was used. XPS analysis shows that pure In_2S_3 was present only for one etching cycle of the device. From the second etching cycle onwards, binding energy peaks

correspond to Cu was observed in In_2S_3 buffer layer, which indicates the diffusion of Cu from $CuInS_2$ absorber layer to In_2S_3. Cu has high diffusion coefficient [12], moreover, the device fabrication is at a temperature of 350 °C i.e., the circumstances are favoring diffusion of Cu from $CuInS_2$. As result of this Cu diffusion, some portion of the In_2S_3 buffer layer converted to $CuInS_2$, which reduces the effective buffer layer thickness in the cell structure. Even the device may get shorted for lower buffer layer thicknesses. Hence Cu diffusion is observed to be a major deterioration factor that limits the performance of $CuInS_2/In_2S_3$ heterojunction solar cells.

3.2.4 Cross sectional SEM of the device

The cross sectional SEM of one of the sample in the efficiency range 2.33 ± 0.26 % is shown in Figure 3.4. SEM analysis was performed without coating the top Ag electrodes.

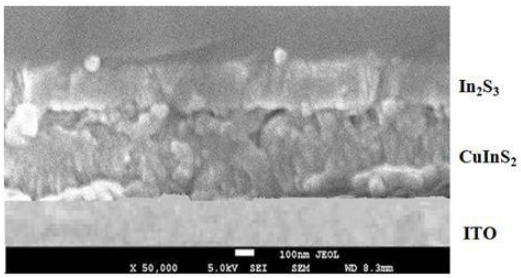

Figure. 3.4 Cross sectional SEM image of ITO/$CuInS_2$/In_2S_3/Ag solar cell.

Individual layers in the cell structure are well distinguished from the SEM image. As discussed in section 3.2.1 and 3.2.2, the expected thicknesses of absorber and buffer layer were ~ 320 nm and 300 nm respectively. XPS depth profile analyses of the device clearly indicate Cu diffusion from absorber to buffer layer, which can convert some portion of In_2S_3 to $CuInS_2$. Cross sectional SEM measurement of the device shows that, after all inter diffusion

processes in the cell structure, thicknesses of $CuInS_2$ absorber layer and In_2S_3 buffer layer were ~ 400 nm and ~ 200 nm respectively.

3.2.5 Fabrication of large area (2.5 x 2 cm^2) device

In order to prove the capability of CSP for the fabrication of large area solar cell, $CuInS_2$ absorber and In_2S_3 buffer layers were deposited in sequence over an ITO coated glass substrate having 3 x 3 cm^2 area. The deposition parameters for $CuInS_2$ and In_2S_3 were kept same as that of best cell obtained in an area of 0.03 cm^2. Over this structure silver back contact was deposited in an area of 2.5 x 2 cm^2 by vacuum evaporation. External connections are made possible using copper wires. Silver paste was used for fixing this wire at a corner of the silver electrode. Outdoor measurements (carried out in sunlight intensity of 50m W/cm^2) showed short circuit current of 10.15 mA and V_{oc} of 416 mV (Figure.3.5) [13].

Figure. 3.5 Outdoor measurements of ITO/$CuInS_2$/In_2S_3/Ag solar cells with an active area of 5cm^2 to study the performance of the device under direct sunlight.

The indoor measurement of the device was also recorded using class AAA solar simulator. The device showed V_{oc} of 432 mV and J_{sc} of 6.33 mA/cm^2. Fill factor and efficiency were 34 % and 0.94 % respectively [13].

The performance parameters are low for large area devices when comparing with small area device (area = 0.03 cm^2) having same spray deposition parameters for individual layers. This is because in large area cells, the external connection from the solar cell is taken from a corner of the silver electrode. This will increase the series resistance of the device and adversely affects all PV parameters [14]. The PV parameters of the device were also monitored for 100 days. Table 3.3 shows the variation in PV parameters with time. It is to be noted that the cell was kept in ordinary atmosphere without any protective coatings [13].

Days	V_{oc} (mV)	J_{sc} (mA/cm^2)	Fill factor (%)	Efficiency (%)	R_s ($\Omega. cm^2$)	R_{sh} ($\Omega. cm^2$)
1	432	6.33	34	0.94	34	125
20	395	5.95	32	0.75	37	125
40	386	5.50	33	0.71	53	166
60	372	5.28	32	0.63	50	143
80	350	4.9	32	0.54	50	119
100	301	4.19	26	0.33	63	76

Table. 3.3 Photovoltaic parameters of the large area device with time.

Even after 100 days, the device works with an efficiency of 0.33 %, which was 0.94 % for freshly prepared device. After 100 days, V_{oc} of the device decreased to 301 mV from 432 mV and J_{sc} decreased to 4.19 mA/cm^2 from 6.33 mA/cm^2 [13]. The percentage decreases in V_{oc}, J_{sc}, fill factor and efficiency were 30.3 %, 33.8 %, 23.5 % and 64.9 % respectively. The decrease in PV parameters with time can explain on the basis of series (R_s) and shunt resistances (R_{sh}). With ageing, silver top electrode can be diffused to In_2S_3 buffer layer as a result the contact resistance (series resistance) of the device

increased drastically from 34 to 63 Ω.cm^2 after 100 days [15]. On the other hand shunt resistance decreases from 125 to 76 Ω.cm^2. As the device was kept in open atmosphere, there was a possibility of getting impurities in to the cell, which can promote the recombination of light generated carriers [16]. It should be noted that the device maintains almost same fill factor (~ 33 %) up to 80 days, which indicates the quality of the device.

3.2.6 Fabrication of 'all sprayed' solar cells

Sputtered ITO back contact in the device structure was replaced with FTO films (thickness = 300 nm, sheet resistance = 20 Ω/□, transparency of 75 % in the visible region) prepared through spray pyrolysis, in our own lab. Thus by spray depositing the buffer, absorber, and back contact, we were able to fabricate an 'all sprayed' solar cell. A schematic diagram of the fabricated device is shown in Figure 3.6.

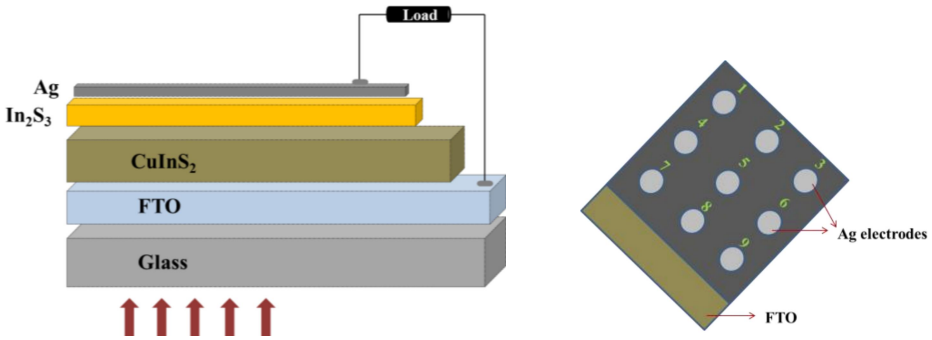

Figure. 3.6 (a) Schematic diagram of all sprayed $CuInS_2$/In_2S_3 solar cell (b) Top view of the device.

For $CuInS_2$ deposition over FTO, Cu: In: S ratio was 1.4: 1: 5 and spray rate was fixed at 4 ml/min. It was observed that, at 350 °C (optimized temperature for $CuInS_2$ deposition over ITO surface) adhesion of $CuInS_2$ over FTO was very poor. Hence initially the substrate temperature was reduced to 275 °C for improving the adhesion of $CuInS_2$ over FTO and the thickness of this layer was ~ 100 nm. After this, substrate temperature was set at 350 °C for further deposition of $CuInS_2$. In_2S_3 buffer layer was then spray deposited over $CuInS_2$ and the spray parameters were kept same as discussed in section 2.5. The optimized thicknesses for $CuInS_2$ absorber layer and In_2S_3 buffer layer for this configuration was ~ 500 nm and ~ 200 nm respectively. Finally silver electrodes are deposited by vacuum evaporation over this cell structure for top contact. Nine silver electrodes each having an area of 0.03 cm^2 and thickness of 50 nm were deposited (Figure 3.6 (b)). The best device in this study shows a V_{oc} of 457 mV and J_{sc} of 5.45 mA/cm^2. The fill factor and efficiency are 38 % and 0.94 % respectively [17]. Dark and illuminated J-V characteristics of the device are shown in Figure 3.7. On comparing with best cell fabricated on ITO back contacts (section 3.2.2), the percentage decreases in J_{sc}, V_{oc} and fill factor for the 'all sprayed' solar cells are 55 %, 4.4 % and 15.5 % respectively. Higher value of sheet resistance (20 Ω/□) and low transparency (75 %) for FTO back contacts when comparing with ITO back contacts (sheet resistance of 12 Ω/□ and transparency of above 85 %) adversely affected the carrier generation and collection of all sprayed solar cells. As a result J_{sc} value is very much affected and device exhibits 63.7 % decrease in efficiency. If we can reduce the sheet resistance of FTO films, better device parameters that are equivalent to device with ITO back contacts can be achieved.

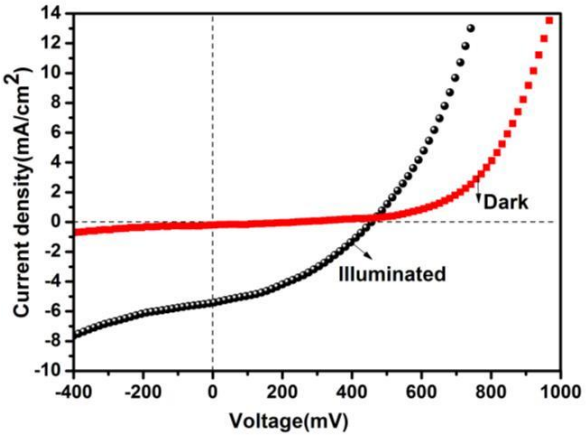

Figure. 3.7 Dark and illuminated J-V characteristics of all sprayed $CuInS_2/In_2S_3$ solar cell.

3.2.7 Effect of Al_2O_3 inter layer on the performance of $CuInS_2/In_2S_3$ solar cell

It was reported that the presence of an ultra-thin Al_2O_3 insulator coating in the cell structure can decrease the Cu diffusion in $CuInS_2$ based solar cell. This insulator coating decreases the interface recombination rate. The origin of beneficial effect of these coatings is still under discussion [18]. For the present work also Cu diffusion was observed from $CuInS_2$ absorber layer to In_2S_3 buffer layer (Figure 3.3). In order to control this Cu diffusion, ultra-thin (2 nm) insulator coating of Al_2O_3 was deposited using atomic layer deposition (ALD) as an interlayer in between $CuInS_2$ and In_2S_3 in the optimized cell configuration. Hence the device structure for the present study is ITO/$CuInS_2$/Al_2O_3/In_2S_3/Ag.

XPS depth profile analysis of the solar cell with Al_2O_3 inter layer is shown in Figure 3.8. On comparing with device without Al_2O_3 inter layer (Figure 3.3), the binding energy peaks corresponding to Cu in In_2S_3 portion is

very much reduced in devices with Al_2O_3 inter layer. Hence the copper diffusion to In_2S_3 buffer layer is very much controlled on introducing an Al_2O_3 inter layer. The J-V characteristics of the devices with and without this Al_2O_3 inter layer is shown in Figure 3.9.

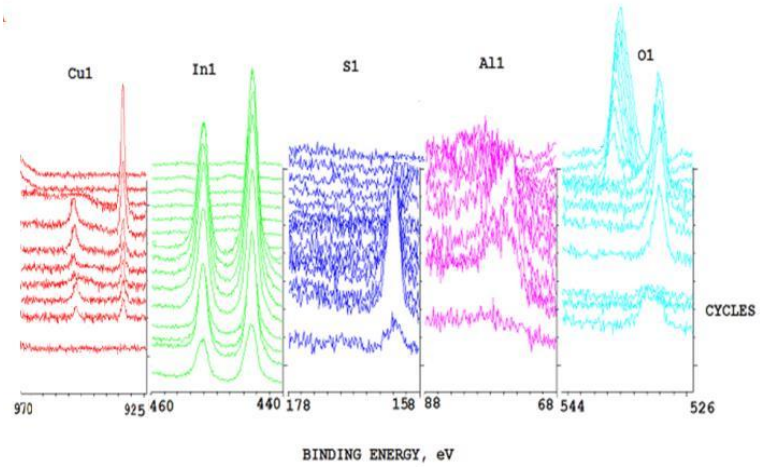

Figure. 3.8 XPS depth profile analysis of $CuInS_2/In_2S_3$ heterojunction with Al_2O_3 inter layer. Presence of peaks corresponding to B.E of Al_2O_3 layer at middle of the cell (depth-wise) is clearly visible.

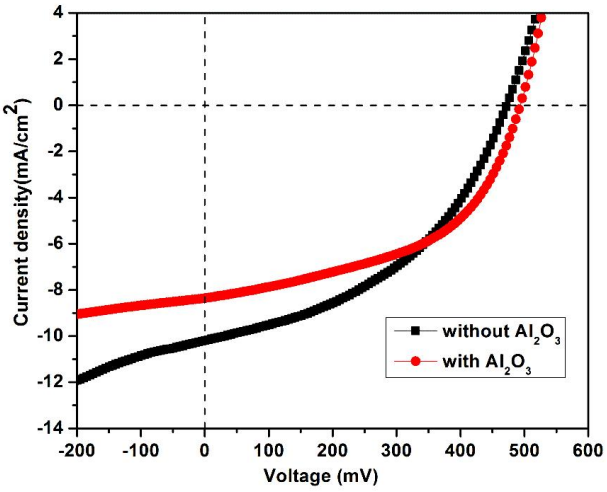

Figure. 3.9 Illuminated J-V characteristics of the $CuInS_2/In_2S_3$ heterojunction with and without Al_2O_3 inter layer.

For device with Al_2O_3 inter layer V_{oc} increases only by a small value (to 484 mV from 473 mV) and fill factor improves from 44 % to 50 %. This is due to the increase in shunt resistance of the device from 151 $\Omega.cm^2$ to 250 $\Omega.cm^2$, which reduces the recombination rate of light generated carriers [19, 20]. But due to the presence of Al_2O_3 insulator layer, J_{sc} value decreased to 8.34 mA/cm^2 from 10.16 mA/cm^2. In effect, the efficiency values for both configurations are almost same (i.e., 2.1 % and 2 %). The PV parameters for the two configurations are tabulated in Table 3.4.

	V_{oc} (mV)	J_{sc} (mA/cm^2)	FF (%)	η (%)	R_s ($\Omega.cm^2$)	R_{sh} ($\Omega.cm^2$)
Without Al_2O_3	473	10.16	44	2.1	14	151
With Al_2O_3	484	8.34	50	2	10	250

Table. 3.4 PV parameters of device with and without Al_2O_3 inter layer.

3.3 Double layered $CuInS_2$ for ITO/$CuInS_2$/In_2S_3/Ag solar cells.

On introducing an ultra-thin insulator interlayer of Al_2O_3 in the cell structure, Cu diffusion to In_2S_3 buffer layer was reduced and the device showed significant improvement in fill factor. Al_2O_3 inter layer for the device was prepared using atomic layer deposition (ALD). By combining CSP and ALD for cell fabrication, the overall deposition process becomes sophisticated and not cost effective. Hence we thought of utilizing CSP technique itself to deposit a resistive $CuInS_2$ layer in the cell structure instead of Al_2O_3 insulator layer. Resistivity of $CuInS_2$ layer can be manipulated by reducing Cu/In ratio in the precursor solution [17, 21-23]. The resistive, "Cu-poor" $CuInS_2$ inter layer can accommodate the diffused Cu ions from the absorber layer. As a

result, Cu diffusion to In_2S_3 is very much controlled and there is a probability for the existence of "Cu-free" In_2S_3 buffer layer in the cell structure. Also, by introducing this resistive inter layer near $CuInS_2/In_2S_3$ junction, probability of recombination of light generated carriers are reduced appreciably and the device can have a better value of shunt resistance (R_{sh}). For solar cell fabrication, the spray deposition conditions (on ITO layer) for $CuInS_2$ absorber and In_2S_3 buffer layer were kept same as discussed in section 3.2. The only difference is that we are introducing a resistive $CuInS_2$ inter layer with Cu: In: S ratio 0.6: 1: 5 [**17**]. Thickness of this resistive layer was varied as 40 nm, 80 nm, 110 nm and 140 nm to find the optimum thickness for the device. Here also five samples were prepared for each thickness of the inter layer. Thickness of $CuInS_2$ and In_2S_3 layers are 320 nm and 300 nm respectively for all samples. The photovoltaic parameters like V_{oc}, J_{sc}, fill factor and efficiency were monitored for each trial. Average value, (along with upper and lower limit values) of these parameters for each thickness of the inter layer is tabulated in Table 3.5.

Thickness of $CuInS_2$ inter layer (~ nm)	V_{oc} (mV)	J_{sc} (mA/cm^2)	Fill factor (%)	Efficiency (%)
40	475±22	9.64±1.48	50±9	1.98±0.29
80	**492±12**	**8.8±0.45**	**53±4**	**2.34±0.21**
110	477±27	7.87±1.85	46±4	1.81±0.45
140	384±48	7.65±1.33	44±9	1.32±0.37

Table. 3.5 PV parameters of $ITO/CuInS_2/In_2S_3/Ag$ solar cells with different thickness of the $CuInS_2$ inter layer.

Studies show that the device exhibits better PV responses when fabricated with an interlayer thickness of ~ 80 nm. Best efficiency was in the

range 2.34 ± 0.21 % for these devices. Out of the measurements from 45 cells of this configuration, 30 exhibited this efficiency range. As the thickness of the inter layer increases, the effective thickness of the absorber layer also increases. Since the illumination is from substrate side, enough light may not be reaching the junction. This may be a reason for the decrease in PV parameters for higher thickness (above 80 nm) of the inter layer. Average value of efficiency decreases from 2.34 % to 1.32 % as inter layer thickness increases from 80 nm to 140 nm. The best device under this study has a V_{oc} of 495 mV and J_{sc} of 9.07 mA/cm^2. Fill factor and efficiency were 57 % and 2.55 % respectively. Illuminated J-V characteristics of the device is shown in Figure 3.10. On comparing with the best device without resistive $CuInS_2$ inter layer, present configuration exhibits improvements in V_{oc} (from 478 mV to 495 mV) and fill factor (from 45 % to 57 %). This is attributed to the reduced recombination rate of light generated carriers due to the presence of resistive $CuInS_2$ inter layer in the cell structure. At the same time resistive nature of the inter layer decreases the J_{sc} obtained from the device (from 12.13 mA/cm^2 to 9.07 mA/cm^2). In effect, the efficiency values for both configurations are almost same (i.e., 2.59 % and 2.55 % for devices without and with resistive inter layer)

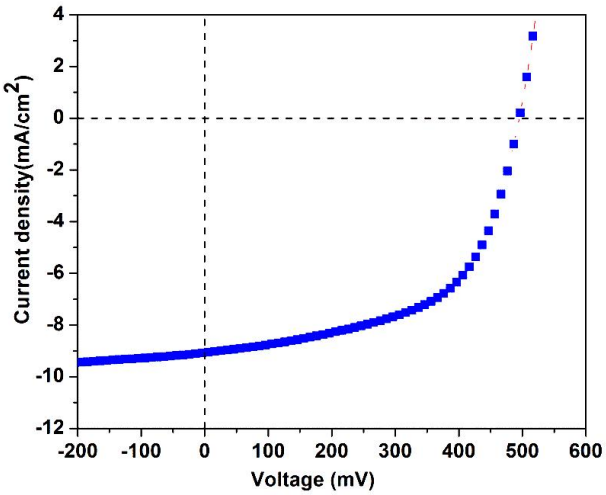

Figure. 3.10 Illuminated J-V characteristics of ITO/$CuInS_2$/In_2S_3/Ag solar cells with 80 nm thick $CuInS_2$ inter layer.

3.3.1 XPS analysis of the device

XPS depth profile analysis of the device with the optimum thickness of inter layer (~ 80 nm) is shown in Figure 3.11. Intensity of binding energy peaks corresponding to copper is very much reduced in In_2S_3, when comparing with that of device without this resistive inter layer (see Figure 3.3). Hence copper diffusion from the absorber to buffer layer was very much in control for the device with resistive inter layer. Moreover, oxygen was absent inside the device which is also favorable for the device [11]. XPS depth profile analysis of Cu in ITO/$CuInS_2$/Al_2O_3/In_2S_3/Ag cell structure (see Figure 3.8) also has similar trends as observed in Figure 3.11.

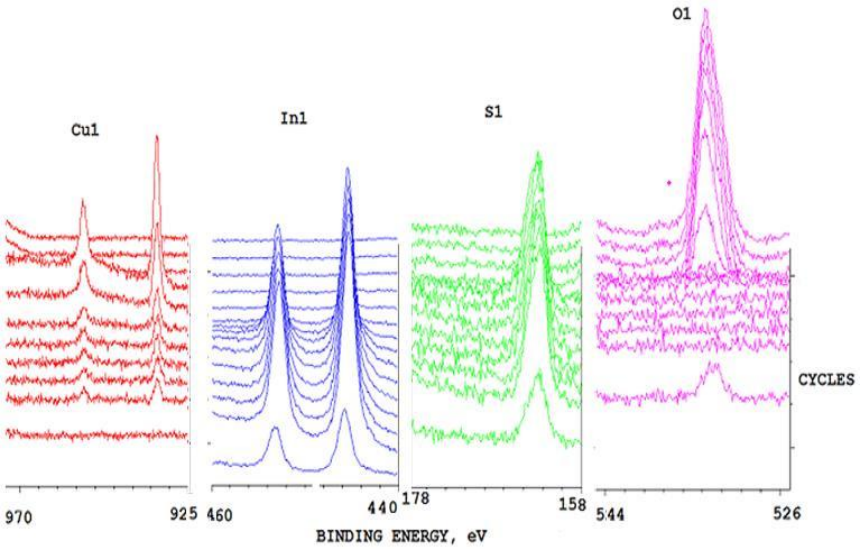

Figure. 3.11 XPS depth profile analysis of ITO/$CuInS_2$/In_2S_3/Ag solar cells with $CuInS_2$ inter layer. There is 'no' oxygen inside the cell.

3.3.2 Cross sectional SEM of the device

Cross sectional view of $CuInS_2$/In_2S_3 solar cell fabricated with the resistive $CuInS_2$ inter layer is shown in Figure 3.12. The component layers of the cell structure i.e., $CuInS_2$ absorber layer, $CuInS_2$ inter layer and a "Cu-free" In_2S_3 layer are well distinguished from the SEM image and layers are almost free from voids. A compact grain structure having columnar growth is observed for both $CuInS_2$ and In_2S_3 layers. As discussed in section 3.3, the deposited thicknesses of $CuInS_2$ absorber layer, $CuInS_2$ inter layer and In_2S_3 buffer layers were 320 nm, 80 nm, 300 nm respectively. But SEM measurements shows that, after all inter diffusion processes in cell structure, thickness of $CuInS_2$ absorber layer, $CuInS_2$ inter layer and In_2S_3 buffer layer were ~ 300 nm, ~ 200 nm and ~ 150 nm respectively. It should be noted that, due to Cu diffusion there are significant increase in thickness of $CuInS_2$ inter layer and decrease in thickness of In_2S_3 buffer layer from the expected values.

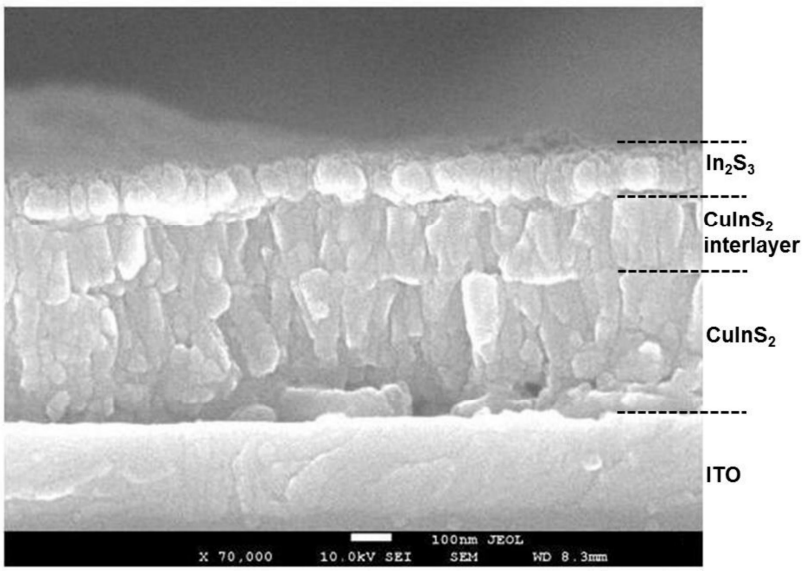

Figure. 3.12 Cross sectional image of ITO/$CuInS_2$/In_2S_3/Ag solar cells with $CuInS_2$ inter layer.

3.4 Conclusions

$CuInS_2$/In_2S_3 heterojunction solar cells were fabricated using ITO as back contact and Ag as front contact having the structure ITO/$CuInS_2$/In_2S_3/Ag. Thicknesses of $CuInS_2$ absorber and In_2S_3 buffer layer are optimized for the better performance of this device. The best cell fabricated using the optimized conditions has V_{oc} = 478 mV, J_{sc} = 12.13 mA/cm^2, fill factor = 45 % and efficiency = 2.59 %. In order to explore the potential of spray deposition for large area coatings, solar cell having an active area of 2.5 x 2 cm^2 was fabricated using this optimized configuration. Performance of this device was monitored up to 100 days and we observed that the device was working even after 100 days without any protective coatings. The cell was kept in open air condition and minimum damage of the device was observed from 20 days onwards. In next step, ITO back contacts are replaced with sprayed FTO to realize a cost effective "all sprayed" solar cells and the device shows

an efficiency of 0.94 %. XPS depth profile analysis of the device revealed the diffusion of Cu from $CuInS_2$ absorber to In_2S_3 buffer layer, which can deteriorates the device performance. An ultra-thin insulator coating of Al_2O_3 deposited employing ALD was used as interlayer in the cell structure and we observed that Cu diffusion to In_2S_3 buffer layer was very much reduced in this case. The device exhibited an improvement in V_{oc} and fill factor; but J_{sc} decreased. In effect there was no improvement in efficiency for these structures. As Al_2O_3 deposition using ALD was sophisticated and not cost effective, we employed spray pyrolysis itself to deposit a resistive $CuInS_2$ inter layer in the cell structure. Copper diffusion to In_2S_3 was reduced on introducing this inter layer. Although the device exhibits repeatability, in this case also, there is not much improvement in efficiency.

References

[1] Sebastian T, Ph.D. Thesis, Cochin University of Science and Technology, India (2009).

[2] John T T, Ph.D. Thesis, Cochin University of Science and Technology, India (2009).

[3] John T T, Mathew M, Kartha C S, Vijayakumar K P, Abe T, Kashiwaba Y, Solar Energy Materials & Solar cells, 2005, **89**, 27-36.

[4] Kaiser I, Ernst K, Fischer Ch- H, Konenkamp R, Rost C, Sieber I, Lux-steiner M. Ch, Solar Energy Materials & Solar Cells, 2001, **67,** 89-96.

[5] Machlin E, Materials Science in Microelectronics II: The effects of structure on properties in thin films, 2010**.**

[6] Cherian A S, Abe T, Kashiwaba Y, Sudha Kartha C, Vijayakumar K P, Energy Procedia, 2012, **15**, 283-290.

[7] Rau U, Schmidt M, Thin Solid Films, 2001, **387**, 141-146.

[8] Aslan F, Adam G, Stadler P, Goktas A, Mutlu I H, Sariciftci N S, Solar Energy, 2014, **108**, 230-237.

[9] Hsia Y, Lu C, Ji L, Meen T, Chen Y, Chi H, Nanoscale Research Letters, 2014, **9**, 32.

[10] Zouaghi M C, Ben Nasrallah T, Marsillac S, Bernede J C, Belgacem S, Thin Solid Films, 2001, **382**, 39.

[11] Ryo T, Nguyen D, Nakagiri M, Toyoda N, Matsuyoshi H, Ito S, Thin Solid Films, 2011, **519**, 7184–7188.

[12] Butrymowicz D B, Manning J R, Read M E, Journal of Physical Chemical Reference Data, 1974, **3**, 2.

[13] Santhosh M V, Kartha C S, Vijayakumar K P,AIP Conference Proceedings, 2014, **1591**, 639-641.

[14] Pysch D, Mette A, Glunz S W, Solar Energy Materials & Solar Cells, 2007, **91**, 1698-1706.

[15] Chiba K, Nakatani K, Thin Solid Films, 1984, **112**, 359-367.

[16] Priyanka, Lal M, Singh S N, Solar Energy Materials & Solar Cells, 2007, **91**, 137-142.

[17] Santhosh M V, Deepu D R, Kartha C S, Rajeev Kumar K, Vijayakumar K P, Solar Energy, 2014, **108**, 508-514.

[18] Nanu M, Schoonman J and Goossens A, Advanced Functional Materials, 2005, **15**, 95-100.

[19] Dhass A D, Natarajan E, Ponnusamy L, International Conference on Emerging Trends in Electrical Engineering and Energy Management, 2012, 382-386.

[20] Yoon W, Boercker J E, Lumb M P, Placencia D, Foos E E, Tischler J G, Scientific reports, 2013, **3**, 2225.

[21] Mere A, Kijatkina O, Rebane H, Krustok J, Krunks M, Journal of Physics and Chemistry of Solids, 2003, **64**, 2025-2029.

[22] Yoshino K, Nomoto K, Kinoshita A, Ikari T, Akaki Y, Yoshitake T, Journal of Materials Science: Materials in Electronics, 2008, **19**, 301-304.

[23] Shi Y, Jin Z, Li C, An H, Qiu J, Applied Surface Science, 2006, **252**, 3737-3743.

……..✷ ♦ ✷……..

Chapter **4**

Extremely thin absorber layer solar cells using mixed phases of $CuInS_2$ and Cu_2S in absorber layer

4.1 Introduction

In 'Extremely Thin Absorber (ETA)' solar cells, absorber layer thickness is reduced to few hundreds of nanometer to overcome the efficiency limits due to low mobility values and defects in solar cells based on thicker absorber layer. As thickness of absorber layer is reduced, light absorption in the absorber layer also decreases. Light absorption in the absorber can be improved either by introducing defect levels or by creating multiple band gaps in the absorber layer. In the present work, a 'multiple band gap' absorber was made possible by incorporating both $CuInS_2$ (E_g = 1.45 eV) and Cu_2S (E_g = 1.80 eV) in a single film employing simple, versatile and cost effective CSP technique (section 4.2.3). For the present case, two conduction bands at different energy levels are available in the same absorber material which can promote multiple photon absorption and this result in improvement of carrier collection in the device.

$CuInS_2$ and Cu_2S are important chalcogenide compounds for using as absorber layer in thin film solar cells. The interest lies mainly because of eco-friendly nature and earth abundance of their elements. Simple production techniques for cell fabrication are also available for these materials. Moreover, their electrical and optical properties are highly suitable as an absorber layer in solar cells [1-4]. $CuInS_2$ films deposited using various technique show high absorption coefficient (~ 10^5 cm^{-1}) and optimum band gap (~ 1.5 eV) for PV conversion [5-7]. Theoretically its conversion efficiency is 28.5 %, which is the highest value when comparing with other chalcopyrites [4]. Cu_2S is also a

well-established absorber material with high absorption coefficient (10^5 cm^{-1}) and band gap values in the range suitable for efficient PV conversion (1.2 - 2 eV) [2, 8]. Improvement in light absorption was possible with these two materials together in a single film due to the presence of multiple absorption bands. This new material is an excellent choice for ETA layer in solar cells as it enhances optical absorption. Generally in ETA solar cells, the absorber layer having few hundreds of nanometer is deposited over micro or nanostructured electron conducting layer (TiO_2 or ZnO) [9, 10]. As the extremely thin absorber was deposited over micro or nanostructures, light undergoes multiple scattering and increasing effective path length in the absorber layer [11, 12]. As a result efficient light absorption was possible in ETA cells. In our case $CuInS_2$-Cu_2S layer exhibits efficient light absorption and micro/nanostructured electron conducting layer is hence avoided, which makes the cell fabrication process very simple. Also due to the reduced absorber layer thickness, the recombination probability of light generated carriers within the absorber layer is very much reduced making collection probability at the contacts better.

Toxic CdS was the proven buffer layer for both $CuInS_2$ and Cu_2S absorber layers [6, 13-16]. However, due to the high diffusion coefficient of Cu ions, diffusion of Cu from absorber layer to CdS buffer layer is an easy process, which adversely affects the stability of these devices. For the present study, spray deposited In_2S_3 is the buffer layer for mixed phase $CuInS_2$-Cu_2S absorber layer and the cell structure followed was ITO/$CuInS_2$-Cu_2S/In_2S_3/Ag. In_2S_3 is non-toxic, easy to prepare and has better light transmission in the blue wave length region [1, 5]. Cu diffusion can also occur from $CuInS_2$-Cu_2S absorber to In_2S_3 buffer layer and converts some In_2S_3 portion into $CuInS_2$. Due to this process In_2S_3 in the solar cell should have enough thickness, to maintain Cu free In_2S_3 buffer layer, even after the diffusion process. Trials on cell fabrication show that, thick In_2S_3 layer (~ 250 nm) can be easily deposited

over thin $CuInS_2$-Cu_2S absorber layer (~ 150 nm) without peeling off. Due to Cu diffusion, there should be $CuInS_2$ inter layer between $CuInS_2$-Cu_2S absorber layer and In_2S_3 buffer layer in the cell structure. Comparing with $CuInS_2$-Cu_2S (5.15×10^{-3} Ω.cm; section 4.2.4) absorber layer $CuInS_2$ (2.49 Ω.cm; section 2.4.3) is resistive in nature. Hence, in effect $CuInS_2$ acts as a resistive inter layer and it was already observed that these resistive inter layer in the cell structure improves V_{oc} and fill factor of the device (section 3.3).

4.2 Deposition of $CuInS_2$-Cu_2S absorber layer

The mixed phase $CuInS_2$-Cu_2S absorber can be easily deposited by reducing the concentration of indium chloride in the precursor solution of $CuInS_2$. Ultrasonically cleaned soda lime glass plates were used initially as the substrate to do all characterizations. For the present study indium chloride concentration in precursor solution for $CuInS_2$ was reduced in steps so that Cu/In ratio in the solution was varied like 1.4/1, 1.4/0.8, 1.4/0.6, 1.4/0.4 and 1.4/0.2. These samples were named as I-1, I-0.8, I-0.6, I-0.4 and I-0.2 respectively. Five samples prepared from five different trials (for each Cu/In ratio) were used for characterizations. Cu/S ratio was kept as 1.4/5 for all these samples. Volume of the precursors sprayed was 70 ml for each sample. Substrate temperature (350 °C) and spray rate (4 ml/min) were fixed same as that of $CuInS_2$ samples.

4.2.1 XRD analysis

Result of XRD analyses (Figure 4.1) show only (112) and (220) planes, which represent tetragonal $CuInS_2$ phase [1]. However sample I-0.2 shows (103) plane corresponding to tetragonal Cu_2S phase also (JCPDS file no 72-1071) [2]. Preferential orientation for all samples are along (112) plane even though Cu/In ratio was varied from 1.4/1 to 1.4/0.2. In spray pyrolysis different binary phases of Cu and S like CuS, $Cu_{1.8}S$, $Cu_{1.9}S$ and Cu_2S were observed in

the deposited films [2, 17]. Among these binary phases, Cu_2S is better absorber [2, 8]. XRD results shows that besides Cu_2S, other binary phases of Cu and S were absent in the deposited films.

For solar cell fabrication in the present study In_2S_3 was the buffer layer, which also was tetragonal in nature [18]. Hence the lattice structural mismatch in the process of junction fabrication is not a big problem here. Grain sizes of the films with different indium concentrations were calculated using well known Scherrer formula and the variation (30 to 35 nm) was not in order. Thickness of the samples decreased drastically on decreasing indium concentration (450 nm, 420 nm, 330 nm, 280 nm, 250 nm for I-1, I-0.8, I-0.6, I-0.4, I-0.2 respectively).

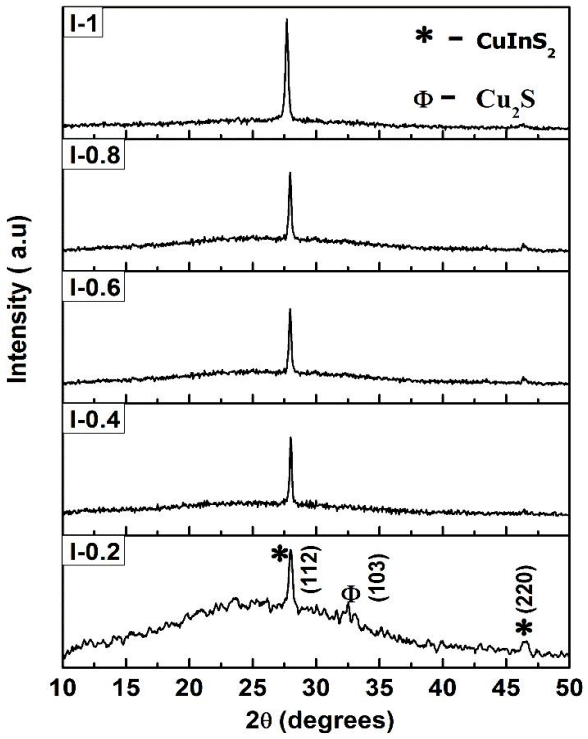

Figure. 4. 1 XRD analyses of the samples with different Cu/In ratios.

4.2.2 Raman analysis

In order to obtain a clear picture of any other binary phases (if present) in the samples, Raman analysis was carried out (Figure 4.2). Unlike XRD analysis, Raman analysis proved that Cu_2S phase exists from I-0.8 onwards which is revealed by the Raman peak at 472 cm^{-1} [19]. All samples showed Raman peak at 300 cm^{-1} corresponding to A_1 mode of $CuInS_2$ [20], whose height decreases with decrease is indium concentration. For I-0.2 samples alone, Raman peak corresponding to Cu_2S phase dominates over $CuInS_2$ phase.

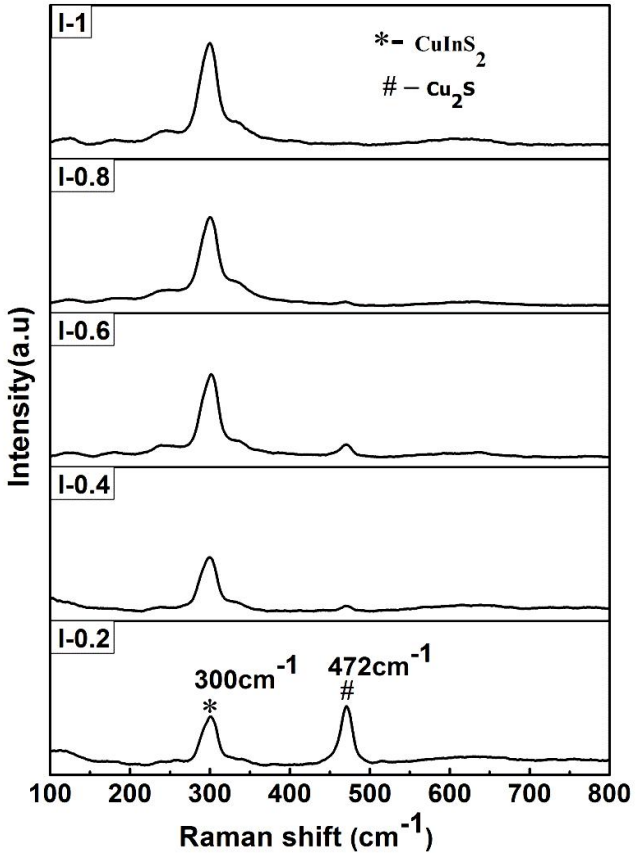

Figure. 4.2 Raman analysis of the films with different Cu/In ratios.

4.2.3 Optical studies

Optical responses of the samples with indium variation was studied by plotting (hν) vs $(\alpha h\nu)^2$ graphs (Figure 4.3). Here 'α' is the absorption coefficient of the material and 'hν' is the energy of the incident photons. Optical studies reveal that samples in I-1 series possess band gap of 1.45 eV, which indicates formation of $CuInS_2$ thin films [21]. On reducing indium concentration in the samples, band gap corresponding to Cu_2S was also visible (from samples I-0.8 onwards). As a result, a double band gap nature was observed for samples from I-0.8 onwards. Interestingly, band gap of Cu_2S phase in the samples increases on decreasing indium concentration. Band gap corresponding to Cu_2S for I-0.8 sample was 1.6 eV and it increases to 1.8 eV for I-0.2 samples.

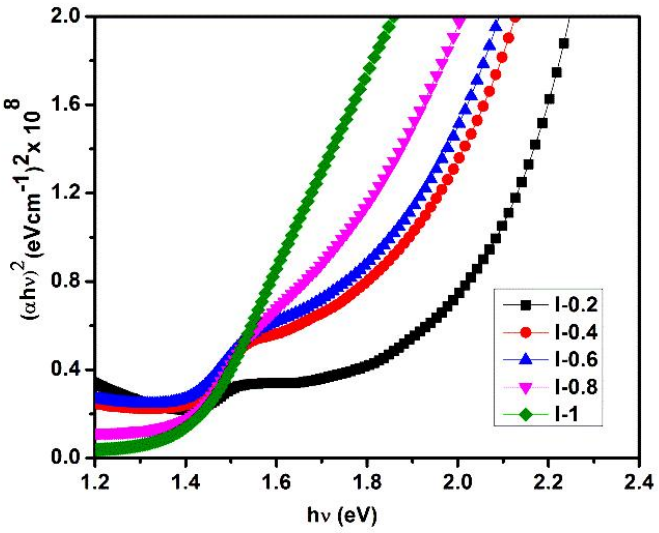

Figure. 4.3 Optical absorption spectra of the samples with different Cu/In ratios.

Multiple band gaps in I-0.2 samples can compensate its low absorption (comparing to I-1 samples) which is evident from Table 4.3.

4.2.4 Electrical studies

The average values of electrical properties for samples prepared with each Cu/In ratio are furnished in Table 4.1. For $CuInS_2$ samples (I-1), bulk concentration of carriers was 1.87 x $10^{19}/cm^3$. On reducing concentration of indium in $CuInS_2$, indium vacancies (V_{in}) as well as Cu in indium sites (Cu_{In}) increases in the samples. These defect levels can act as shallow acceptor levels [22, 23]. As a direct consequence of this process, bulk concentration of majority carriers increases with decreasing indium concentration in $CuInS_2$ films. Bulk concentration for majority carriers was increased to 1.36 x 10^{21} $/cm^3$ for I-0.2 samples making resistivity of the sample low. For I-1 samples resistivity value is 2.49 Ω.cm and it reduced by 3 orders reaching 5.15 x 10^{-3} Ω.cm for I-0.2 samples. Mobility values are better for I-0.2 and all samples showed p-type conductivity.

Sample name	Bulk concentration (cm^{-3})	Resistivity (Ω.cm)	Mobility (cm^2/Vs)	Conductivity type
I-1	$1.87x10^{19}$	2.49	$1.34x10^{-1}$	p-type
I-0.8	$4.91x10^{20}$	$4.63x10^{-1}$	$2.75x10^{-2}$	p-type
I-0.6	$3.75x10^{20}$	$1.60x10^{-1}$	$1.04x10^{-1}$	p-type
I-0.4	$1.46x10^{21}$	$9.26x10^{-2}$	$4.62x10^{-2}$	p-type
I-0.2	$1.36x10^{21}$	$5.15x10^{-3}$	$8.03x10^{-1}$	p-type

Table. 4.1 Electrical characterization of the films with different Cu/In ratios.

4.2.5 AFM studies

Surface topography of the samples on reducing indium concentration in $CuInS_2$ was analyzed using 3D AFM analysis [24]. Results of AFM analyses of I-1, I-0.6 and I-0.2 samples are shown in the Figure 4.4. It is clear from the results that RMS value of roughness decreases on decreasing the indium

concentration. For I-1, the roughness is 56 nm while it decreases to 46 nm for I-0.6 samples. I-0.2 samples possess the lowest surface roughness of 37 nm.

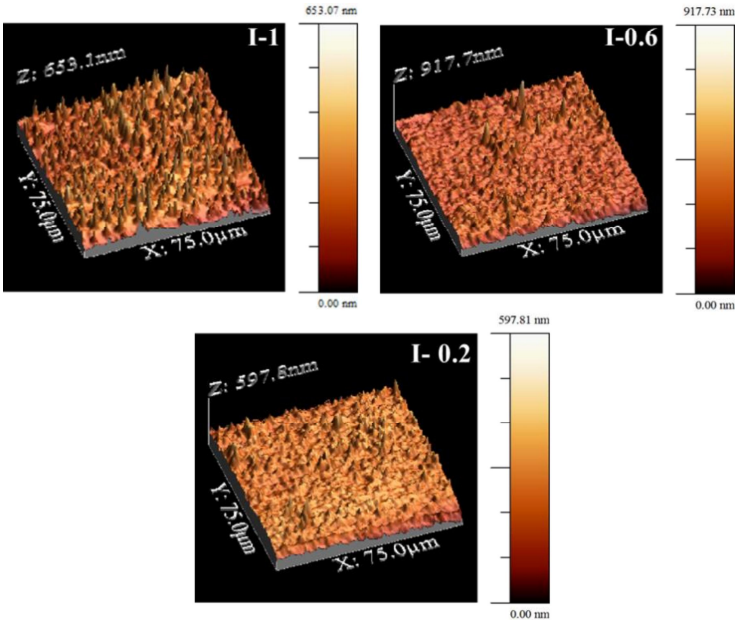

Figure. 4.4 Results of AFM analyses of I-1, I-0.6 and I-0.2 samples.

4.2.6 SEM analysis

Figure 4.5 shows SEM images of I-1 and I-0.2 samples. In samples I-1, some agglomerations are observed throughout the surface. EDAX measurements are performed specifically on these agglomerated regions. These regions exhibit higher copper concentration. These 'Cu-agglomerated' regions are the characteristics of $CuInS_2$ thin films having higher copper concentration [22]. AFM analysis already indicated the higher value of surface roughness for these samples and this higher surface roughness can be correlated with the presence of these 'Cu-agglomerated' regions. As indium concentration reduces in $CuInS_2$, 'Cu-agglomerated' regions disappear; samples I-0.2 consists of densely packed particles. EDAX analysis was also performed in I-1 and I-0.2 samples (Table 4.2) and non-stoichiometry parameter ($\Delta y = [2S/(Cu+3In)]-1$) was calculated for these samples. Δy values for both samples are greater than

zero which confirms their p-type conductivity [25]. Table 4.2 shows the atomic concentration of various elements and the non-stoichiometry parameters for I-1 and I-0.2 samples obtained from EDAX analysis.

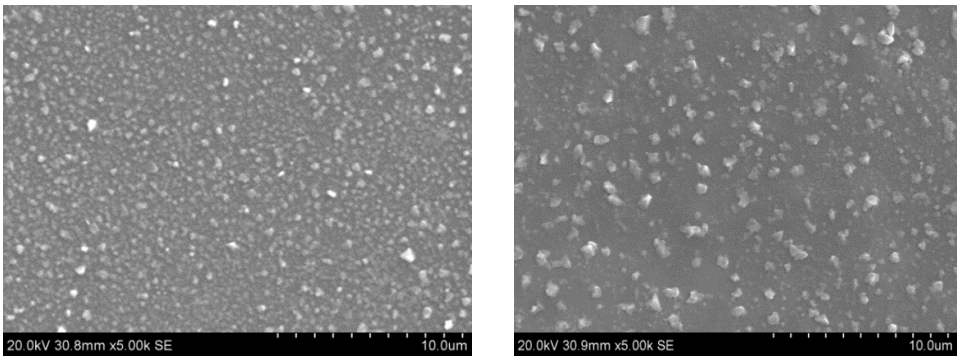

(a) (b)

Figure. 4.5. SEM pictures of (a) I-1 and (b) I-0.2 samples.

Sample name	Cu (at %)	In (at %)	S (at %)	Cu:In:S (actual)	Δy
I-1	27.15	22.71	50.14	1.19:1:2.20	0.05
I-0.2	46.26	10.35	43.39	4.46:1:4.19	0.12

Table. 4.2. Atomic compositions of I-1 and I-0.2 samples.

4.3 Fabrication and analysis of ITO/$CuInS_2$-Cu_2S/ In_2S_3/Ag solar cells

Since present work has emphasis on the fabrication of solar cells based on $CuInS_2$-Cu_2S absorber layer, cells with structure ITO/$CuInS_2$-Cu_2S/ In_2S_3/Ag were fabricated. Earlier studies pointed out that both $CuInS_2$ and Cu_2S phases were significant in the sample series I-0.2, these were suitable for device fabrication. Devices fabricated with I-0.8, I-0.6, I-0.4 samples do not show efficiency beyond that of $CuInS_2$ absorber layer (as discussed in section 3.2.1). Hence samples I-0.2 was used as absorber layer in the present studies.

For top electrode, silver is a good choice because the presence of silver in In_2S_3 improves its crystallinity [5]. A schematic diagram of the fabricated device is shown in Figure 4.6 (a). Each cell under the electrode was isolated using sharp edged blade.

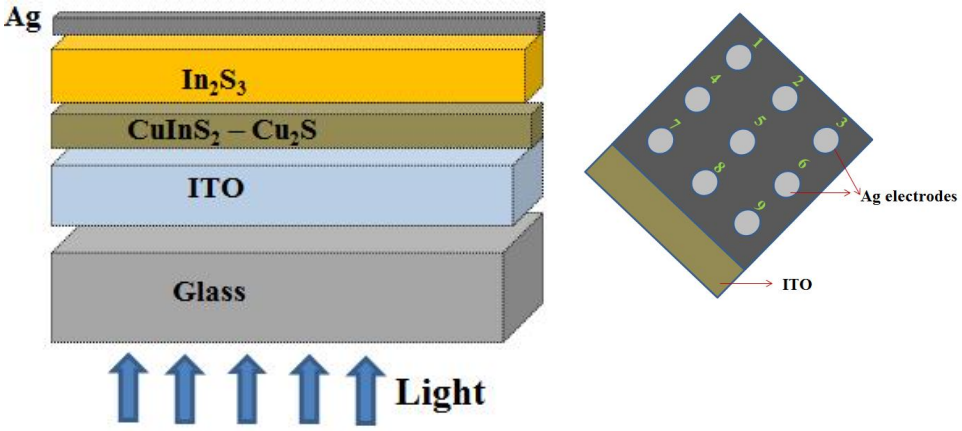

(a) (b)

Figure. 4.6 (a) Schematic diagram of the solar cell fabricated with $CuInS_2$-Cu_2S absorber layer (b) Top view of the device.

For thin film solar cells, thickness of the absorber layer is crucial parameter that determines the overall performance of the device [26]. In order to optimize thickness of the absorber layer, it was varied simply by varying the spray volume of the precursor solution. Thicknesses of the films thus deposited were measured by placing soda lime glass plates along with ITO coated glass substrates during the spray. Volume of the precursor solution used for depositing absorber was varied as 32 ml, 40 ml, 48 ml, 56 ml and 64 ml. Respective thicknesses of the films were measured as 100 ± 8 nm, 125 ± 10 nm, 150 ± 10 nm, 180 ± 15 nm and 205 ± 15 nm. In all cases, thickness of the In_2S_3 buffer layer was kept constant at ~ 250 nm by fixing spray volume of the precursors at 36 ml. Finally, for top contact, silver is vacuum evaporated over

the cell structure. Here silver is deposited as an array of 9 electrodes each having area of 0.03 cm^2 and thickness of 50 nm (Figure 4.6(b)). Five trials were performed for each thickness of the absorber layer (45 cells were considered for this study). The photovoltaic parameters like V_{oc}, J_{sc}, fill factor and efficiency were monitored for each cell. Average value, (along with upper and lower limit values) of these parameters for each thickness of the absorber is tabulated in Table 4.3.

$CuInS_2$:Cu_2S spray volume (ml)	Thickness (~ nm)	V_{oc} (mV)	J_{sc} (mA/cm^2)	FF (%)	Efficiency (%)
32	100±8	410±18	6.90±1.72	40±6	1.19±0.47
40	125±10	465±30	9.77±1.83	50±4	2.11±0.27
48	**150±10**	**488±30**	**12.12±2.13**	**52±6**	**3.19±0.63**
56	180±15	458±33	8.93±1.08	48±13	2.12±0.64
64	205±15	432±38	7.54±1.51	48±5	1.69±0.24

Table. 4.3 Photovoltaic parameters of devices with different thicknesses of the absorber layer.

From the data furnished in Table 4.3, it was observed that as thickness of the absorber layer was increased to 150 nm from 100 nm, PV parameters are improving and beyond this cell parameters deteriorated. Hence there is an optimum thickness (~ 150 nm) of the absorber layer for better performance of the device. At this thickness, devices showed efficiencies in the range 3.19 ± 0.63 %. Out of the measurements from 45 devices (five trials), 20 devices (44 % of total cells) exhibited this efficiency range. The best device in this study has V_{oc} = 518 mV, J_{sc} = 14.25 mA/cm^2, fill factor = 52 % and efficiency = 3.82 %.

Variations in PV parameters are also studied with In_2S_3 buffer layer thickness. Here thickness of the absorber layer was kept at ~ 150 nm, optimized from above trials and buffer layer thickness was decreased from 250 nm to 180 nm by reducing spray volume from 36 ml to 26 ml. Also buffer layer thickness was increased from 250 nm to 310 nm by increasing spray volume from 36 ml to 46 ml. The variations in PV parameters with In_2S_3 buffer layer thickness was tabulated in Table 4.4.

In_2S_3 spray volume (ml)	Thickness (nm)	V_{oc} (mV)	J_{sc} (mA/cm^2)	Fill factor (%)	Efficiency (%)
26	180±10	433±17	11.13±2.61	47±13	2.05±0.69
36	**250±12**	**488±30**	**12.12±2.13**	**52±6**	**3.19±0.63**
46	310±15	489±18	7.15±1.58	53±6	1.99±0.56

Table. 4.4 Photovoltaic parameters of the devices with different thicknesses of the buffer layer.

Analysis shows that on increasing and decreasing thickness of the buffer layer, with respect to 250 nm, does not provide any improvement in overall cell performance. On increasing thickness of the resistive buffer layer (resistivity ~ 10^3 Ω.cm) from 250 nm to 310 nm, series resistance increases and the collection probability of light generated carriers at the top electrode decreases. Effectively, J_{sc} decreases significantly and results in low efficiency devices. On decreasing thickness of the buffer layer from 250 nm to 180 nm, PV parameters are decreasing; this is because Cu diffusion from the absorber layer may be significant in devices with thin buffer layer leading to an improper junction. As a conclusion, optimum values for absorber and buffer layer thicknesses for the present study were found to be ~ 150 nm and ~ 250

nm for better performance of ITO/$CuInS_2$-Cu_2S/In_2S_3/Ag solar cells. Considering each values obtained for different trials, an average value for PV parameters for the best configuration in this study is V_{oc} ~ 488mV, J_{sc} ~ 12.12 mA/cm^2, fill factor ~ 52 % and efficiency ~ 3.19 %. The dark and illuminated J-V characteristics of the best cell fabricated is shown in Figure 4.7.

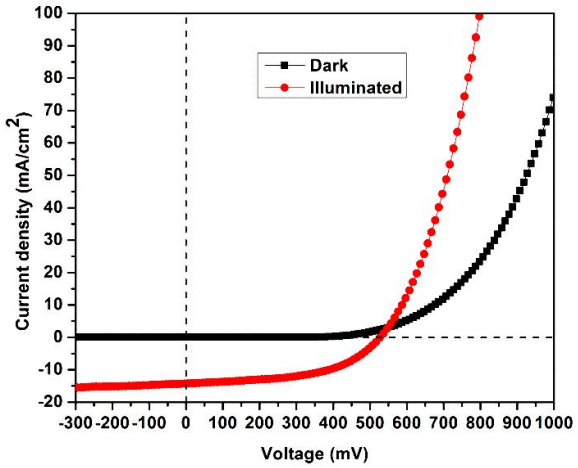

Figure. 4.7 Dark and illuminated J-V characteristics of the best device fabricated.

4.4 Transmission spectra of the device

Transmission spectra of solar cell fabricated with the optimum thickness of $CuInS_2$-Cu_2S absorber layer and In_2S_3 buffer layer (Figure 4.9) (performed without coating silver top contact) proves that there is an average transmittance of ~ 45 % in the visible region of the spectra. By considering that the solar cell utilizes only ~ 55 % of the incident light, efficiency of the device becomes ~ 6 %. By depositing a suitable transparent conducting electrode instead of silver, these solar cells can be connected in parallel for better utilization of sunlight leading to further improvement of performance parameters of the cell.

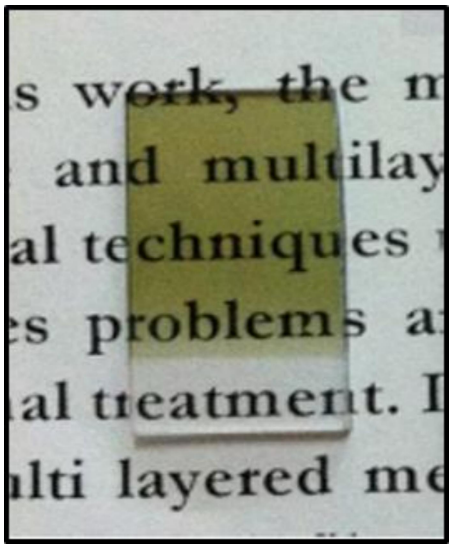

Figure. 4.8 Image of ETA solar cells (without Ag electrode) using $CuInS_2$-Cu_2S absorber layer.

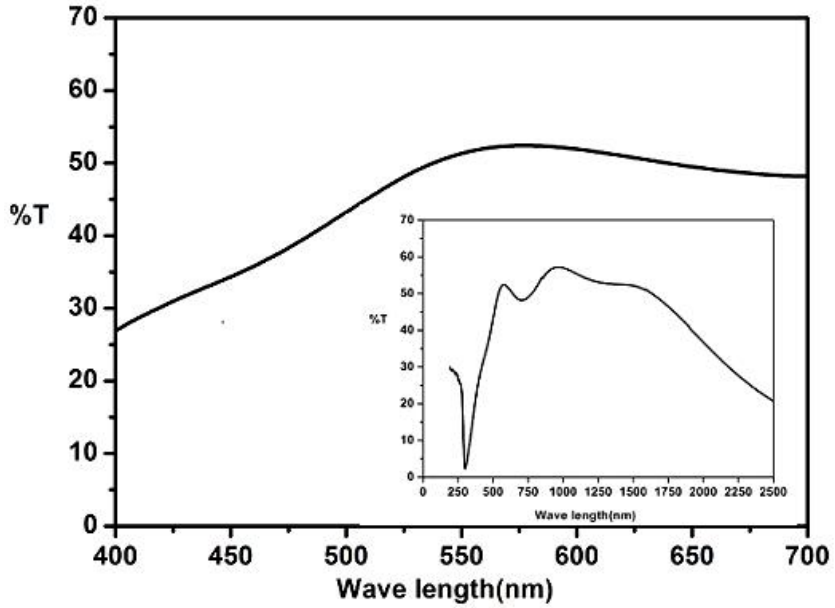

Figure. 4.9 Transmission spectra of ETA solar cells using $CuInS_2$-Cu_2S absorber layer.

4.5 Conclusions

A new absorber material having mixed phases of both $CuInS_2$ and Cu_2S was deposited by CSP method. For depositing this mixed phase absorber, indium concentration was reduced in the precursor solution of $CuInS_2$. Structural analyses using XRD and Raman, optical studies by taking absorption spectra reveal the presence of $CuInS_2$ and Cu_2S phases in the same samples. Interestingly, resistivity was found to decrease by 3 orders and reached a value of 5.15 x 10^{-3} Ω.cm. New absorber was employed for the fabrication of ETA solar cells for the first time by following the structure ITO/$CuInS_2$-Cu_2S/In_2S_3/Ag. Dependence of absorber and buffer layer thicknesses in the overall performance of the device was explored by simply varying the spray volumes of the respective precursor solutions. The best device under this study has V_{oc} = 518 mV, J_{sc} = 14.25 mA/cm^2, fill factor = 52 % and efficiency = 3.82 %. As these solar cells show ~ 45 % transmission in visible region of sunlight, it can be suitable for window glasses that can simultaneously transmit sunlight and capture power from it.

References

[1] Santhosh M V, Deepu D R, Kartha C S, Rajeev Kumar K, Vijayakumar K P, Solar Energy, 2014, **108**, 508-514**.**

[2] Isac L, Duta A, Kriza A, Manolache S, Nanu M, Thin Solid Films, 2007, **515**, 5755- 5758.

[3] Hadley H C, Jr, Tseng W F, Journal of Crystal Growth, 1977, **39**, 61-72.

[4] Siebentritt S, Thin Solid Films, 2002, **403-404**, 1–8**.**

[5] John T T, Mathew M, Kartha C S, Vijayakumar K P, Abe T, Kashiwaba Y, Solar Energy Materials & Solar Cells, 2005, **89**, 27–36.

[6] Klaer J, Bruns J, Henninger R, Sieme K, Klenk R, Ellmer K, Braunig D,Semiconductor Science and Technology, 1998, **13**, 1456-1458.

[7] Braunger D, Hariskos D, Walter T, Schock H W, Solar Energy Materials & Solar Cells, 1996, **40**, 97-102.

[8] Isac L, Popovici I, Enesca A, Duta A, Energy Procedia, 2010, **2**, 71–78.

[9] Krunks M, Katerski A, Dedova T, Oja Acik I, Mere A, Solar Energy Materials & Solar Cells, 2008, **92**, 1016-1019**.**

[10] Santhosh M V, Deepu D R, Geethu R, Rajeev Kumar K , Kartha C S, Vijayakumar K P, Semiconductor Science and Technology, 2014, **29**, 115026 (7pp).

[11] Kaiser I, Ernst K, Fischer Ch- H, Konenkamp R, Rost C, Sieber I, Lux-steiner M. Ch, Solar Energy Materials & Solar Cells, 2001, **67**, 89-96.

[12] Goossens A, Hofhuis J, Nanotechnology, 2008, **19,** 424018**.**

[13] Siemer K, Klaer J, Luck I, Bruns J, Klenk R, Braunig D, Solar Energy Materials & Solar Cells, 2001, **67**, 159-166.

[14] Das S R, Vankar V D, Nath P, Chopra K L, Thin Solid Films, 1978, **51**, 257-264.

[15] Ashour A, Journal of Optoelectronics and Advanced Materials, 2006, **8**, 1447-1451**.**

[16] Saraf R, IOSR Journal of Electrical and Electronics Engineering, 2012, **2**, 47-51.

[17] Pathan H M, Desai J D, Lokhande C D, Applied Surface Science, 2002, **202**, 47-56**.**

[18] Ratheesh Kumar P M, John T T, Kartha C S, Vijayakumar K P, Abe T, Kashiwaba Y, Journal of Material Science, 2006, **41**, 5519-5525.

[19] Wang S, Wang W, Lu Z, Materials Science and Engineering B, 2003, **103**, 184-188.

[20] Chung W, Jung H, Lee C H, Kim S H, Optic Express, 2012, **20**, 25071.

[21] John T T, Kartha C S, Vijayakumar K P, Abe T, Kashiwaba Y, Applied Physics A, 2006, **82**, 703-707**.**

[22] Shi Y, Jin Z, Li C, An H, Qiu J, Applied Surface Science, 2006, **252**, 3737-743**.**

[23] Lewerenz H J, Solar Energy Materials & Solar Cells, 2004, **83**, 395-407**.**

[24] HorcasI, Fernandas R, Gomez-Rodriguez J M, Colchero J,Gomez-Herrero J, Baro AM, Review of Scientific Instruments, 2007, **78**, 013705 .

[25] Xu X H, Wang F, Liu J J, Park K C, Fujishige M, Solar Energy Materials & Solar Cells , 2011, **95**, 791-796.

[26] Ryo T, Nguyen D, Nakagiri M , Toyoda N, Matsuyoshi H, Ito S, Thin Solid Films, 2011, **519**, 7184-7188.

……..✷♦✷……..

Chapter **5**

ETA solar cells fabricated using mixed phase $CuInS_2$-Cu_2S absorber by utilizing Cu diffusion in Cu_2S/In_2S_3 heterojunction

5.1 Introduction

Cu_2S is an important absorber layer for thin film solar cells because of its simple production possibilities using a variety of chemical deposition methods such as spray pyrolysis, chemical bath deposition, electrodeposition etc. High absorption coefficient (10^5 cm^{-1}) and favorable band gap (1.2 to 2 eV) for efficient solar energy absorption are its exceptional material properties as an absorber layer [1-5]. Moreover, the constituents of this compound are non-toxic and earth abundant. Even though this is a good absorber, only CdS and ZnCdS are found to be suitable buffer layer for Cu_2S. Efficiencies of 9.15 % and 10.2 % were attained for Cu_2S/CdS and Cu_2S/ZnCdS solar cells respectively [6, 7]. Theoretical analyses show that Cu_2S/CdS and Cu_2S/ZnCdS solar cells are capable of achieving practical conversion efficiencies of 11 % and 14-15 % respectively [8]. These solar cells were extensively investigated way back in 1960s to 1980s and showed significant promise. However, the diffusion of copper from Cu_2S to CdS was the major issue that adversely affected the reproducibility and long-term stability of these devices. Ultimately these factors and toxic nature of cadmium in the buffer layer lead to the abandonment of this type of cells. In the present work, non-toxic In_2S_3 was used as the buffer layer for Cu_2S absorber layer. Both absorber and buffer layer were deposited by CSP method.

5.2 Prospects of Cu_2S/In_2S_3 solar cells

For Cu_2S absorber layer, the highest efficiency of 10.2 % was obtained for chemi-plated Cu_2S/evaporated $Zn_xCd_{1-x}S$ thin film solar cells [7]. But the instability due to Cu diffusion and toxic nature of cadmium are the two constraints that prevented their commercial exploitation [9]. For the present work, CdS in the cell structure is replaced with sprayed In_2S_3 buffer layer. In_2S_3 has several advantages over CdS. First of all, there are no environmental hazards connected with production and disposal of In_2S_3 thin films [10, 11]. In_2S_3 based photovoltaic technology offers simple and cost effective production possibilities using chemical methods such as chemical spray pyrolysis (CSP), spin coating and chemical bath deposition (CBD) [12-14]. Solar cells using In_2S_3 give better response in blue region due to wider bandgap when comparing with that of CdS. CSP already proved as an efficient deposition method of In_2S_3 buffer layer for fabricating thin film solar cells with absorber layers like $CuInS_2$, CuZnS and Cu_2ZnSnS_4 [15-17].

Due to high diffusion coefficient, diffusion of Cu from Cu_2S to In_2S_3 was easy process in Cu_2S/In_2S_3 junction also. But for the present case, Cu diffusion to In_2S_3 converts some part of In_2S_3 into $CuInS_2$, which is a good absorber material. This $CuInS_2$ layer is formed in between Cu_2S and In_2S_3 layer. The resistivity of $CuInS_2$ (~ 2.49 Ω.cm) is higher when compared with that of Cu_2S (10^{-4} Ω.cm). In effect, there is a resistive layer near the junction and a conductive layer near the external contact. The resistive layer ($CuInS_2$) promotes effective charge carrier separation by reducing the recombination probability of light generated charge carriers and the conductive layer (Cu_2S) promotes effective charge collection by the external contact. 'Cu diffusion' is the major problem for Cu_2S/CdS solar cells, but for Cu_2S/In_2S_3 junction, we are utilizing this process for the better performance of the device. The light activity in Cu_2S/In_2S_3 solar cell is mainly attributed to the formation of

$CuInS_2/In_2S_3$ heterojunction by Cu diffusion. Solar cells using the combinations of $CuInS_2$ absorber layer and In_2S_3 buffer layer had already proved their significance among thin film solar cells [15, 18, 19]. Moreover, theoretical efficiencies of $CuInS_2$ based solar cells are around 28 %, which is higher than that of 15 % predicted for well-established Cu_2S/ZnCdS hetero junction solar cells. Again in the present case, Cu_2S, $CuInS_2$ and In_2S_3 layers are tetragonal in nature. As a result, lattice structural mismatch during junction formation is not a serious problem here.

The solar cell performance depends mainly on two types of loss mechanisms: optical and electronic. Optical loss mechanism controls the efficiency of creation of minority charge carriers by the absorption of light in the device. In the present solar cell configuration, the absorber layer consists of both $CuInS_2$ and Cu_2S. Multiple band gaps corresponding to these materials offer efficient light absorption within the absorber layer. The electronic loss is the other significant loss mechanism in a solar cell which relates to the effectiveness with which the minority carriers are collected at the opposite contacts of the device [20]. In order to minimize this loss, the absorber layer thickness in the present cell configuration was kept very small (~ 160 nm only). By reducing absorber layer thickness probability of recombination of light generated carriers within the absorber layer is reduced significantly. In effect minority carrier diffusion length improves, which promotes efficient charge collection at the external contacts.

5.3 Deposition and characterization of Cu_2S thin films

Ultrasonically cleaned soda lime glass plates were used as substrate for depositing Cu_2S using our automated CSP machine. Copper chloride ($CuCl_2$) and thiourea [$CS(NH_2)_2$] were used as precursors for copper and sulphur. Cu/S

ratio in the precursor solution was maintained as 1.4/5. Substrate temperature and spray rate were kept at 280 °C and 4 ml/min respectively.

5.3.1 XRD analysis

XRD pattern of the deposited sample is shown in Figure 5.1. The d values calculated coincided with that of tetragonal Cu_2S (JCPDS data card 72-1071) with preferential orientation along (103) plane [2, 21, 22].

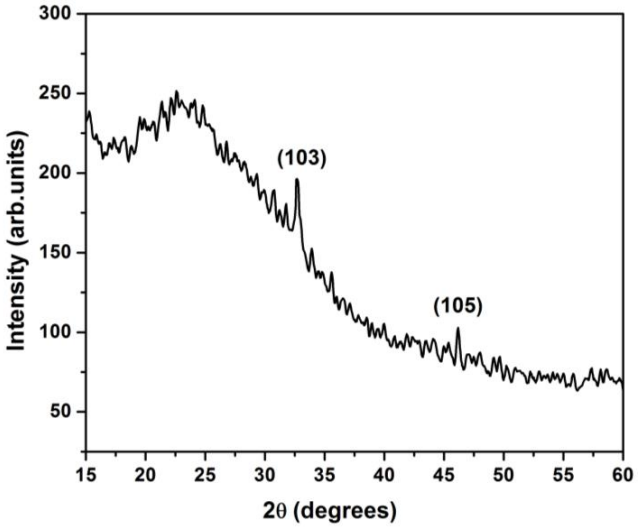

Figure. 5.1 XRD pattern of Cu_2S thin film.

For a tetragonal system, inter planar spacing (d) and lattice parameters ('a' and 'c') are related as

$$\frac{1}{d^2} = \frac{(h^2 + k^2)}{a^2} + \frac{l^2}{c^2}$$

Lattice constants were calculated to be a = 4 Å and c = 11.33 Å, which well matched with standard values, a = 3.99 Å and c = 11.28 Å. The grain size (D) was calculated using well known Scherrer's formula.

$$D = \frac{k\lambda}{\beta \cos\theta}$$

Where k is a dimensionless shape factor with a value close to unity, λ is the X-ray wavelength (1.54 Å), β is the full width at half the maximum intensity (FWHM) and θ is the Bragg angle. Grain size of the prepared Cu_2S film was calculated to be 36 nm. Copper sulfide thin films prepared using CSP technique have different phases such as chalcocite (Cu_2S), djurleite ($Cu_{1.95}S$), digenite ($Cu_{1.8}S$) and covellite (CuS). Among these, Cu_2S is observed to be a better absorber for thin film solar cells [2]. In our case, binary phases of Cu and S other than Cu_2S were not observed in the deposited films and hence the films are suitable candidate for absorber layer.

5.3.2 Raman analysis

Results from Raman analysis of the deposited film are shown in Figure 5.2. Strong and sharp Raman peaks at 262 cm^{-1} and 472 cm^{-1} are the characteristics of Cu_2S phase [23, 24]. Like XRD analysis, Raman analysis also shows that binary phases other than Cu_2S were not present in the deposited film.

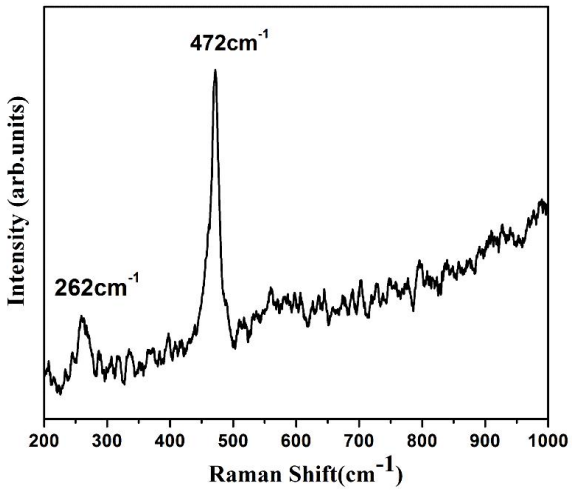

Figure. 5.2 Raman spectra of Cu_2S thin film.

5.3.3 Optical studies

Optical absorption spectrum of Cu_2S samples are shown in Figure 5.3. From $(\alpha h\nu)^2$ - $h\nu$ plot, band gap of ~ 2.2 eV is obtained, which is well matching with the reported values [4, 25, 26]. Absorption spectrum clearly shows that the sample is absorbing higher energies of visible light (from 550 nm to 400 nm), and this improves short-wavelength spectral response (blue response). For the present study, Cu_2S and $CuInS_2$ are the absorber layers. Light is falling on the device through Cu_2S and it absorbs higher energy portion of the light. After that, the transmitted low energy portion of light is absorbed by $CuInS_2$ (E_g = 1.5 eV). For devices with only $CuInS_2$ absorber layer can also absorb the high energy portion of visible spectra; but the excess energy (E_{ph}-E_g, where E_{ph} is the energy of photon and E_g is the band gap energy) is not used effectively due to thermalization of electrons. Thus by introducing a Cu_2S-$CuInS_2$ absorber layer, improved light absorption can be attained.

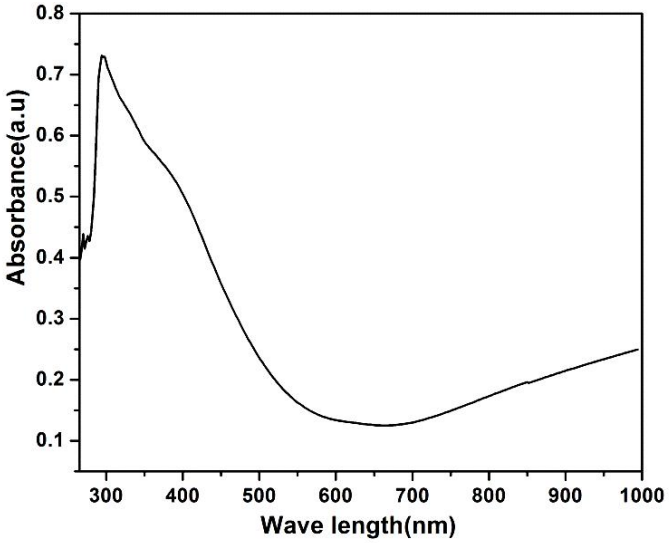

Figure. 5.3 Absorption spectrum of Cu_2S sample.

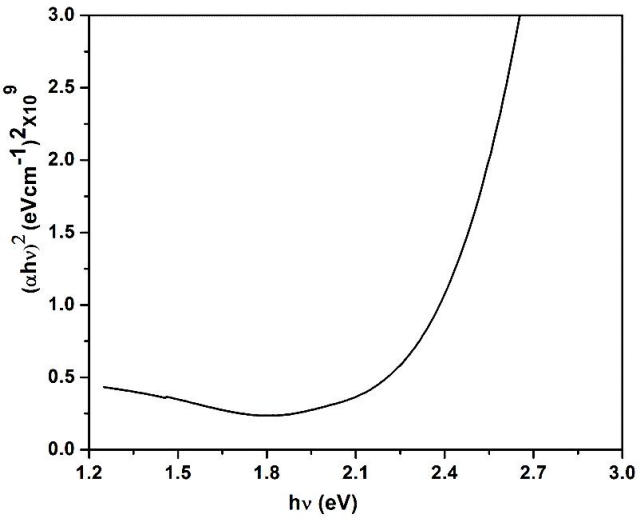

Figure. 5.4 $(\alpha h\nu)^2$ vs hν graph of Cu_2S sample.

5.3.4 Electrical studies

Electrical studies were performed at room temperature using Hall measurement system (Table 5.1). Sample shows only p-type conductivity and the bulk concentration of majority carrier was 3.63 x 10^{21} cm^{-3}. Resistivity and mobility are 9.06 x 10^{-4} Ω.cm and 1.89 cm^2/Vs respectively.

Bulk concentration	$3.63x10^{21}$ cm^{-3}
Sheet concentration	$5.45x10^{16}$ cm^{-2}
Resistivity	$9.06x10^{-4}$ Ω.cm
Mobility	1.89 cm^2/Vs
Average Hall coefficient	$1.71x10^{-3}$ cm^3/C

Table. 5.1 Results of Hall measurements of Cu_2S sample.

5.3.5 EDAX analysis

Composition of the sample was studied using EDAX analysis. The atomic percentage of Cu and S were 61.37 % and 38.63 % respectively. Deficiency of copper is responsible for p-type conductivity of Cu_2S film.

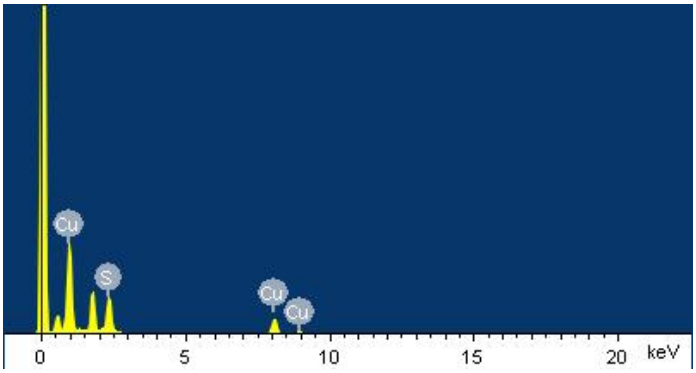

Figure. 5.5 EDAX analysis of Cu_2S thin film.

5.3.6 AFM analysis

AFM analysis of Cu_2S sample is depicted in Figure 5.6. Sample surface is almost uniform without any abrupt change in surface morphology. Average value of surface roughness was calculated as 39 nm. Value of surface roughness for Cu_2S was comparable to that of $CuInS_2$ films (40 nm) used for device fabrication in our previous studies.

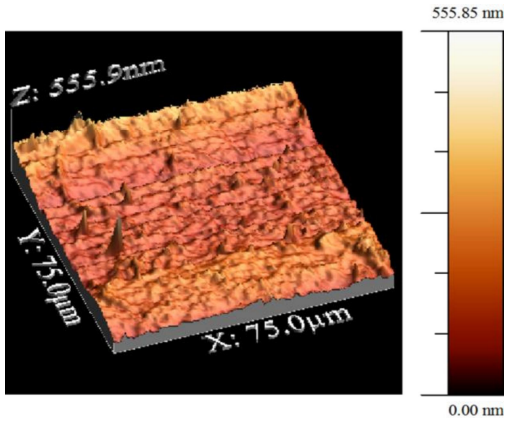

Figure. 5.6 AFM analysis of Cu_2S thin film.

5.4 ITO/Cu_2S/In_2S_3/Ag solar cell fabrication

For solar cell fabrication ITO coated glass plates (Geomatec, Japan; sheet resistance ~ 12 Ω/□) were used as the substrate. Over ITO, Cu_2S absorber layer was deposited by CSP method as discussed in section 5.3. In_2S_3 buffer layer was spray deposited (as discussed in chapter 2, section 2.5) over Cu_2S absorber layer to form a heterojunction. Finally for taking front contact from the device, silver was vacuum evaporated over the cell structure. Silver was deposited as array of 9 electrodes each having area of 0.03 cm^2 and thickness of 50 nm (Figure 5.7(b)). A schematic diagram of the fabricated device is shown in Figure 5.7(a).

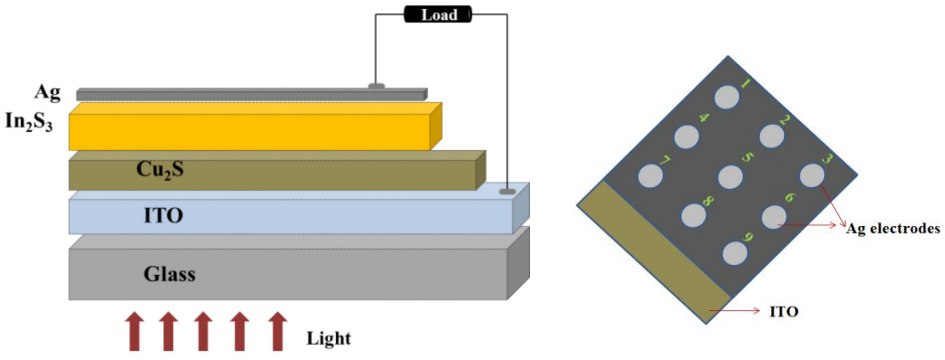

(a) (b)

Figure. 5.7 (a) Schematic diagram of the fabricated solar cell using Cu_2S (b) Top view of the device.

5.4.1 Raman analysis of the device

Results of Raman analysis of the fabricated solar cell (without coating Ag top electrode) is shown in Figure 5.8. Raman peaks corresponding to Cu_2S and In_2S_3 are present in Raman spectrum. Raman peaks at 472 cm^{-1} and 330 cm^{-1} correspond to that of Cu_2S and In_2S_3 respectively [23, 24, 28]. Besides these, Raman peak corresponding to $CuInS_2$ (300 cm^{-1}) also exists in the

spectrum [29]. The diffusion of Cu from Cu_2S to In_2S_3 converts some portion of In_2S_3 to $CuInS_2$. In effect the device structure became ITO/Cu_2S/$CuInS_2$/In_2S_3/Ag. Diffusion of Cu from Cu_2S is an easy process due to its high diffusion coefficient. Moreover, In_2S_3 is sprayed over Cu_2S at a temperature of 350 °C, which also promotes Cu diffusion.

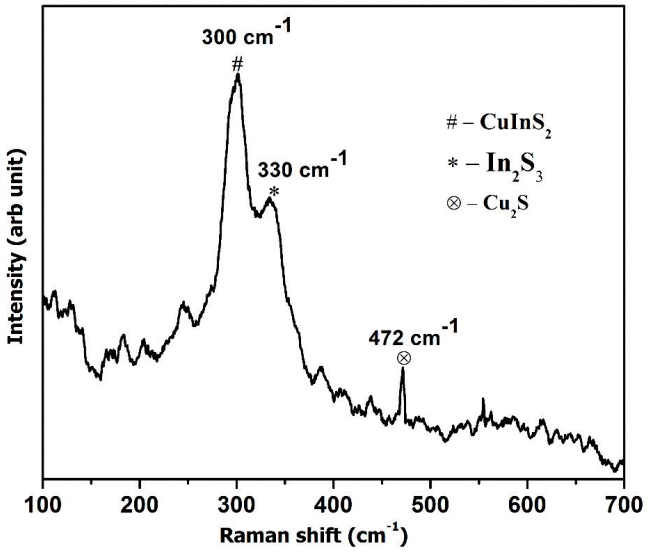

Figure. 5.8 Raman analysis of the fabricated device using Cu_2S absorber layer.

5.4.2 Effect of absorber layer thickness on device performance

In order to study effect of absorber layer thickness on the performance of the device, its thickness was varied by simply adjusting the spray volume of the precursor solution. This is extremely easy with CSP technique. Cells were fabricated with different thickness of the absorber, keeping thickness of In_2S_3 buffer layer (~ 250 nm) same for all configurations. The PV parameters such as open circuit voltage (V_{oc}), short circuit current density (J_{sc}), fill factor and efficiency were monitored for all configurations. Five solar cells were

fabricated for a particular thickness of the absorber layer. Highest, lowest and average values of PV parameters for each thickness of the absorber layer are tabulated in Table 5.2.

Spray volume (ml)	Thickness (~ nm)	V_{oc} (mV)	J_{sc} (mA/cm^2)	Fill factor (%)	Efficiency (%)
24	140±10	461±20	12.01±1.75	49±1	2.61±0.43
36	**160±15**	**479±8**	**17.14±0.86**	**45±5**	**3.78±0.33**
48	210±15	457±25	14.78±1.43	47±1	3.21±0.54
60	265±18	392±34	13.51±0.30	41±4	2.18±0.35

Table. 5.2 PV parameters of the device with different thicknesses of the absorber layer.

Analyses show that device with an absorber layer thickness of ~ 160 nm has better values of PV parameters when comparing with other configurations. For lower absorber layer thickness, V_{oc} and J_{sc} are observed to be low. This may be due to the inefficient absorption in thinner absorber layer. For higher absorber layer thickness (above 160 nm), the diffusion length of light generated minority carrier may be low due to the higher recombination rate in thicker absorber layer. Hence best device in this study has an absorber layer thickness of ~ 160 nm and buffer layer thickness of ~ 250 nm and the device shows V_{oc} = 487 mV, J_{sc} = 17.09 mA/cm^2, fill factor = 50 % and efficiency = 4.11 %. This value was observed for only one device out of the 45 devices fabricated in five different trials. Including this cell, 14 cells showed almost stable efficiency in the range 3.78 ± 0.33 %.

5.4.3 Effect of buffer layer thickness on device performance

In_2S_3 buffer layer thickness in the cell structure was also varied above and below 250 nm to study the variations in PV parameters. Absorber layer

thickness was kept ~ 160 nm for all these cases. It was observed that there was not much improvement in efficiency by varying the buffer layer thickness from 250 nm. On decreasing buffer layer thickness below 250 nm, Cu diffusion became significant in In_2S_3 layer which reduces the PV parameters. On increasing the thickness of resistive In_2S_3 layer (above 250 nm), series resistance of the device increased which reduced the PV parameters. PV parameters of the device with different thickness of the buffer layer were tabulated in Table 5.3. J-V characteristic of the best device fabricated under this study is shown in Figure 5.9.

In_2S_3 spray volume (ml)	Thickness (nm)	V_{oc} (mV)	J_{sc} (mA/cm^2)	Fill factor (%)	Efficiency (%)
26	180±10	413±42	14.21±2.05	40±7	2.2±0.69
36	**250±12**	**479±8**	**17.14±0.86**	**45±5**	**3.78±0.33**
46	310±15	483±22	9.84±1.91	50±3	2.23±0.3

Table. 5.3 PV parameters of the device with different thicknesses of the buffer layer.

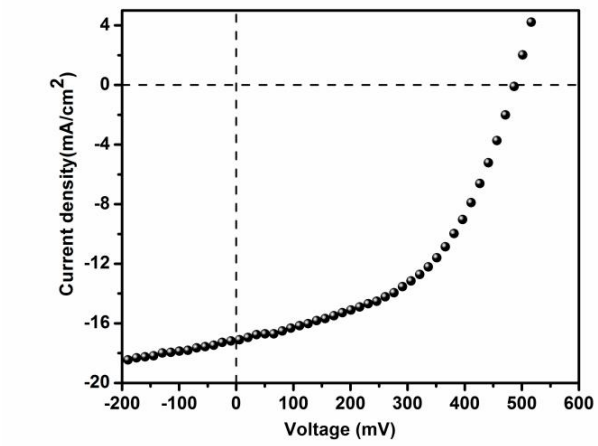

Figure. 5.9 Illuminated J-V characteristic of the best device.

5.4.4 Deposition time for the device

For solar cell fabrication, ITO was kept for 5 minutes over the heater for getting 280 °C. After this, Cu_2S absorber layer was sprayed over ITO and it takes just 9 minutes. Without any further delay, In_2S_3 buffer layer was sprayed over Cu_2S and this process requires another 9 minutes. After these processes, the device was suddenly taken from the heater for silver deposition (top contact) using vacuum evaporation. For silver deposition, it requires approximately 20 minutes. Thus cell fabrication process is completed within 45 minutes. Hence it is clear that besides cost effectiveness, CSP offers faster PV production possibilities.

5.4.5 Electrical energy requirement for device fabrication: an approximate calculation

For the fabrication of best device in the present study, electric energies are consumed by automated spray pyrolysis unit (1 kWh), air compressor (0.245 kWh) and vacuum coating unit (2.85 kWh). Hence considering that 45 minutes is the total time required for device fabrication, the total energy consumed during the device fabrication is ~ 4.1 kWh. For a single solar cell, energy consumption will be still lower than this value, as CSP and vacuum evaporation allows the deposition of larger number of cells in a batch.

5.5 Conclusions

Cu_2S thin films were deposited using automated spray pyrolysis machine. XRD and Raman analyses clearly indicated the presence of Cu_2S phase. Other binary phases of Cu and S were absent in the films. Optical studies revealed that band gap was ~ 2.2 eV for the Cu_2S films. From Hall measurements, bulk concentration of majority carrier and resistivity of the film were estimated as 3.63 x 10^{21} cm^{-3} and 9.06 x 10^{-4} Ω.cm respectively. Solar

cells were fabricated using Cu_2S absorber layer by following the structure ITO/Cu_2S/In_2S_3/Ag. Raman analysis of the cell indicated the formation of $CuInS_2$ also in the cell structure and this is due to the diffusion of Cu from Cu_2S to In_2S_3 buffer layer. Effect of absorber and buffer layer thickness on the performance of the device was monitored. Optimized thicknesses for absorber and buffer layers are ~ 160 nm and ~ 250 nm respectively. The devices under this study possessed efficiency of 3.78 ± 0.33 %. $V_{oc,}$ J_{sc} and fill factor were 479 ± 8 mV, 17.14 ± 0.86 mA/cm^2 and 45 ± 5 % respectively. Cell fabrication process was completed within 45 minutes, which offers faster PV production possibilities. Better light absorption and efficient charge carrier separation in multiple band gap absorber enabled the device to possess a better value of J_{sc} (17.09 mA/cm^2) when comparing with that of $CuInS_2$ based device. For $CuInS_2$ based solar cell, better values of J_{sc} and efficiency were 12.13 mA/cm^2 and 2.59 % respectively.

References

[1] Reijnen L, Meester B, Goossens A, Schoonman J, Materials Science and Engineering: C, 2002, **19**, 311-314.

[2] Isac L, Duta A, Kriza A, Manolache S, Nanu M, Thin Solid Films, 2007, **515**, 5755-5758.

[3] Page M, Niitsoo O, Itzhaik Y, Cahen D, Hodes G, Energy and Environmental Science, 2009, **2**, 220-223.

[4] Pathan H M, Desai J D, Lokhande C D, Applied Surface Science, 2002, **202**, 47-56.

[5] Zhuge F, Li X, Gao X, Gan X, Zhou F, Materials Letters, 2009, **63**, 652-654.

[6] Bragagnolo J A, Barnett D E, Allen M, Phillips J E, Hall R B, Rothwarf A, Meakin J D, IEEE Transactions on Electron Devices, 1980, **27**, 645-651.

[7] Hall R B, Birkmire R W, Phillips J E, Meakin J D, Applied Physics Letters, 1981, **38**, 925-926.

[8] Chopra K L, Das S R, Thin Film Solar Cells, Springer Science and Business Media, 1983.

[9] Norian K H, Edington J W, Thin Solid Films, 1981, **75**, 53-65.

[10] Zarbaliyev M Z, Mutlu I H, Aslan F, Journal of Sol-Gel Science and Technology, 2011, **59**, 153-157.

[11] Jayakrishnan R, John T T, Kartha C S, Vijayakumar K P, Abe T, Kashiwaba Y, Semiconductor Science and Technology, 2005, 20, 1162–1167.

[12] Kim W, Kim C, Journal of Applied Physics, 1986, **60**, 2631.

[13] Barreau N, Solar Energy, 2009, **83**, 363-371.

[14] Lokhande C D, Ennaoui A, Patil1P S, Giersig M, Diesner K, Muller M, Tributsch H, Thin Solid Films, 1999, **340**, 18-23.

[15] John T T, Mathew M, Kartha C S, Vijayakumar K P, Abe T, Kashiwab Y, Solar Energy Materials & Solar Cells, 2005, **89**, 27–36.

[16] Kitagawa N, Ito S, Nguyen D, Nishino H, Natural Resources, 2013, **4**, 142-145.

[17] Lin P, Lin L, Yu J, Cheng S, Lu P, Zheng Q, Journal of Applied Science and Engineering, 2014, **17**, 383-390.

[18] Santhosh M V, Deepu D R, Kartha C S, Rajeev Kumar K, Vijayakumar K P, Solar Energy, 2014, **108**, 508-514.

[19] Santhosh M V, Deepu D R, Geethu R, Rajeev Kumar K, Kartha C S, Vijayakumar K P, Semiconductor Science and Technology, 2014, **29**, 115026 (7pp).

[20] Hall R B, Meakin J D, Thin SolidFilms, 1979, **63**, 203-211.

[21] Machani T, Rossi D P, Golden B J, Jones E C, Lotfipour M, Plass K E, Chemistry of Materials, 2011, **23**, 5491-5495.

[22] Grozdanov I, Journal of Solid state Chemistry, 1995, **114**, 469-475.

[23] Wang S, Wang W, Lu Z, Materials Science and Engineering B, 2003, **103**, 184-188.

[24] Minceva-Sukarova B, Najdoski M, Grozdanov I, Chunnilall C J, Journal of Molecular Structure,1997, **410-411**, 267-270.

[25] Shinde M S, Ahirrao P B, Patil J, Patil R S, Indian Journal of Pure and Applied Physics, 2012, **50**, 657-660.

[26] Allouche N K, Nasr T B, Guasch C, Turki N K, ComptesRendusChimie, 2010, **13,** 1364-1369.

[27] Bharathi B, Thanikaikarasan S, Ramesh K, International Journal of Chemical Technology Research, 2014, **6**, 1907-1909.

[28] Spasevska H, Kitts C C, Ancora C, Ruani G, International Journal of Photo energy, 2012, Article I D **637943**, 7 pages.

[29] Ojaa I, Nanu M, Katerski A, Krunks M, Mere A, Raudoja J, Goossens A, Thin Solid Films, 2005, **480–481**, 82–86.

……..✷♦✷……..

Chapter **6**

Concluding remarks and future prospects

Thin film solar cells can play major role in satisfying world's growing energy demands. While choosing thin film materials, especially for energy devices, one should be careful in having eco-friendly, earth abundant, economic and stable ones. Moreover, the deposition technique should be simple and cost effective. Copper based chalcogenide compounds such as $CuInS_2$ and Cu_2S are capable of satisfying all these demands. For solar cell fabrication, toxic CdS is the proven buffer layer for these materials. In present study, $CuInS_2$ and Cu_2S are the absorber materials and In_2S_3 is the buffer layer. An automated CSP machine was employed for their deposition.

First, $CuInS_2$ absorber layer was deposited by maintaining Cu/In ratio in the precursor solution as 1.4 at substrate temperature of 350 °C. It was observed that surface roughness of the deposited films has strong dependence on spray rate of the precursor solution. Even though low spray rate (2 ml/min) was found to be suitable for getting smooth films, intermediate spray rate (4 ml/min) was selected to avoid long time for spray without affecting good quality device using $CuInS_2$. Initially superstrate configuration (glass/TCO/TiO_2/In_2S_3/$CuInS_2$/Ag) was tried. For this, microporous TiO_2 films were prepared employing CSP keeping substrate temperature at 350 °C. Deposited TiO_2 films are almost amorphous in nature. Air annealing of these films at 400 °C for 2 hour improved the crystallinity without changing the microporous nature. These optimized $CuInS_2$ and TiO_2 are used for the fabrication of 'all sprayed solar cell' using spray deposited FTO film as back contact. Cell parameters obtained were V_{oc} = 409 mV, J_{sc} = 3.90 mA/cm^2, fill

factor = 38 % and efficiency = 0.61 %. FTO back contacts were also replaced with ITO films prepared through sputtering. Cell parameters obtained for this configurations were V_{oc} = 428 mV, J_{sc} = 7.97 mA/cm^2, fill factor = 34 % and efficiency = 1.17 %. Performance of the device in superstrate configuration was not up to our expectation and hence this study was restricted to this much.

In the next step, devices were fabricated without TiO_2 films by following glass/ITO/In_2S_3/$CuInS_2$/Ag structure and this configuration showed feeble light activity. On the other hand, trials on glass/ITO/$CuInS_2$/In_2S_3/Ag configuration showed significant light activity and this configuration were used for further studies. The best device under this study with optimized thickness of absorber and buffer layer has V_{oc} = 478 mV, J_{sc} = 12.13 mA/cm^2. Fill factor and efficiencies were 45 % and 2.59 % respectively. XPS depth profile analysis of this device indicated diffusion of Cu from absorber to buffer layer. Using this configuration, large area device having active area of 2.5 x 2 cm^2 was also fabricated with efficiency of 0.94 %. PV parameters of this device were monitored up to 100 days. The cell was kept in open air condition without any protective coating and minimum damage of the device was observed from 20 days onwards. Even though PV parameters were low, cell works even after 100 days. By replacing ITO back contacts by spray deposited FTO, we fabricated "all sprayed" solar cell with efficiency of 0.94 %. For the purpose of controlling Cu diffusion, Al_2O_3 layer (2 nm) deposited using ALD was introduced in the cell structure (glass/ITO/$CuInS_2$/Al_2O_3/In_2S_3/Ag). XPS analysis of this device clearly showed that Cu diffusion to In_2S_3 was very much controlled in this structure. Comparing with device without Al_2O_3 inter layer, it showed improvements in V_{oc} and fill factor. But J_{sc} value was low, and hence there was no improvement in efficiency. In the next step, CSP method itself was used to deposit resistive $CuInS_2$ inter layer in the cell structure instead of Al_2O_3. Cu diffusion was very much controlled in these structures also and the

device showed improvements in V_{oc} and fill factor comparing with device without this resistive inter layer. But here also J_{sc} decreased leading to comparable efficiencies for both devices. The best device with resistive $CuInS_2$ has V_{oc} of 495 mV and J_{sc} of 9.07 mA/cm^2, while fill factor and efficiency were 57 % and 2.55 % respectively.

CSP was employed for the deposition of a new absorber layer with phases of both $CuInS_2$ and Cu_2S. This material was deposited simply by reducing indium concentration in the precursor for $CuInS_2$. Presence of both $CuInS_2$ and Cu_2S in the sample was confirmed using XRD and Raman analyses. From optical absorption studies, band gaps corresponding to $CuInS_2$ phase (1.45 eV) and that of Cu_2S phase (1.80 eV) were measured. Solar cells were fabricated with this new absorber material by following 'glass/ITO/$CuInS_2$-Cu_2S/In_2S_3/Ag' configuration. The best device with optimized thicknesses of absorber and buffer layer has V_{oc} = 518 mV, J_{sc}= 14.25 mA/cm^2, FF = 52 % and η = 3.82 %. As these cells exhibited ~ 45 % transmission in the visible region, they can be used in window glasses that can simultaneously transmit sunlight and capture power from it.

Finally, Cu_2S absorber was deposited again with CSP technique and used for the fabrication of glass/ITO/$CuInS_2$-Cu_2S/In_2S_3/Ag solar cells. One device among this group with optimized thicknesses of absorber and buffer layer had V_{oc} = 487 mV, J_{sc} = 17.09 mA/cm^2, Fill factor = 50 % and efficiency = 4.11 %. Raman analysis of the device was also performed. Besides the Raman peaks of Cu_2S and In_2S_3, peak corresponding to $CuInS_2$ also existed in the device, which indicated diffusion of copper from the absorber to In_2S_3 buffer layer. Overall cell fabrication processes are completed within 45 minutes. Thus, besides cost effectiveness CSP offers faster PV production possibilities. It was observed that, for entire solar cell fabrication ~ 4.1 kWh

energy is consumed. As we can deposit large number of cells in a single batch, energy consumption for a single solar cell will reduce further.

Future prospects

Copper diffusion into the buffer layer is the main challenge for $CuInS_2$ based devices, prepared using CSP technique in particular. For the present study, double layered $CuInS_2$ was used to control Cu diffusion in $CuInS_2/In_2S_3$ solar cell. By depositing $CuInS_2$ as three layers more control over Cu diffusion can be achieved and this can be easily done with CSP technique. Continuous monitoring of copper diffusion in the device with XPS analysis is also mandatory for this attempt. Small grain size for $CuInS_2$ is another challenge. Doping and post deposition treatments of $CuInS_2$ can improve its grain size.

Lower value for fill factor stands as another issue. In order to improve the fill factor, series resistance of the device can be decreased by lowering the resistivity of In_2S_3 buffer layer. Resistivity of spray deposited In_2S_3 can be manipulated by doping with indium, tin and silver. Doping can be simply performed by incorporating salts of the dopant in the precursor solution of In_2S_3 (in-situ doping). Ex-situ doping can also performed in the cell by depositing a layer of dopant metal on top In_2S_3 layer in the cell before Ag electrode deposition and followed by vacuum annealing. It was observed that, ex situ doping of In_2S_3 with indium and tin decreases the resistivity of In_2S_3. By doing so, device can have a conductive In_2S_3 layer near the electrode and resistive layer near the junction, which can promote effective charge carrier separation and collection.

Solar cells fabricated with $CuInS_2$-Cu_2S absorber layer exhibits ~ 45 % transmission in the visible region. By selecting a suitable transparent front contact, these solar cells can be arranged one over the other to utilize maximum available sunlight.

Sputtered ITO back contacts in multi band gap ETA cell structure can be replaced with spray deposited FTO films for the realization of cost effective 'all sprayed solar cells'. For further reduction in cost, indium free and non-toxic buffer layers such as ZnS and ZnO can be tried for both $CuInS_2$ and Cu_2S absorber layers.

……..✷♦✷……..